



**Research Topic:** Structure-based hit-to-lead design, optimization, and synthesis of tetrahydro-1,3,5-triazine-2-amine derivatives as potential inhibitors of *Mycobacterium tuberculosis* Dihydrofolate Reductase (*MtbDHFR*).

By

ALBERT ZINDOGA

C20142247X

SUPERVISORS: PROFESSOR GRACE MUGUMBATE

Dr. GADZIKANO MUNYUKI

A THESIS SUBMITTED TO CHINHOYI UNIVERSITY OF TECHNOLOGY IN  
FULFILLMENT OF THE REQUIREMENTS OF THE MASTER OF PHILOSOPHY IN  
MEDICINAL CHEMISTRY DEGREE IN THE DEPARTMENT OF CHEMISTRY

MARCH 2023

Endorsement by **Prof Grace Mugumbate**, Main Supervisor:

Date .....15 March 2023....

Signature

*Mugumbate*

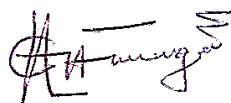
## DECLARATION

Albert Zindoga declares that this thesis, “Structure-based hit-to-lead optimization, and synthesis of tetrahydro-1,3,5-triazine-2-amine derivatives as potential inhibitors of anti-tuberculosis” is originally authored by himself under supervision of Prof. Grace Mugumbate and Dr. Gadzikano Munyuki. Every other ideas and information that are not his, are referenced.

Candidate name: **Albert Zindoga.**

Date .....15 March 2023....

Signature:

A handwritten signature in black ink, appearing to read 'A. Zindoga', with a stylized flourish at the end.

## **DEDICATION**

I dedicate this work to the Creator of this beautiful planet, and future wife and family.

## ACKNOWLEDGMENTS

Everything in this Thesis and research could not have been accomplished without the intervention and mediation of the Almighty God and Christ. I would like to express my heartfelt gratitude to Prof Grace Mugumbate for her unwavering commitment to high academic standards, caring, support, and offering breakthroughs during difficult moments. Dr. G. Munyuki for providing wisdom and a way through when the research hit a brick wall. Dr. G. Munyuki would borrow from his packed schedule, enough moments and time to ensure the progress of this research.

I would like to express special thanks to Dr. N. Siziba and Dr. S. Nyoni the dean of the school and the chairperson of the department respectively for their continued mentorship and, for their frequent assistance in the completion of research experiments. I would also like to extend my special gratitude to Dr. M. Manyeruke for his sincerity, kindness, persistence, and unfaltering positive attitude regardless of what difficulty I faced in the lab during synthesis.

I would also like to thank my parents, my girlfriend, and relatives, for their endless love, guidance, support, and encouragement while I worked toward the completion of my dissertation. My Father has motivated me to follow a path of lifelong education, and for this (and so much more) I am forever grateful. To all my friends some of whom are also my colleagues, it was going to be more than difficult to have been able to navigate through some challenging times without your best wishes and support. My sincere and special thanks to my church “Still Waters Seventh day Multicultural Church” for many answered prayers and an unbelievable act of kindness and love when my father was critically ill in hospital after a severe stroke.

Last but not least I would like to recognize The World Academy of Science (TWAS) for funding the research efficiently, the Holistic Drug Design and Development (H3D) for the characterization of samples, and the Chemistry department for providing considerable assistance.

## OUTPUTS FROM THE STUDY

1. This study helped establish a validated and quintessential protocol for the design and synthesis of tetrahydro-1-3-5-triazine derivatives and a data set for novel bioactive compounds that can be modified into anti-tuberculosis drugs.
2. Furthermore, the inter-disciplinary project could advance basic science at CUT and boosted molecule design and synthesis in addition to encouraging inter-disciplinary collaborations
3. Poster presentation titled, “Structure-based Hit-Lead Optimization of Tetrahydro-1, 3, 5-Triazin-2-Amine derivatives and anti-tuberculosis compounds”, at Holistic Drug Design and Development (H3D) Center in the Stellenbosch Winelands at Webersburg Estate (South Africa) over the period 25-28 October 2022 (**Appendix A**).
4. Research Article (**Published**) titled, “Application of Computational Methods in Understanding Mutations in *Mycobacterium tuberculosis* Drug Resistance”. <https://doi.org/10.3389/fmolb.2021.643849>. (**Appendix B**).
5. Research Manuscript (**Drafted**) titled, “Structure-based Hit to Lead Optimization of Tetrahydro-1, 3, 5-Triazin-2-Amine derivatives and anti-tuberculosis compounds”, (**Appendix C**).
6. Book Chapter (**Under peer review**) titled, “Application of Computational approaches in studies of Bioactives in *Catha edulis*, Cannabis, and their derivatives”.
7. Research Manuscript (**Drafted**) titled, “Application of computer-aided drug design of natural products for malaria, tuberculosis, and, breast cancer”.
8. Book of Abstract, and Oral Presentation  
**Title:** Structure-based Hit to Lead Optimization of Tetrahydro-1, 3, 5-Triazin-2-Amine derivatives and anti-tuberculosis compounds, (**Appendix D**).

## ABSTRACT

Among several *Mycobacterium tuberculosis* potential drug targets, *Mycobacterium tuberculosis* Dihydrofolate Reductase (*MtbDHFR*) is a key enzyme involved in folate metabolism. It is an important target in which its inhibition results in mycobacterial cell death. Several successful anti-folates against infectious diseases exist, but none have been developed to combat tuberculosis. Previously, two potent anti-tuberculosis phenotypic hits belonging to the tetrahydro-1,3,5-triazine-2-amine (THT) family, were predicted and confirmed as inhibitors of *MtbDHFR*. Therefore, optimizing these confirmed hits can lead to a new class of anti-tuberculosis compounds that are target specific and highly potent. The study aims to design and synthesize tetrahydro-1,3,5-triazine-2-amine derivatives as potential anti-TB hit based on the 3D structure of *MtbDHFR*. Structure-activity relationship (SAR) was applied in the design of 113 tetrahydro-1,3,5-triazine-2-amine based on the 3D structure of *MtbDHFR*. The rest of the compounds were designed by scaffold hopping via the synergy of Marvin Sketch (manual design) and Spark software program to inflate the library to a capacity of 1700 compounds. By considering the key distinguishing features between human-DHFR and *MtbDHFR*, the matter of selectivity was well addressed. Resultantly 23 out of 40 tested compounds favored *MtbDHFR* inhibition over *Human DHFR* in terms of selectivity. The generated compound library was subjected to virtual screening using Auto-Dock Vina to predict the binding affinities and the best binding pose of each compound inside the binding site of the *MtbDHFR* target. Next, ADMET studies were then performed to predict the pharmacokinetics and toxicity profiles of the designed compounds. Furthermore, Molecular Dynamics (MD) simulations were done on four ligand complexes where conformational stability, residue flexibility (RMSF), compactness (Rg), and hydrogen bonding were analyzed. The Molecular Dynamics (MD) simulation results support excellent binding affinities of these ligands observed earlier by molecular docking. The study demonstrated a successful hit to lead optimization and all compounds were identified with, binding affinities ranging from -6.5 to -14.1 kcal/mol, improved drug-like, and ADMET properties. Two of the high-ranked compounds were selected for synthesis. The carbodiimide, DCC-mediated coupling reaction was used to synthesize two of the pre-qualified compounds AZ01 and TB1 which had a percentage yield of 74 and 67% respectively, paving the way for further exploration and experimentation work such as biological assays and potentially preclinical testing. Conclusively it is imperative to mention that 1,3,5-triazine scaffolds holds a great promise to the design of novel effective anti-TB leads and may be a beacon of hope for the eradication of this global burdensome TB disease.

Furthermore, the inter-disciplinary project has advanced basic science at CUT and boosted molecule design and synthesis in addition to encouraging inter-disciplinary collaborations.



## TABLE OF CONTENTS

DECLARATION .....	i
DEDICATION .....	ii
ACKNOWLEDGMENTS .....	iii
OUTPUTS FROM THE STUDY .....	iv
ABSTRACT.....	v
TABLE OF CONTENTS.....	vii
ABBREVIATIONS .....	xiv
CHAPTER 1 INTRODUCTION.....	1
1.1 Background .....	1
1.2 Problem Statement .....	3
CHAPTER 2 LITERATURE REVIEW.....	4
2.1 Epidemiology of Tuberculosis .....	4
2.2 Attributes of <i>Mycobacterium Tuberculosis</i> .....	5
2.3 Dihydrofolate Reductase, DHFR .....	7
2.4 Differences between <i>Mtb</i> -DHFR and <i>h</i> -DHFR.....	8
2.5 Application of <i>In-silico</i> Technics in Anti-Tuberculosis drug discovery.....	9
2.6 Chirality and Its Role in Drug Research .....	12
2.6.1 Anti-TB Chiral Drugs .....	13
2.7 Molecular Dynamics Application in Drug Discovery .....	15
2.8 Databases of <i>Mycobacterium Tuberculosis</i> .....	17
2.9 Scaffold-Hopping Technique .....	20
2.9.1 Heterocycle replacement or 1° Hop: .....	21
2.9.2 Ring opening/closure 2° Hop .....	21
2.9.3 Peptidomimetics 3° Hop.....	22
2.9.4 Topology/Shape-Based Scaffold Hopping 4° Hop.....	23
2.10 Synthesis of Triazine Amine derivative molecule via Amid Coupling .....	24
2.11 Justification of the Study.....	26
2.12 Objectives of the Study .....	27
2.12.1 Main Objective.....	27
2.12.2 Specific objectives .....	27

CHAPTER 3	MATERIALS AND METHODS	28
3.1	Research Design	28
3.2	Computational Designing of Compounds	29
3.2.1	Structure-Activity relationship (SAR)	29
3.2.2	Scaffold-Hopping	29
3.2.3	Library Molecular Structure Curation	30
3.3	Structure-based Virtual Screening (SBVS) and ADMET analysis	31
3.4	Macromolecule Structure Preparation	31
3.5	Preparation of Ligands	32
3.6	Reference Ligands	32
3.7	Virtual Screening against <i>Mtb</i> -DHFR and <i>h</i> -DHFR	33
3.8	Validation of the Docking Protocol	33
3.9	ADMET Studies	33
3.10	Validation of the molecular docking results	34
3.10.1	Molecular Dynamics Simulations	34
3.11	Synthesis	35
3.11.1	Synthesis of tetrahydro-1,3,5-triazine-2-amine derivatives	35
3.11.2	Synthesis: DCC-Mediated Amide Coupling	36
3.11.3	The general procedure for the carbodiimide coupling using DCC	36
3.11.4	Reaction Workup	37
CHAPTER 4	RESULTS AND DISCUSSION	39
4.1	Library Generation Results	39
4.2	Compounds designed by Scaffold Hopping	43
4.2.1	Two Degree (2°) Scaffold-Hopping	44
4.3	Validation of the docking protocol	48
4.4	<i>In-silico</i> ADMET Studies	49
4.4.1	Computational Quantitative Characterization of Physicochemical Properties	54
4.4.2	Brain or Intestinal Estimated (BOILED EGG)	58
4.5	Analysis of interactions between 1,3,5-triazine-derivative ligands and <i>Mtb</i> -DHFR receptor	62
4.6	Selectivity Studies	71
4.7	Molecular Dynamics	75
4.7.1	Root mean square fluctuation (RMSF)	77
4.7.2	The radius of gyration, Rg	79
4.7.3	Hydrogen bonds Analysis	80

4.7.4	The outcomes of carbodiimide coupling using DCC.....	81
CHAPTER 5	CONCLUSION .....	84
5.1	Recommendations and Future Work.....	85
APPENDICES	.....	87
5.2	Appendix A: Poster presentation.....	87
5.3	Appendix B: Research Paper.....	88
5.4	Appendix C: Manuscript .....	89
5.5	Appendix D: Book Chapter.....	90
5.6	Appendix 1: Structure-Activity Studies .....	91
5.7	Appendix 2: Lipinski rule of five, Synthetic Accessibility, and ADME Studies.....	100
5.8	Appendix 3: 2D -Structures, and common amino acid residue interacting across all receptors, and binding affinities conjoined to three docked macromolecules (4kne, 4kl9, 1dg8), of 10 pre-qualified ligands. ....	116
5.9	Appendix 4: Ligand-target interactions of 10 best ligands for all three receptors (PDB ID: 4KNE, PDB ID: 4KL9, PDB ID: 1DG8) along with their type of interactions.	118
5.10	Appendix 5: Virtual screening of the glycerol mimicking molecules and the prequalified drug-like molecules to evaluate their selectivity properties towards h (human) DHFR (PDB ID: 1OHJ) and Mtb-DHFR (PDB ID: 1DG8). ....	122
CHAPTER 6	REFERENCES.....	124

## List of Tables

Table 2. 1: Global TB commitments and The End TB Strategy and Targets. This information was derived from the Global tuberculosis report 2021. Geneva: World Health Organization; 2021.....	4
Table 2. 2: Some examples of molecular dynamic (MD) packages commonly applied in drug discovery.....	15
Table 2. 3: Examples of drugs approved by <i>In-silico</i> drug discovery techniques.....	17
Table 2. 4: Classes of Scaffold hopping and examples of some tools used.....	23
Table 4. 1: Structure-Activity Relationship studies.....	40
Table 4. 2: RMSD Calculation of all aligned receptor molecules against each other.....	47
Table 4. 3: 1-3-5-triazine-2-amine derivative compounds along with their Lipinski rule, drug-like score consensus (DLScons), synthetic accessibility (SAscore), Quantitative Estimate of Drug-Likeness (QED), Aqueous Solubility, Cytochrome 450 inhibition prediction of 5 isoforms (1a2, 2c9, 2c19, 2d6, and 3a4), and binding affinity against DHFR enzyme receptors PDB ID: 4kne, 4kl9 and 1dg8.....	49
Table 4. 4: Univariate statistical analysis of <i>In-silico</i> predicted physicochemical properties of selected 16 compounds.....	54
Table 4. 5: ADME properties and Toxicity predictions among selected 24 compounds.....	60
Table 4. 6: 2D -Structures, molecular formula, amino acid residues per each macromolecule, common amino acid residue interacting across all receptors, and binding affinities conjoined to three docked macromolecules (4kne, 4kl9, 1dg8), of 10 pre-qualified ligands.....	62
Table 4. 7: Ligand-target interactions of 10 best ligands for all three receptors (PDB ID: 4KNE, PDB ID: 4KL9, PDB ID: 1DG8) along with their type of interactions.....	66
Table 4. 8: Virtual screening of the glycerol mimicking molecules and the prequalified drug-like molecules to evaluate their selectivity properties towards h (human) DHFR (PDB ID: 1OHJ) and Mtb-DHFR (PDB ID: 1DG8).....	71
Table 4. 9: Binding affinity and some druglike properties of the reference ligand, NSC-339579.....	74
Table 4. 10: Characteristics of the compounds crystals.....	83

## List of Figures

Figure 2. 1: The cell components of the <i>M. tuberculosis</i> structure and sites (potential attractive targets) of inhibition by anti-TB drugs .....	6
Figure 2. 2: The DHFR structure in complex with NADPH (purple) and methotrexate (yellow). The functional loops are F–G (blue), Met20 (red), G–H (green) while G121V signposted by a sphere (cyan) symbolizes the scene of mutation.....	7
Figure 2. 3: Binding site structure of (a) Mtb-DHFR versus (b) h-DHFR. The glycerol binding moiety seen in (a) Mtb-DHFR close to MXT is absent in (b) h-DHFR (Li et al. 2000). .....	8
Figure 2. 4: First-line drugs in their 2D structures.....	14
Figure 2. 5: Structures of antihistamine drugs as examples of 1° Hop (a) pheniramine, (b) cyproheptadine, (c) pizotifen, (d) azatadine, (e) superposition of drugs (a) in magenta and (b) in green and (d) in magenta. ....	21
Figure 2. 6: Prostaglandin EP1 receptor antagonists: (a) biaryl amine series and (b) indole series .....	22
Figure 2. 7: Structures of pain-killing drugs: (a) morphine, (b) tramadol, and (c) 3D .....	22
Figure 2. 8: Amide bond formation by boron reagent. ....	25
Figure 2. 9: DCC-Mediated synthesis of an amide bond.....	26
Figure 3. 1: Summary and workflow of the computational medicinal chemistry and organic synthetic chemistry concepts adopted for the design and synthesis of <i>Mtb</i> -DHFR inhibitor compounds. ....	28
Figure 3. 2: Structure of NSC-339679 compound used as a reference ligand.....	32
Figure 3. 3: DCC-Mediated Amide Coupling.....	35
Figure 3. 4 Scheme for the DCC-Mediated Amide coupling reaction mechanism .....	37
Figure 4. 1: The illustration of typical erroneous issues resolved by molecular structure curation. ....	39

Figure 4. 2: 4kne-BTHT1 interactions with amino acids of the binding pocket. (a) 3D-interactions (b) 3D surface representation, ligand (purple), polar interactions (ILE: 14 & SER: 49), polar contacts (red), non-polar contacts (light green), .....	42
Figure 4. 3: 1° target-based Scaffold Hopping technique using THT1 and THT2 as the starter molecules, 2D/3D similarities of the starter molecules to the product molecules, and virtual screening of the daughter analogs to determine the binding energies imparted by alterations on each scaffold. The displayed $\Delta G$ -value represents the average docking score obtained against Mtb-DHFR macromolecular receptors PDB ID: 4kne, 4kl9, & 1dg8.....	43
Figure 4. 4: Two degree, 2° Scaffold-Hopping product molecules, 2D and 3D Similarities (dark green=starter molecule, pink = product molecule), and Virtual Screening of 1-3-5-Triazine derivative molecules. ....	46
Figure 4. 5: Superimposition/Sequence alignment of (a) PDB ID: 4kne and 4kl9, (b) PDB ID: 4kne and 1dg8, (c) PDB ID: 4kl9 and 1dg8, PDB ID 4kne (blue), PDB ID 4kl9 (cyan), PDB ID 1dg8 (yellow).....	47
Figure 4. 6: Co-crystallized ligands (green) superimposed with predicted ligands (yellow), presented for validation of the docking protocol [a]. 4kne in complex with cycloguanil, b). 4kl9 in complex with NADPH, c). 1dg8 complexed with NADPH d). 1ohj complexed with PT523].....	48
Figure 4. 7: Assessment of the Lipinski rule of five, (a) Molecular weight (MW), (b) LOGP (consensus), (c) number of hydrogen bond donors (nHDon), (d) number of hydrogen bond acceptors (nHAcc). ....	56
Figure 4. 8: Computational quantitative characterization of compounds' physicochemical properties, (a) Chiral centers, Molar refractivity consensus (MRcons), Topological polar surface are using N and O polar contributions, (d) number of rotatable bonds (RBN), (e) Synthetic accessibility score (SAscore) and (f) Estimated solubility (ESOL).....	57
Figure 4. 9: Predicted boiled egg representation of the selected designed 1,3,5-triazine based derivatives using the Swiss ADME web tool. ....	59
Figure 4. 10: Complex structures of MtbDhfr and humanDhfr with molecule (ligand) GM10 and RF28.....	73

Figure 4. 11: RMSD as a function of 50 ns MD simulation time of schematic plots for docked complexes (a) MtbDHFR-AS100, (b) MtbDHFR-MOL15, (c) MtbDHFR-TB1, and (d) MtbDHFR-RM15.....	76
Figure 4. 12: Root mean square fluctuation (RMSF) graph (Fig 4.12a) showing minimum, maximum and average RMSF (Fig 4.12b) of Mtb-DHFR target when complexed with selected (4) ligands during a 50 ns Molecular dynamics (MD) simulation time.....	78
Figure 4. 13: Root mean square fluctuation (RMSF) for ligands .....	79
Figure 4. 14 : The radius of gyration (Rg) for ligands (a) and for protein (b) to which ligands bound during a 50 ns MD Simulation period.....	80
Figure 4. 15: The total number of hydrogen bonds between MtbDHFR protein and ligands AS100, MOL15, RM15, and TB1 .....	81
Figure 4. 16: Scheme for the DCC-Mediated Amide coupling reaction mechanism .....	82

## ABBREVIATIONS

ADMET	Absorption, Distribution, Metabolism, Excretion, Toxicity
BBB	Blood-Brain Barrier
BOILED EGG	Brain Or Interstitial Estimated
YASARA	Yet Another Scientific Artificial Reality Application
CADD	Computer Aided Drug Design
CYP450	Cytochrome P450
DCC	N, N'-dicyclohexylcarbodiimide
DCU	N, N'-dicyclohexylurea
DHFR	Dihydrofolate reductase
e.g.	<i>exempli gratia</i> (Latin for "for example")
EDC	1-ethyl-3-(3'-dimethylaminopropyl)-carbodiimide hydrochloride
ESOL	Estimated Solubility
FDA	Food and Drug Administration
i.e.	<i>id est</i> (Latin for "that is")
LBDD	Ligand-Based Drug Design
MD	Molecular Dynamics
MDR-TB	Multi-drug resistant tuberculosis
MM-GBSA	Molecular Mechanics Generalized Born Surface Area
MM-PBSA	Molecular Mechanics Poisson-Boltzmann Surface Area
MRcons	Molar Refractivity consensus
MW	Molecular Weight
nHAcc	Number of Hydrogen bond acceptors
nHDon	Number of Hydrogen bond donors



PDB	Protein Data Bank
QED	Quantitative Estimate of Drug Likeness
RBN	Number of rotatable bonds
Rg	Radius of gyration
RMSD	Root Mean Square Deviation
RMSF	Root Mean Square Fluctuation
SAR	Structure-activity relationship,
SAscore	Synthetic Accessibility score
SBDD	Structure-based drug design
SMILES	Simplified Molecular Input Line Entry System
TPSA (N, O)	Topological Polar Surface Area using N and O polar contributions
WHO	World Health Organization

## CHAPTER 1

### INTRODUCTION

#### 1.1 Background

*Mycobacterium tuberculosis*, a causative agent of a deadly respiratory and communicable disease called Tuberculosis (TB) has persisted as a major global threat to human life. TB infected and killed a total of 1.5 million people in 2018 as established by the World Health Organization (WHO) in 2020. The gravity of the TB epidemic is in the vicinity of 1.7 billion people reportedly at the *Mtb* latent stage and the infected have a higher probability of developing TB (Chakaya et al., 2021). Resultantly the current progress to the End TB Strategy by 2035 vision as observed by the 2020 global TB report is sluggish and still ‘beyond the black stump’ having yielded a decrement of 9% instead of the targeted 20% since 2015. The length of TB treatment often extends to Multi-Drug Resistant (MDR) and several other health complications such as patient non-compliance (Wajja, 2004). Recently, Allué-Guardia (2021) projected MDR-TB mortality rising to 75 million people, coupled with a massive \$16.7 trillion in financial implications to the global economy in a timeframe of just 35 years. Stakeholders, advocates, and researchers are working together to develop treatment regimens shorter in duration, more effective, safer, and well-tolerated (Tiberi et al., 2018). Among several TB drug targets, Dihydrofolate reductase (DHFR), a key enzyme involved in folate metabolism, is an important target and its inhibition can result in mycobacterial cell death. Although several antifolates have proved successful in the treatment of infectious diseases, none have been developed to combat TB, thus finding novel agents with a promising pharmacological profile remains one of the major challenges for medicinal chemists, as testified by the literature trends of the last 20 years. Thus, as evidenced by the literature trend over the last 20 years, finding novel agents with a promising pharmacological profile remains one of the major challenges for medicinal chemists. Failure of many drugs to obtain FDA approval as a result of several unsatisfactory attributes such as low efficacy, potency, selectivity, toxicity, have delayed the availability of a new drug to patients. The realization that 90% of the drugs entering clinical trials fail to get FDA approval (Leelananda, & Lindert, 2016) is an undesirable characteristic and therefore calls for urgency in the utilization of high-minded methodologies in drug discovery.

Methotrexate (MTX) and trimetrexate are antifolate drugs that have a high affinity for DHFR and can inhibit DNA synthesis and cell proliferation (Lin & Gerson, 2014). These compounds are not useful as antibacterial drugs because of their poor selectivity despite having antibacterial activities (Li et al., 2011). Among many of their medicinal uses, including bactericidal effects, antifolates are also used in cancer chemotherapy.

The approach of Structure-based drug design (SBDD) in this study made use of 3D Crystal structure of *Mtb*-DHFR target to actualize and predict those ligands that are likely to establish optimal interactions with the binding site.

From a design standpoint, compound library generation or build-up was executed with factors such as selectivity, affinity, potency, efficacy, and toxicity in mind. With a cognitive understanding of one of the most noteworthy distinguishing features between the crystal structure of *Mtb*-DHFR and *H*-DHFR which is the absence of a glycerol-binding motif in *H*-DHFR but contrarily is ubiquitous and tightly bound in *Mtb*-DHFR., therefore we designed a series of small-molecule compound analogs in which the non-triazine moiety was joined to a 1, 2, 3-triol. This school of thought was derived from El-Hamamsy et al. (2007) with the agenda to mimic the binding signature of Methotrexate deep in the dihydrofolate-binding pocket to optimize DHFR enzyme selectivity. Adopting El-Hamamsy et al.'s idea in designing a better triazine derivative molecule containing a glycerol-mimicking triol should occupy both the DHFR binding pocket and the glycerol binding pocket giving rise to better selectivity toward *Mtb*DHFR inhibition. All these insights inspired the research to apply two techniques *i.e* structure-activity relationship and scaffold-hopping concepts to design compounds with modified selectivity, improved affinities, or bio-activities, and essentially to attain novel patentable isolobal analogs. In these research endeavors to discover new tuberculosis drugs, the polypharmacology approach could be realized to gain mastery over the issues of resistance. Polypharmacology is referred to as a phenomenon involving (a) one drug acting on diverse targets of a specific distinctive disease pathway or (b) a promiscuous drug related to several or more than one disease pathway (Stelitano et al., 2020; Reddy & Zhang, 2013). This concept is similar to drug promiscuity and it seems to conflict with drug selectivity, which describes the ability of a drug to affect a specific intended receptor target or macromolecule, however, both selectivity and promiscuity are important attributes in drug discovery. Additionally, many successful drugs are promiscuous (Mencher & Wang, 2005). During Structure-based design with respect to selectivity, one of our prime goals was to hyperbolize desirable and favorable

[triazine ligand(s) – MtbDHFR] interactions while making unfavorable the [triazine ligand(s) – *h*-DHFR] and other undesirable off-target interactions.

In building our compound dataset it was imperative and a prerequisite to consider but strike a balance between structural novelty and its physicochemical properties, including lead-like (Congreve et al. 2003) and drug-like (Lipinski, 2004) properties. Consequently, it is of paramount importance to leverage the available chemoinformatics approaches to assess and determine their lead-like properties. This is a wise ideology before synthesis because it serves time and laboratory costs. This research was therefore inspired to yield lead-like anti-TB molecules.

## 1.2 Problem Statement

Tuberculosis (TB) is ubiquitous in all corners of the world. While humans in all age brackets are at risk, TB is dreadfully infecting adults at their productive age, and more than 95% of recorded cases and deaths emanate from developing countries (WHO, 2021). Inexpedient contributors such as the attrition rate in drug development, and the available treatment options, which are stultified by drug resistance, poor-patient compliance, slow-acting drugs, technological demerits of the presently used therapeutics, etc. (Hussain *et al.*, 2019) have turned out to be abortive to the 2030 SDG and WHO's End TB Strategy (WHO., 2015). This problem is being further catastrophized by the emerging MDR-TB which mortality was predicted to acclimatize to 75 million people with a penalty of \$16.7 trillion in financial implications to the global economy in a timeframe of just 35 years if appropriate efforts are not enacted. Stakeholders, advocates, and researchers are working together to develop treatment regimens shorter in duration, more effective, safer, and more well-tolerated (Tiberi et al., 2018). Among several potential *Mycobacterium tuberculosis* drug targets, Dihydrofolate Reductase (DHFR) a key enzyme involved in folate metabolism is an important target, and its inhibition results in mycobacterial cell death. Several successful anti-folates against infectious diseases exist, but none have been developed to combat tuberculosis. Previously, two potent anti-tuberculosis phenotypic hits belonging to the tetrahydro-1,3,5-triazin-2-amine (THT) family, were predicted and confirmed as inhibitors of *Mtb* DHFR. Therefore, optimizing the confirmed hits would lead to a new class of anti-tuberculosis compounds that are target specific and highly potent.

## CHAPTER 2

### LITERATURE REVIEW

#### 2.1 Epidemiology of Tuberculosis

Following a UN high-level-TB meeting that brought about the resolution that an annual US\$13 billion must be provided for TB diagnosis, treatment, and prevention (Tuberculosis n.d.), it is clear that tuberculosis is undeniably a global catastrophe. When the same meeting (UN-high-level TB meeting) was held in 2018 in which they established 2018-2022 goals, they agreed in the meeting, to provide treatment for 40 million people, TB immunization to 30 million people, 1.5 million people with MDR-TB, as well as 6 million HIV infected persons ([UNHLM ON TB Key Targets and Commitments | Stop TB Partnership](#)). Tuberculosis is not only a global concern but a threat to all age groups therefore the UN-high-level TB meeting also prescribed treatment provisions at the household level to 4 million children with ages between 0 to 5 years and 20 million to those within the age group above five years (Stop TB Partnership, 2020). Early diagnosis of TB patients should be prioritized if the world is determined to curtail the mortality rate together with the treatment costs. The End TB Strategy incorporates systematic screening, which can achieve early TB diagnosis effectively (WHO, 2021). Table 2.1 shows the TB commitments at the global level and the End TB Strategy.

Table 2. 1: Global TB commitments and The End TB Strategy and Targets. This information was derived from the Global tuberculosis report 2021. Geneva: World Health Organization; 2021

<b>VISION</b>	<b>A WORLD FREE OF TB</b> -zero death, disease, and suffering due to TB			
<b>GOAL</b>	<b>END THE GLOBAL TB EPIDEMIC</b>			
<b>INDICATORS</b>	<b>MILESTONES</b>		<b>TARGETS</b>	
	2020	2025	2030	2035

Percentage reduction in the absolute number of TB death (Compared with the 2015 baseline)	35%	75%	90%	95%
Percentage reduction in the TB incidence rate (compared	20%	50%	80%	90%
Percentage of TB-affected households facing catastrophic costs due to TB (level in 2015 unknown	0%	0%	0%	0%

The information in Table 2.1 describes the resolutions of a joint venture between the World Health Organization (WHO)’s End TB Strategy and the UN Sustainable Development Goals (SDGs). The TB mortality growth in 2020 was largely attributed to diagnosis obstructions and treatment disturbances at the hands of the COVID-19 pandemic (<https://tbfacts.org/tb-statistics/>). Since both tuberculosis and COVID-19 are respiratory diseases, it is imperative to promote and conduct COVID-19 coinfection in patients with TB. Investigations determining coinfection are of paramount importance because patients with TB can experience a much more intense illness with a higher probability of succumbing to death from COVID-19 (Coronel et al., 2021).

## 2.2 Attributes of *Mycobacterium Tuberculosis*

*Mycobacterial tuberculosis* virulence is centered on its capacity to invade and stay inside host cells and its ability to combat and survive the microbicidal effects of macrophages (Echeverria et al., 2018). The arrangement of the critical and unique features of the Mycobacterial cell wall, such as mycolyl-arabinogalactan-peptidoglycan complex, and the phosphatidyl-myo-inositol-based lipoglycans, provide an attractive target for the anti-tuberculosis agent development (Jankute *et al.* 2015). Some potentially rich sources of TB drug targets are found in cell wall biosynthesis, and energy metabolism (Cardoso et al., 2022).

The *Mycobacterium tuberculosis* (*Mtb*) pathogen exercises varying intrinsic mechanisms that enable it to resist and survive six months of drug therapy. *Mtb* leverages to its advantage the possession of an exceedingly impermeable and thick lipid-rich hydrophobic cell wall envelope that suppresses the influx of many anti-TB chemotypes especially hydrophobic drugs (Sarathy et al.,

2012). The peptidoglycan determines the shape of the *Mtb* cell wall structure ( Figure 2.1), by helping it withstand turgor pressure, providing a communication interface, and defense barrier against the threats of its external environment (Alvarez et al., 2014; Cava, 2014). *M. tuberculosis* is neither categorized as gram-positive nor gram-negative because of its unique structural components, such as the peptidoglycan, which is the determining factor and the reason *Mtb* falls into the class of acid-fast bacteria (Vilchèze & Kremer, 2017; Baker et al., 2019).

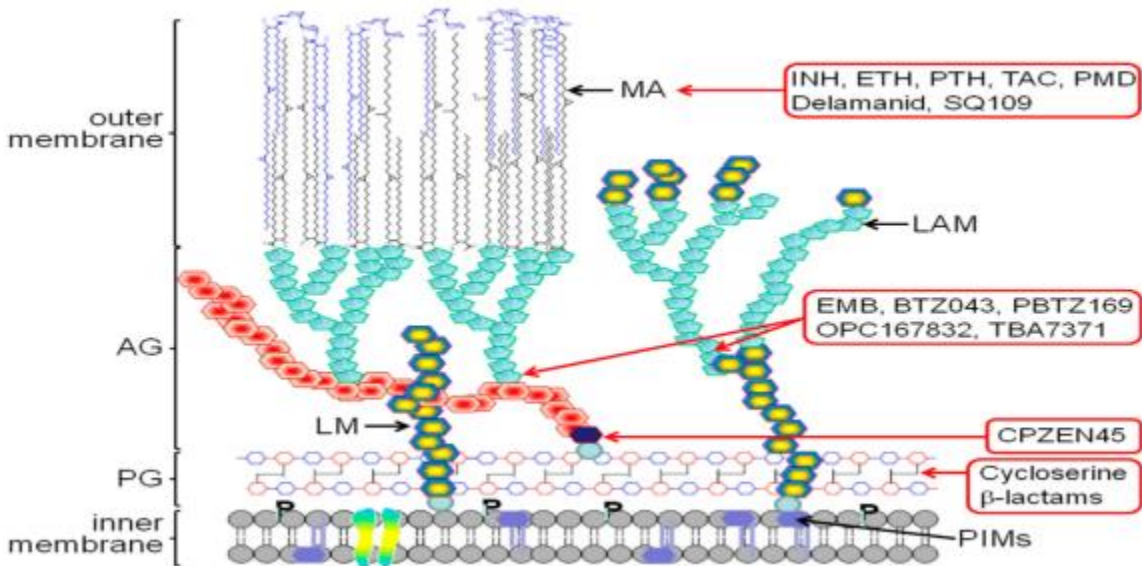


Figure 2. 1: The cell components of the *M. tuberculosis* structure and sites (potential attractive targets) of inhibition by anti-TB drugs

It is more likely that tuberculosis distribution and incidence could hike globally in 2022-2023 on account of the COVID-19 pandemic impact (WHO, 2021). The new cases (about 500 000) regarding multidrug or rifampicin-resistant TB have been reported to occur annually, and statistically only one in three cases were confirmed to have received treatment (WHO, 2022). Newly developed, drug-resistant TB treatment-approved anti-TB drugs such as delamanid, bedaquiline and pretomanid can effectively regulate and control TB if made available to patients (WHO, 2020). One major concern which has also plummeted political debate and advocacy in both developing and developed countries is the urgent need to avail these new anti-TB drugs at affordable drugs, especially in poor or developing countries (Gunther et al. 2023).

Regarding drug resistance, some recent researches investigated several factors, such as efflux pumps, membrane energetics as well as cell wall biosynthesis processes. Porin channels are transporters outside the *M. tuberculosis* cell wall, which can mediate the influx of drugs but are

also thought to be connected to the interior walls imparting efflux of drugs detrimentally contributing to antibiotic resistance (Niederweis et al, 2010). These efflux pumps can provide a striking target for designing and developing next-generation anti-TB agents. However, research findings by Remm and co-workers could not significantly point out any of these factors as responsible for drug resistance (Remm et al., 2022).

### 2.3 Dihydrofolate Reductase, DHFR

*Dihydrofolate reductase (DHFR)* is a key enzyme that plays an integral role in the biosynthesis of co-factors such as tetrahydrofolate, which in turn is an essential precursor to the biosynthesis of purines, thymidine nucleotides, and several amino acids like glycine, and methionine, (Bertacine et al, 2018). As far as its catalytic phenomena, DHFR structure has three crucial functional loops, which include the Met20 loop that possesses 9–23 residues, the F-G loop has 116–132 residues, and the G-H loop of 142–149 residues. The structure of DHFR is illustrated in Figure 2.2 (Mauldin, 2012). Based on experimental (Bhabha et al, 2011) and theoretical techniques (Agarwal et al. 2002; Rod, Radkiewicz, & Brooks III, 2003) catalysis is also imparted by motions among the loops.

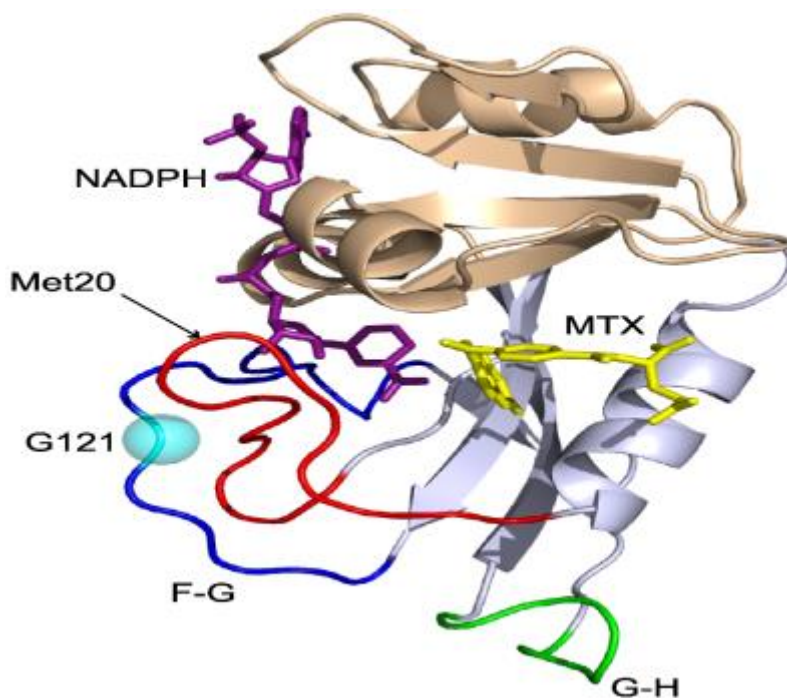


Figure 2. 2: The DHFR structure in complex with NADPH (purple) and methotrexate (yellow). The functional loops are F-G (blue), Met20 (red), G-H (green) while G121V signposted by a sphere (cyan) symbolizes the scene of mutation.



Mutation in the structure of DHFR commonly occurs in glycine (Watney, Agarwal, & Hammes-Schiffer, 2003). (G121) highlighted in Figure 2.2.

## 2.4 Differences between *Mtb*-DHFR and *h*-DHFR

The DHFR enzyme is ubiquitous in both microorganisms and humans. There are however distinctive features between human DHFR (*h*-DHFR) and *M. tuberculosis* DHFR (*Mtb*-DHFR) that are key to the discovery or identification of next-generation anti-TB agents. This consideration is crucial when designing *Mtb*-DHFR selective inhibitors to minimize the probability of inhibiting off-target molecules like *h*-DHFR, thus minimizing side effects. However, clinically effective anti-TB drugs have more or similar selectivity and affinity to the *h*-DHFR (Sharma et al., 2020).

Despite its universality in humans and *Mtb*DHFR structure accounts for only 26% of similarities differing only in their active binding pockets (Kobayashi, 2014). In *M. tuberculosis*, DHFR (*Mtb*-DHFR) binding site is a glycerol binding motif usually bonded to Asp 27, Gln 28 and Leu 24, and this glycerol binding motif is absent in human DHFR leaving its site occupied by hydrophobic Leu 22, Pro 26 and Phe 31 residues (Sharma, 2018; Niederweis et al, 2010). Some of these fundamental differences are highlighted in figure 2.3.

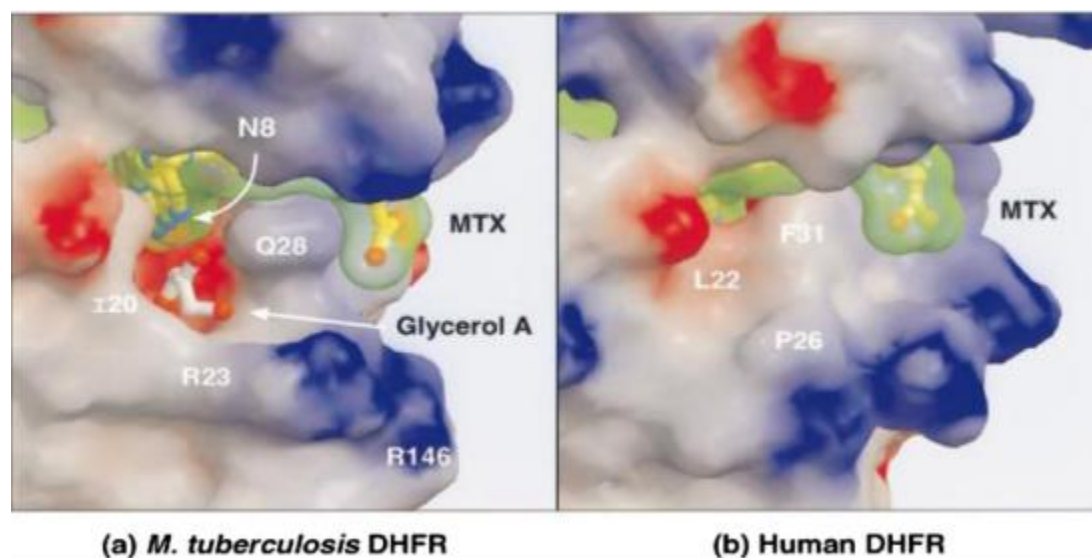


Figure 2. 3: Binding site structure of (a) *Mtb*-DHFR versus (b) *h*-DHFR. The glycerol binding moiety seen in (a) *Mtb*-DHFR close to MXT is absent in (b) *h*-DHFR (Li et al. 2000).

The other distinguishing feature between *h*-DHFR and *Mtb*-DHFR is 187 amino acid residues of *h*-DHFR compared to 159 of *Mtb*-DHFR (El-Hamamsy et al., 2007). This also, therefore, implies

that the h-DHFR is larger than the *Mtb*-DHFR. Exploration of these differences provides the basis for designing novel selective *Mtb*-DHFR inhibitors that will not favor the binding of human DHFR.

## **2.5 Application of *In-silico* Technics in Anti-Tuberculosis drug discovery**

This section focuses on applying chemoinformatics in TB drug discovery in synthetic and natural products. In the quest for more effective drugs, remarkable improvements in computational power coupled with advancements in AI technology can be used to revolutionize the drug development process (Mak & Pichika., 2019). The combination of factors such as the phenomenal increase in compound databases, remarkable boosts in computing power, transformational achievement in learning algorithms, etc., are at the prime of adoption by medicinal chemists in the actualization of effective therapeutic medicines. Artificial Intelligence (AI) is widely applied in disease diagnosis in which. Xiong *et al.* (2018) in their study investigated the clinical efficacy of artificial intelligence (AI)-assisted detection method for acid-fast stained TB bacillus. In their investigation, Xiong *et al.* (2018) also concluded that TB-AI can be a potential support system to detect stained TB bacilli and help make sound clinical decisions. In addition, TB-AI holds the potential to relieve the heavy workload of pathologists and increase detectability and chances of accuracy in diagnosis. We are focusing on the modernistic *In-silico* approaches in TB drug designing and discovery from natural products by a glimpse of the great intervention of the cutting edge, highest level general development of cheminformatics.

Almost every society globally has skimmed and substantiated the medicinal value of plants and natural products. Thus, the world has benefited from natural products emanating from various sources, including marine organisms, terrestrial plants, vertebrates and invertebrates, and terrestrial microorganisms (Newman *et al.*, 2000). Nature being depended upon as a source of folk medicines brought about bioactive organics such as salicylic acid (the precursor of aspirin), antimalarial quinine, and morphine, which was isolated from the opium poppy, etc. (Raja *et al.*, 2010). Yuan *et al.* (2016) realized that the discovery of new drugs by entirely depending on modern technologies was almost unrewarding because the adoption of high throughput screening and combinatorial chemistry-based-drug development could not deliver expected drug productivity since the 1980s. However, beyond the traditional use of folk medicines, *in-silico* approaches have

been widely recognized as useful for drug discovery (Lagunin *et al.*, 2014). *In-silico* drug discovery can take advantage of many available chemical databases, medicinal plants, and chemo- and bioinformatics tools. The number of existing databases grows annually. The contribution of computational technics (*in-silico* methods) in drug discovery will grow soon. In these research endeavors to discover new tuberculosis drugs, the polypharmacology approach could be implemented to gain mastery over the resistance issues. Polypharmacology can be defined in two ways which are (a) a phenomenon involving a single drug acting on multiple different targets of a unique disease pathway or (b) a single drug acting on multiple targets of multiple disease pathways (Stelitano *et al.* 2020; Reddy & Zhang, 2013).

Using DNA sequencing data, Machine Learning (ML) can be used to predict tuberculosis drug resistance. Several machine learning tools have found applications in drug discovery, including GOLD, Deep PVP, LIB, and SVM. Machine learning has algorithms such as support vector machine (SVM), random forest (RF), decision tree, and Artificial Neural Networks (ANN) (Nayarisseri *et al.*, 2021). Within the drug discovery pipeline, Machine Learning (ML) techniques are employed in various methods and stages that comprise Structure-based Virtual Screening (SBVS), Ligand-based Virtual Screening (LBVS), Structure-based Drug Design (SBDD), ligand-based drug design (LBDD), drug repurposing, quantitative structure-activity relationship (QSAR) modeling, and ADMET analysis (Antolín, 2021).

From the kingdom Fungi, endophytic fungi can produce two natural bisanthraquinone, (+)-1,1'-Bislunatin (Bis) and (+)-2,2'-Epicytoskyrin A (Epi). These two secondary metabolites, Bis and Epi, possess potent bactericidal effects in which *in-silico* virtual screening using glide confirmed good biological activity against *Mtb* H37Rv with docking scores of -8.427 kcal/mol and -7.481 kcal/mol (Oktavia *et al.* 2020). The applied *in-silico* approach is an example of structure-based drug design. Oktavia *et al.* 2020 capitalized on the knowledge of the 3D macromolecular receptor/target of *Mtb* H37Rv and employed molecular docking using the glide docking tool. The anti-*Mtb* properties of Indonesian natural products isolated from *Rhoeo spathacea* and *Pluchea indica* were gratified and confirmed using structure-based drug discovery to be inhibitors of *M. tuberculosis* CYP121 target following a virtual screening of ligands by AutoDock Vina software. Subsequently, the mechanism of inhibition of the identified secondary metabolites was full-fledged by molecular dynamics simulation using YASARA software (Prasasty *et al.*, 2020). Zhang

et al. (2021) performed structure-based virtual screening using Discovery Studio, a molecular docking software tool using a commercial library of natural products provided by Enamine (Kyiv, Ukraine). After applying these chemoinformatics tools, Zhang *et al.*, 2021 identified the F0414 compound as a potent inhibitor of the Mt-dUTPase target with confirmed bioactivity against *M. tuberculosis*.

Ligand-based approaches for TB drug discovery have consisted primarily of quantitative structure-activity relationship (QSAR), three-dimensional (3D)-QSAR, and pharmacophore models. Agrawal *et al.* (2007) used ligand-based pharmacophore modeling and structure-based virtual screening by molecular docking to identify and shortlist 15 natural product compounds with better anti-*Mtb* activities.

Data analytics software called KNIME provides a rich palette of tools that can remarkably empower ligand and structure-based drug design and optimization in the search for potent and selective inhibitors of *Mycobacterium tuberculosis* (*Mtb*) from natural products. For example, KNIME pipeline software was used to filter 350 compounds from the Zinc database before virtual screening (docking) by virtue of 20 calculated molecular descriptors on the knowledge of the *Mtb*-*EthR* target binding pocket (Tatum *et al.*, 2017).

For building compound libraries, ChemT (<http://www.esa.ipb.pt/>) software from BioChemCore is an ideal, easy-to-use open-source chemoinformatic tool (Abreu et al. 2011). Using approved drugs, for example, TB drugs such as isoniazid, rifampicin, ethionamide, natural product anti-TB agents, or even any other drug that has been removed from the market for various reasons not limited to risks outweighing benefits and many other reasons such as resistance, ChemT can take center stage to automatically generate custom-made template-based chemical libraries at the heart of drug optimization, drug repurposing. Data Warrior (<https://openmolecules.org/datawarrior>), the open-source software for Data Visualization and Analysis with Chemical Intelligence, is also vital to chemical library generation and expedites Lipinski rule of five among its several exploits (Sander & Freyss, 2015). Therefore all these *in-silico* approaches can find their application in TB drug discovery.

For the calculation and analysis of various molecular descriptors and several molecular fingerprints, a new generation software tool called alvaDesc, provided by alvascience, has been made available (Mauri, 2020). Another companion software provided again by alvascience is the

alvaMolecules tool ([www.alvascience.com](http://www.alvascience.com)), which can help standardize data structures and molecular structure curation. This includes rectifying erroneous structures such as unusual valence, multiple structures, chirality, aromaticity, excess hydrogens, etc. Another alvascience software called alvaModel <http://www.alvascience.com/alvamodel/> can be appropriately devoted to ligand-based drug discovery approach due to its ability to create Quantitative Structure-Activity/Property Relationship (QSAR/QSPR) models. To determine the lead-like and drug-like properties of compound structure and, even during lead optimization, the QSAR/QSPR) models are paramount in their ability to predict physicochemical, biological, and environmental properties, promoting potential anti-TB molecules to the next stages of the drug discovery pipeline. From the aptitude of these prowess software programs, the application of alvaDesc, alvaMolecules, and alvaModel in anti-TB natural product discovery can be successful and handy in streamlining the discovery process.

Driven by this evidence of technological breakthroughs, chemoinformatics can circumvent *M. tuberculosis*'s formidable burdensome emerging strains through the diverse chemical space of anti-TB secondary metabolites in natural plant products.

## **2.6 Chirality and Its Role in Drug Research**

By definition, chirality is the potential and ability of the compound molecule to exist in two enantiomeric asymmetrical non-superimposable mirror images of each other. Maintaining bond orders, atomic composition and atomic composition chirality phenomenon can occur nonetheless. One of the critical objectives in drug discovery is to develop drug molecules that are safe and target-specific. The property of molecular chirality comprehensively offers a great deal of complexity in navigating toward achieving this objective (LaPlante et al., 2011). Enantiomers of the chiral molecule are most likely to be significantly distinctive in various properties including biological activity, toxicity, pharmacodynamics, and pharmacokinetics (Eichelbaum & Gross 1996). When both mirror-image enantiomers occur in equal proportions are called racemates and there are adverse effects attributable to one of the enantiomer present in the racemic mixture. The second enantiomer may be toxic and less biologically active and could have the ability to interfere with the more biologically active enantiomer by competitively binding to the same active site. An example of chiral molecules include thalidomide and perhexiline, whereas the left-hand

enantiomers of these respective two renowned drugs were potent and effective, their right-hand molecules were revealed with teratogenic effects and unsafe (Vargesson, 2019). Each enantiomeric pair molecule may form distinct interactions inside the target's binding site, resulting in undesirable ADMET effects. In the case of thalidomide which was past prescribed to pregnant women to alleviate morning sickness, the impact of the right-hand enantiomer resulted in many around 100000 infants being born with severe birth defects (Smithells & Newton, 1992; Vargesson, 2019; Johnson, 2018; Magazanik, 2015). The enantiomeric pair may also have different drug-drug interaction experiences. Owing to this fact, it is highly recommended to take into account stereoselectivity in the early stages of drug development to get the better of associated adverse effects. Chirality in drugs can also evolve from atropisomerism, a phenomenon where a bond rotation is hindered about its axis (Blaser, 2013). Chirality is common in various organic molecules, including amino acids and also glucose. Inspired and necessitate by the motive to develop new drugs, the US Food and Drug Administration (FDA) published new guidelines in 1992 expressing the significance of absolute stereochemistry or enantiopurity for all chiral compounds [www.fda.gov/cder/guidance/stereo.htm](http://www.fda.gov/cder/guidance/stereo.htm) (Amouri & Gruselle, 2008). Regarding chiral molecules, designing and synthesizing enantiopure molecules enhances the chances of producing drugs with safer and improved efficacy. Modern organic synthesis techniques and separation methods of asymmetric synthesis have so far advanced chiral drug discovery and development, and chiral separation, resultantly an influx of at least 75% of new drugs introduced to the market around the year 2011 were single enantiomers (Huang et al., 2011). From 2011 to date, a considerable amount of chiral anti-TB agents have been developed from various sources including natural products, high throughput screening (HTS) hits, and other famous anti-TB agents.

### **2.6.1 Anti-TB Chiral Drugs**

Of the first-line TB drugs (figure 2.4.), 60% (i.e. 3 out of 5) which include rifampicin (RMP), ethambutol (EMB), and streptomycin (SM) can rotate the plane of polarized light (comprise chiral centers) and are administered in their optically active pure forms.

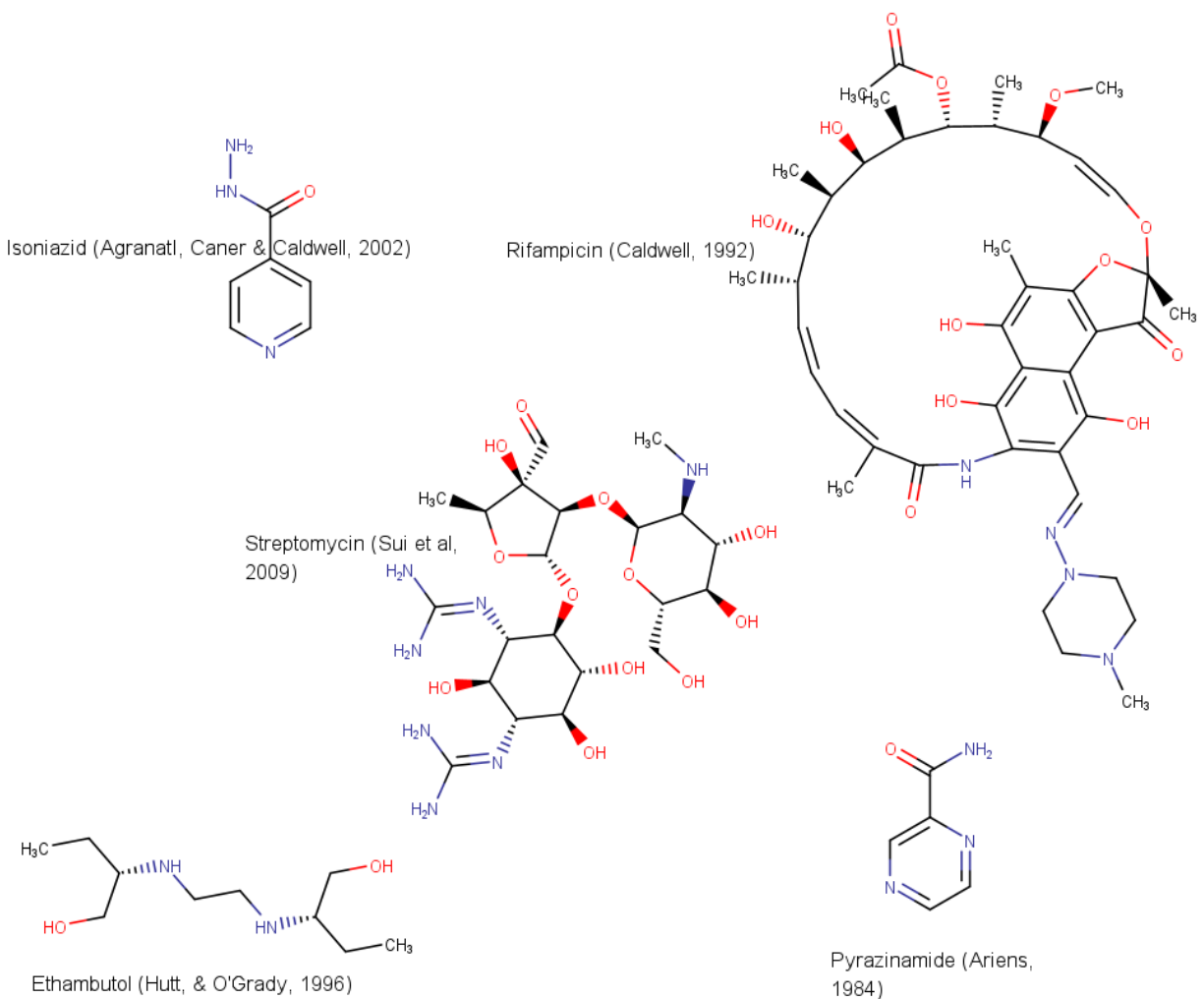


Figure 2. 4: First-line drugs in their 2D structures

It was observed that the *S, S* enantiomer from the chiral EMB is highly antimycobacterial (i.e. 500 fold) than its *R, R* isomer which can cause blindness due to optical neuritis (Upadhyay et al., 2020). Exploiting the cheap chiral source from camphor, Perkova et al. (2014) used the  $\beta$ -aminoalcohol EMB fragment and a chiral camphane scaffold to develop camphor molecule derivatives of which some were 25 times better than EMB in terms of antimycobacterial activity.

The computational examination of chirality is possible with software programs like alvaDesc 2.0 which was adopted for this study. The alvaDesc software can calculate the number of chiral centers, chiral moment (similar to the moment of inertia but centered at the chiral center), and chiralPhMoment (similar to chiralMoment, but only taking the N/O atoms into account).

## 2.7 Molecular Dynamics Application in Drug Discovery

As showcased by vast applications in recent research, Molecular Dynamics simulations have become of paramount importance to drug discovery. Mortier et al. (2015) conducted four-year span research in which they reviewed the influence and impact of MD simulations in the landscape of medicinal chemistry with particular attention to ligand-protein interactions. The accuracy of ligand-target residence time in predicting *in vivo* drug efficacy (Mollica et al., 2016) serves as the archetype of a target that holds allure for the design of next-generation anti-TB agents. Molecular dynamics (MD) simulations are frequently used to leverage their capacity to efficiently sample the configuration space, which enables in-depth examination of structural stability and biochemical processes in drug discovery, such as ligand binding and other enzymatic processes (Marco & Gago, 2007). Several force fields that include AMBER (Duan et al., 2003), OPLS (Kaminski et al., 2001) or CHARMM (Brooks, 2009), etc., are an integral part of molecular dynamics simulations. It has long been primarily recommended to perform all computer simulations in GPU as much as in CPU due to a retarded transfer of data between GPU and CPU. However, this setup has drastically turned in the direction that favors the use of CPU due to technological advancement in recent times (Krieger & Vriend, 2015). Through MD simulations, crucial ligand determinants such as binding energetics and kinetics of the candidate molecules can be evaluated to facilitate further development in the drug discovery pipeline. Examples of software packages for MD simulations include GROMACS (Hess, 2008), CHARMM, NAMD (Phillips et al., 2020), AMBER (Salomon-Ferrer, Case, & Walker, 2013), etc. To streamline the process of MD simulations, a web-based graphical user interface CHARMM-GUI, <http://www.charmm-gui.org> has become of grandest application for preparing complex biomolecular systems. For a number of MD packages such as GROMACS, CHARMM, GENESIS, Desmond, AMBER, LAMMPS, OpenMM, and CHARMM/OpenMM, CHARMM-GUI is handy in executing input file preparation (Jo et al, 2017). Table 2.2 shows some commonly used MD simulation packages in drug discovery.

Table 2. 2: Some examples of molecular dynamic (MD) packages commonly applied in drug discovery.

Software	Simulation system	Reference
----------	-------------------	-----------



GROMACS	Proteins, carbohydrate, lipids, nucleic acids	Van Der Spoel, D., Lindahl, E., Hess, B., Groenhof, G., Mark, A. E., & Berendsen, H. J. (2005). GROMACS: fast, flexible, and free. <i>Journal of computational chemistry</i> , 26(16), 1701-1718.
CHARMM	Proteins, nucleic acids lipids, carbohydrates,	Brooks, B. R., Brooks III, C. L., Mackerell Jr, A. D., Nilsson, L., Petrella, R. J., Roux, B., ... & Karplus, M. (2009). CHARMM: the biomolecular simulation program. <i>Journal of computational chemistry</i> , 30(10), 1545-1614.
Desmond	Proteins, lipids	<a href="https://www.schrodinger.com/desmond">https://www.schrodinger.com/desmond</a>
AMBER	Proteins, carbohydrates nucleic acids,	Case, D. A., Cheatham III, T. E., Darden, T., Gohlke, H., Luo, R., Merz Jr, K. M., ... & Woods, R. J. (2005). The Amber biomolecular simulation programs. <i>Journal of computational chemistry</i> , 26(16), 1668-1688.
NAMD	Proteins, carbohydrates, lipids, nucleic acids,	Phillips, J. C., Zheng, G., Kumar, S., & Kalé, L. V. (2002, November). NAMD: Biomolecular simulation on thousands of processors. In <i>SC'02: Proceedings of the 2002 ACM/IEEE conference on Supercomputing</i> (pp. 36-36). IEEE.
LAMMPS	Proteins, lipids, carbohydrates, nucleic acids	<a href="https://lammmps.sandia.gov/">https://lammmps.sandia.gov/</a>

Post MD simulations, the trajectories of the generated results will be generated after simulation can be subjected to analysis in terms of RMSD (root mean square deviation), RMSF (root mean square fluctuation), Rg (radius of gyration), Hydrogen bond analysis, and either Molecular mechanics Poisson–Boltzmann surface area (MM-PBSA) or Molecular mechanics generalized Born surface area (MM-GBSA) free energy calculations (Elfiky, 2021; Ibrahim et al., 2020). Ligand-binding stability and equilibrium can be determined by root-mean-square

deviations (RMSD) obtained through MD simulations. RMSF (root mean square fluctuation) can measure the flexibility of the enzyme (receptor) backbone structure, while the radius of gyration represents the compactness of the structure (Ferdausi et al, 2022).

## 2.8 Databases of *Mycobacterium Tuberculosis*

The revolution of data repositories, data mining, and management has motivated researchers to leverage the emerged big data era, transforming the pursuit of TB chemotypes from hype to hope. The protein Data Bank ([www.rcsb.org](http://www.rcsb.org)) (Berman., 2000) contains 185,158 biological macromolecular structures for various proteins, including those of *Mycobacterium tuberculosis*, which are empowering breakthroughs in voluminous *in-silico* drug discovery studies worldwide. The lack of drug(s) effective against TB (Peloquin & Davies., 2021) and the sprouting idea of big data and computational approaches can only mean that more rigorous efforts are needed in TB drug discovery to maximize the advantages provided by these computational tools in the search for novel effective TB drugs and even in drug-repurposing. UniProt (<https://www.uniprot.org/>) is also a critical data repository of comprehensive, high-quality, and freely accessible resources of protein sequence and functional information. Linked to UniProt is Mycobrowser (<https://mycobrowser.epfl.ch/>) (Kapopoulou et al., 2011) and together with TB Database ([http://tbdb.bu.edu/tbdb\\_sysbio/MultiHome.html](http://tbdb.bu.edu/tbdb_sysbio/MultiHome.html)) (Reddy et al., 2009; Galagan et al., 2010), the two are the particular specific data repositories for TB or and *Mycobacterium* protein information. TB database and Mycobrowser house genomic and proteomic data for *Mycobacterium*, such as genes, mycobacterium genomes, gene expression correlation, gene epitopes, and experimental and computational models of TB molecular pathways. In table 2.3 we have compiled some of the drugs approved drugs designed by *in-silico* drug discovery techniques.

Table 2. 3: Examples of drugs approved by *In-silico* drug discovery techniques

Drug	Type of Machine Learning employed	Receptor/Target	Approved
Grazoprevir (Zepatier)	Molecular Modelling and Docking-derived	NS3/4 A protease	2016

	approach (Athanasiou et al., 2019)		
Lifitegrast	Structure-based rational design (Macalino et al., 2018)	LFA-1/ICAM-1	2016
Rucaparib (Zepatier)	Ligand-based molecular modeling (Athanasiou et al, 2019)	Poly (ADP-ribose) polymerase (PARP-1)	2016
Venetoclax	Rational design for BCL-2 (Macalino et al, 2018)	Bcl-2/(BAX/BAK)	2016
Acalabrutinib	SAR (Barf et al., 2017), SBDD and Docking (Abdelhameed et al., 2019)	Bruton's tyrosine kinase	2017
Betrixaban	Molecular Docking (Athanasiou et al., 2019)	Serine protease Factor Xa (fXa)	2017
Brigatinib (Alunbrig)	Docking and Homology Modelling (Athanasiou et al., 2019)	AKL	2017
Copanlisib Hydrochloride	SBDD (Xray crystallography and	Phosphoinositide 3-kinase (PI3K)	2017

	Docking) and LBDD (based on lead scaffold) (Scott et al., 2016)		
Ivosidenib	LBDD coupled with broad SAR profiling and modification (Popovici-Muller et al., 2018)	Isocitrate dehydrogenase-1 (IDH1)	2018
Abemaciclib	Structure-activity relationship studies in conjunction with structure-based design (Gelbert et al., 2014)	Cyclin-dependent kinase	2018
Glasdegib Maleate	SAR (Munchhof et al., 2012)	Hedgehog pathway	2018
Apalutamide	SBDD and SAR (Jung et al., 2018)	Androgen receptor inhibitor	2018
Larotrectinib Sulphate	LBDD with SAR and crystal-binding mode similarity (Jiang et al., 2021)	Tropomyosin-related kinase	2018
Duvelisib	SBDD (Molecular docking, virtual screening) and LBDD (lead optimization	PI3K Kinase	2018

	and SAR) (Jia et al., 2019)		
Lorlatinib	SBDD and physical property-based optimization (Nagasaka et al., 2020; Johnson et al., 2014)	Tyrosine kinase	2018
Erdafitinib	Combined FBDD and SBDD (Murray et al., 2019)	FGFR tyrosine	2019
Darolutamide	SBDD (Docking and MD) (Liu et al., 2018)	Androgen receptor	2019
Entrectinib	SBDD and SAR (Menichincheri et al., 2016)	Tyrosine kinase inhibitor	2019
Remdesivir	Homology Modelling, SBDD (Molecular docking) (Biasini et al., 2014; Elfiky, 2020).	SARS-CoV-2 RdRp	2020

## 2.9 Scaffold-Hopping Technique

Scaffold hopping is a subset of bioisosteric replacement (Brown, 2014), defined by Schneider *et al.* as a technique for identifying isofunctional molecular structures with significantly different backbones (Schneider *et al.*, 1999). Scaffold hopping activity can begin with at least one

compound (starter/parent compound) whose structural backbone is judiciously modified to yield structurally diverse novel molecules. According to Boehm *et al.* (2004), two compounds can be considered novel if their synthetic routines are distinct even if their structures have minor differences. Also, they can be granted different patents. The benefits of scaffold hopping comprehend significant improvement in pharmacokinetic and pharmacodynamics properties, physicochemical properties such as solubility, modification of selectivities & affinities, and ultimately to generate novel patentable leads molecules (Böhm *et al.*, 2004; Yang *et al.*, 2018). Based on the degree of alterations of the starter molecule, Sun *et al.* (2012) classified scaffold hopping into four categories:

### 2.9.1 Heterocycle replacement or 1° Hop:

Heterocyclic replacement involves minor modifications characterized by rearrangement or switching of carbon and nitrogen atoms or even other heteroatoms in a ring. Often yield compounds with a low degree of structural novelty. Figure 2.5 shows good examples of drugs designed through heterocycle replacement. We also see that 1° hop has the most success stories among other hops.

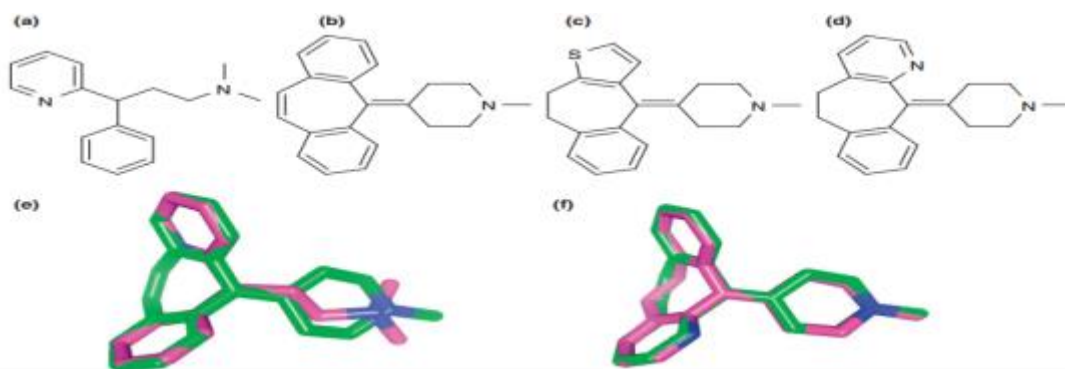


Figure 2. 5: Structures of antihistamine drugs as examples of 1° Hop (a) pheniramine, (b) cyproheptadine, (c) pizotifen, (d) azatadine, (e) superposition of drugs (a) in magenta and (b) in green and (d) in magenta.

### 2.9.2 Ring opening/closure 2° Hop

This type of scaffold-hopping can also be called bond formation and cleavage. Two common examples of ring closure are converting an alkyl chain to cyclohexane or piperidine. In figure 2.6,

the results of the ring closure yielded a bioactive conformation (Hall et al., 2008). Figure 2.7 demonstrates an example of drugs derived through ring opening.

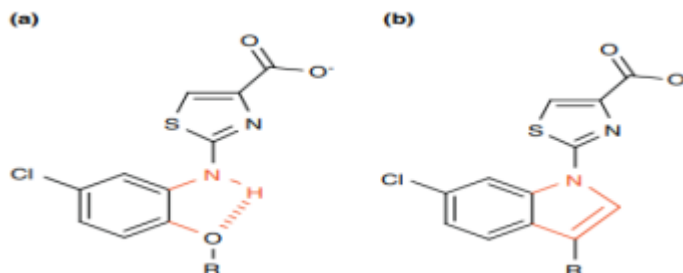


Figure 2. 6: Prostaglandin EP1 receptor antagonists: (a) biaryl amine series and (b) indole series

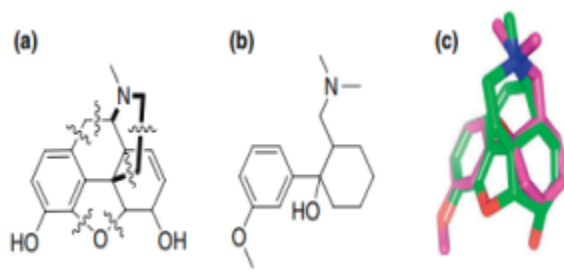


Figure 2. 7: Structures of pain-killing drugs: (a) morphine, (b) tramadol, and (c) 3D

Tramadol (b), a less toxic drug, was designed by breaking six bonds and opening three bonds of a rigid and toxic morphine structure.

### 2.9.3 Peptidomimetics 3° Hop

This involves the replacement of peptide backbones with non-peptic moieties. Assessment of metabolic stability is of paramount importance in drug development, although it is time-consuming, laborious, and costly whether in-vivo or in-vitro (Ryu et al., 2022). The story of peptide-based drugs is, without a doubt, a daunting task due to their poor metabolic stability (Adessi & Soto, 2002). Metabolic stability can be improved by altering the ring size and chirality of the molecule structure and by supplementary structure cyclization (Gajula et al, 2021), of which the scaffold hopping technique can find suitable applications.

## 2.9.4 Topology/Shape-Based Scaffold Hopping 4° Hop

In this type of scaffold hopping, the whole structure of the scaffold is wholly altered but only interactions are preserved. Since it involves extensive modification of the structure, topology/shape-based scaffold hopping presents a tremendous opportunity to achieve the development of novel and patentable drug analogs if attained. However, literature has not yet recorded successful endeavors of new drugs developed through 4° Hop. Table 2.4 is showing four classes of scaffold hopping and their corresponding tools.

Table 2. 4: Classes of Scaffold hopping and examples of some tools used

Class/Scaffold Hop Degree	Software tools Used
1° Hop (Heterocycle replacement)	<ol style="list-style-type: none"><li>1. Mcule (<a href="https://mcule.com/apps/1-click-scaffold-hop">https://mcule.com/apps/1-click-scaffold-hop</a>)</li><li>2. MORPH (Beno &amp; Langley, 2010) and</li><li>3. Recore (Maass, 2007)</li></ol>
2° Hop (Bond formation/cleavage)	<ol style="list-style-type: none"><li>1. Spark (<a href="https://www.cressetgroup.com/software/spark">https://www.cressetgroup.com/software/spark</a>),</li><li>2. alvaBuilder (<a href="https://www.alvascience.com/alvaBuilder">https://www.alvascience.com/alvaBuilder</a>)</li><li>3. CSD (Allen, 2002).</li></ol>
3° Hop (Peptidomimetics)	<ol style="list-style-type: none"><li>1. Recore (Maass, 2007)</li><li>2. CAVEAT (Lauri, &amp; Bartlett, 1994).</li><li>3. Schrodinger <a href="http://www.schrodinger.com/">http://www.schrodinger.com/</a> (accessed July 2022)</li></ol>
4° Hop (Topology/Shape-Based)	<ol style="list-style-type: none"><li>1. SHOP (Bergmann, 2009)</li><li>2. Spark (<a href="https://www.cressetgroup.com/software/spark">https://www.cressetgroup.com/software/spark</a>),</li><li>3. ROCS (Rush, 2005)</li></ol>



## 2.10 Synthesis of Triazine Amine derivative molecule via Amid Coupling

The nitrogen-containing heterocyclic compounds called triazines have sparked great interest in medicinal chemistry research because of their promiscuity and incredibly good binding affinities. Triazine structure is characterized by a benzene ring substituted by three nitrogen atoms. The positions of these nitrogen atoms identify the triazines into three isomeric forms, which are a) 1,2,3-triazine, b) 1,2,4-triazine, and c) 1,3,5-triazine. Compared to benzene, these isomers have much weaker resonance energy and resultantly favor nucleophilic over electrophilic substitution in their reactions (Kumar et al., 2018).

Reminiscing on a plethora of recent research, triazines have proven potential bioactivity with a broad spectrum of pharmacological configurations in the character of anticancer (Cascioferro et al., 2017), anti-tuberculosis (Sunduru et al., 2010), anti-microbial (Kushwaha & Sharma, 2020), etc. In particular, 1,3,5-triazine moiety was labeled a versatile moiety; its scaffold exists in many clinically used drugs, for example, Cycloguanil, Dioxadet, Altretamine, etc. (Kumar et al., 2018). The 1,3,5-triazine isomer can be singled out from the rest of the isomers for its threefold symmetry, which aids in its flexibility to several modifications due to unsophisticated regiochemistry (Zhou et al., 2008).

“Organic synthesis” is the action chemistry of compound-creation activity that mainly pay attention to biologically active small molecules (Schreiber, 2011). In organic synthesis, amide coupling accounts for 16 % of reactions in medicinal chemistry laboratories (Roughley & Jordan, 2011), making it one of the most commonly used reactions. However, the requirement for greener approaches remains pertinent in synthetic organic chemistry. The top six small molecule drugs, the peptidic and all polyamides/ constitute amide-bond-containing drugs in the market (McGrath et al., 2010). Amide coupling requires coupling reagents, and the attributes of a suitable reagent must be considered, such as availability, cost, ease of removal from the matrix, safe, toxicity, etc. (Dunetz et al, 2016). In terms of coupling reagents, this section focused more on carbodiimides and boron reagents.

The performance of every coupling reagent varies depending on the type of reactants (a carboxylic acid and an amine) and other conditions, also looking at factors such as selectivity, yield, epimerization, etc. (Dunetz et al., 2016). Formation of amide should be a straightforward

condensation reaction giving off the water as the waste, but this turns out to be very difficult because of the spontaneous formation of an ammonium salt unless in the presence of a catalyst or other coupling reagents (Valeur & Bradley, 2009; Lundberg et al., 2008; Al-Zoubi et al., 2008). Incorrect stoichiometric proportions of coupling reagents, *in situ* preactivation of the carboxylic activation, is recommended (D'Amaral et al., 2021). Some of the coupling reagents often used are boron reagents, carbodiimides (e.g., DCC, DIC, and EDC), uronium/guanidinium reagents (HBTU), phosphonium salt reagents (BOP ((benzotriazole-1-yloxy)tris(dimethylamino)phosphonium hexafluorophosphate), ethoxyacetylene and dynamite. A reaction similar to scheme one was used to prepare a commercial drug for cancer called efaproxiral.

**Scheme 1: Synthesis of an amide by Boron reagent**

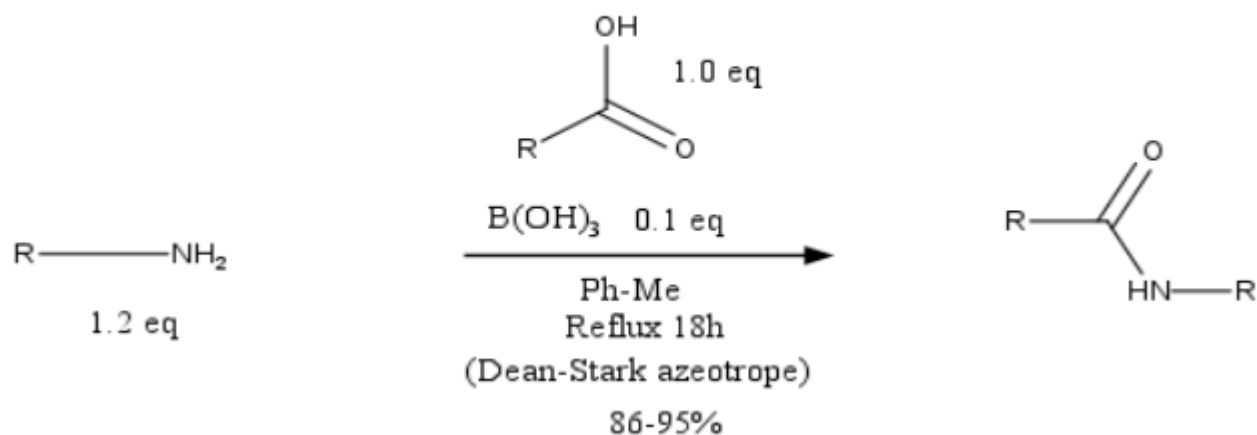


Figure 2. 8: Amide bond formation by boron reagent.

Using the conditions in scheme 1, the amide product can be produced after workup and purification with a yield of about 76% (Ramachandran & Hamann, 2021).

The most popular reaction for the DCC-mediated coupling (Scheme 2) occurs at zero degrees (0 ° C). However, Storace et al. (2002) at Bristol-Myers Squibb had a distinct route. They successfully synthesized human leukocyte elastase inhibitors to treat cystic fibrosis and rheumatoid arthritis.

## Scheme 2: Synthesis of an amide (DCC-Mediated)

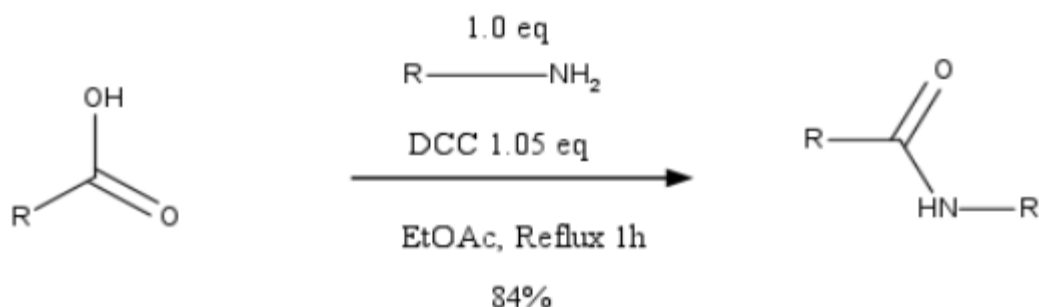


Figure 2. 9: DCC-Mediated synthesis of an amide bond

The challenge with all DCC coupling is forming the by-product called dicyclohexyl urea, which persists and is very difficult to purge from the crude product matrix. However, Storace et al. (2002) removed dicyclohexyl urea by washing it with 2HCl, followed by filtration. Compared to other carbodiimides, another coupling agent EDC is the most commonly used carbodiimide because it renders the dicyclohexyl urea by-product water-soluble making it easy to purge, but it is costly. Therefore its use is limited (Dunetz et al, 2016).

### 2.11 Justification of the Study

Reminiscing on a plethora of recent research, triazines have proven potential bioactivity with a broad spectrum of pharmacological configurations in the character of anticancer (Cascioferro et al., 2017), anti-tuberculosis (Sunduru et al., 2010), anti-microbial (Kushwaha & Sharma, 2020), etc. In particular, 1,3,5-triazine moiety was labeled a versatile moiety. Its scaffold exists in many clinically used drugs, for example, Cycloguanil, Dioxadet, Altretamine, etc. (Kumar et al., 2018). The 1,3,5-triazine isomer can be singled out from the rest of the isomers for its threefold symmetry, which aids in its flexibility to several modifications due to unsophisticated regiochemistry (Zhou et al., 2008). Among several *Mycobacterium tuberculosis* potential drug targets, Dihydrofolate Reductase (DHFR), a key enzyme involved in folate metabolism, is an essential target in which its inhibition results in mycobacterial cell death. Several successful antifolates against infectious diseases exist, but none have been developed to combat tuberculosis. Previously, two potent anti-

tuberculosis phenotypic hits belonging to the tetrahydro-1,3,5-triazine-2-amine (THT) family were predicted and confirmed as inhibitors of *Mtb* DHFR. Therefore, optimizing the confirmed hits would lead to a new class of anti-tuberculosis compounds that are target specific and highly potent.

## **2.12 Objectives of the Study**

### **2.12.1 Main Objective**

- To design and synthesize tetrahydro-1,3,5-triazine-2-amine derivatives as potential inhibitors of *Mtb*-DHFR enzyme.

### **2.12.2 Specific objectives**

1. To design through computational hit-to-lead optimization of **two** tetrahydro - 1, 3, 5-triazine-2-amine derivatives using *Mtb* - DHFR target.
2. To determine the potential anti-TB lead compounds (*Mtb*-DHFR inhibitors) from the generated compound library and prioritize them for synthesis through SBVS and ADMET analysis.
3. Molecular Dynamics Simulation of tetrahydro - 1, 3, 5-triazine-2-amine derivatives lead compounds to validate Structure Based Virtual Screening (SBVS) results.
4. Synthesis of tetrahydro - 1, 3, 5-triazine-2-amine derivatives lead compounds.

## CHAPTER 3

### MATERIALS AND METHODS

#### 3.1 Research Design

This study embraced an amalgam of *in-silico* and synthetic chemistry in the Chinhoyi University's computer and chemistry laboratory. Chief among the applied concepts in this study is the computational medicinal chemistry, pharmacology, bio and chemoinformatics, and all its *in-Silico* drug discovery tools. The schematic display of the study design is shown in figure 3.1.

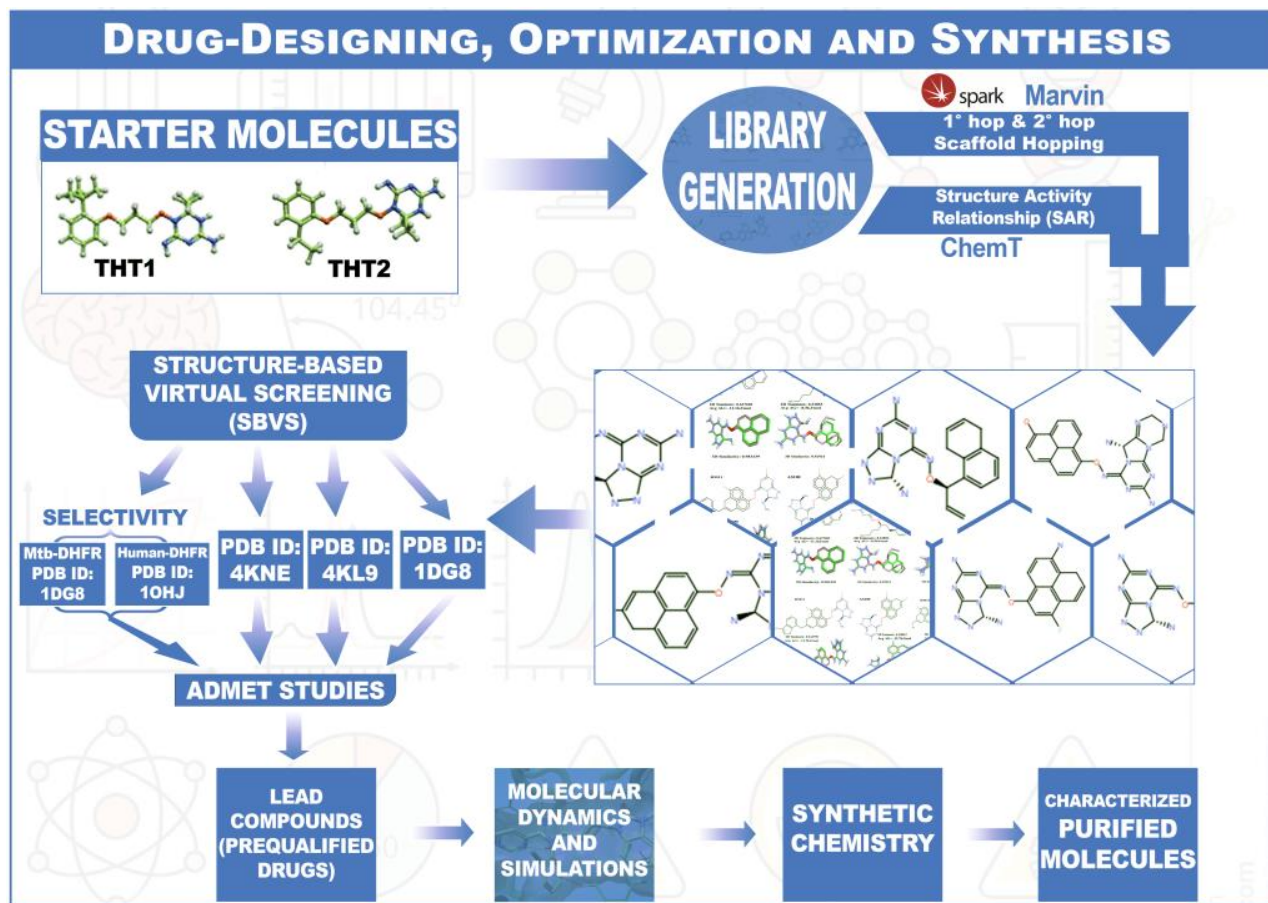


Figure 3. 1: Summary and workflow of the computational medicinal chemistry and organic synthetic chemistry concepts adopted for the design and synthesis of *Mtb*-DHFR inhibitor compounds.

## 3.2 Computational Designing of Compounds

In order to satisfy the first objective, we implemented two main techniques which were structure activity relationship (SAR) and 1° & 2° scaffold-hopping. After that we implemented compound data curation of the resulted compound library that had been generated.

### 3.2.1 Structure-Activity relationship (SAR)

Structure-Activity Relationship is a concept in which drugs/ligands impart their biological activity through the chemical functionalities i.e. groups or atoms within their structures. From this principle, we employed ChemT (<http://www.esa.ipb.pt/>) (Abreu et al., 2011) software to generate a custom-made template-based chemical library at the heart of hit-lead optimization. ChemT requires a template molecule to be inputted for library build-up to launch and in this regard, it is ideal to use an approved TB drug such as isoniazid. **THT1** and **THT2** were used as starter molecules in the recommended SMILES format. These two potent hits belong to the tetrahydro-1, 3, 5-triazine-2-amine (THT) family, and were predicted and confirmed as *Mtb*-DHFR inhibitors by Mugumbate et al. (2015). During the Structure-Activity relationship, we would have some functional groups of choice judiciously removed, added, or modified on selected designated R-positions on the starter molecule. This allowed for the identification of crucial substituted R-positions plus functional groups that are essential to the imparted desired biological activity (Smeyne, 2020). The 3D crystal structures of DHFR which included PDB ID: 4KNE, 4KL9, and 1DG8 were utilized in virtual screening using AutoDock Vina in PyRx. Next, an analysis of the virtual screening was performed with an eye to finding and correlating the binding interactions of the 3D structure of the ligands to their corresponding binding affinities.

### 3.2.2 Scaffold-Hopping

Scaffold-hopping was performed to generate a compound library with new chemistry and novel lead series with modified selectivity, improved efficacy, and the best possible affinities with respect to interactions of ligand-DHFR complexes. Again the active THT1 and THT2 were parent molecules in which their central core structures were modified into novel chemotypes. There are four major classes of Scaffold-hopping: 1. Heterocycle replacement (**1°hop**), 2. Ring-opening, and closure (**2°hop**), 3. Peptidomimetics (**3°hop**), and 4. Topology-based hopping (**4°hop**) (Sun et al.,

2012), depending on the degree of change associated with the parent molecule. We focused in this study on the first two types among the four categories which were **1°hop** scaffold-hopping, and ring-opening and closure also described by Sun et al. (2012), as **2°hop**. The criteria for choosing these two techniques was based on the successful stories associated with the two and the synthetic accessibility (ease of synthesis) of the compounds designed by these two methods. In the 2°hop concept, the parent molecules were transformed into rigid structural analogs by ring closure or opening, either by converting an alkyl chain to cyclohexane, or piperidine (Evelyn et al., 2010), or through ring fusion. Ring closure can impart changes in flexibility by regulating the total number of rotatable bonds and subsequent activity of the resulting compound to a better degree of novelty as well as boosting absorption and membrane permeability (Vieth et al, 2004). The Mucko scaffold definition was also used to design novel compounds with the aid of computer tools by removing all the R-groups (substituents) while retaining the rings and the linker between the triazine moiety and the non-triazine moiety. After modifying the central core structure of the scaffold, some R-groups/substituents were re-introduced to the entire novel compound to grow or enhance some desired physicochemical properties. During analysis, the trade-off between the structural novelty of the newly designed analog and the desired lead-like compound was always considered. The scaffold hopping technique sometimes requires chemical knowledge of starter molecules (Bajorath, 2017) so the parent molecules THT1 and THT2 were chosen on account of their confirmed bioactivity against *MtbDHFR*. The scaffolds of parent molecules typify a broad spectrum of structural relationships which can extend beyond chemically similar compounds to even structurally unrelated ones. Synthetic feasibility was also considered in this expedition since molecule design was done with an eye to creating lead or potential drugs that are synthesizable.

Growing our library, a considerable number of molecules were designed and generated by ‘Spark’ UK; <http://www.cresset-group.com/spark/>; program software packages (Cheeseright et al., 2006), through R-group replacement or scaffold-hopping.

### 3.2.3 Library Molecular Structure Curation

The generated library especially most of the dataset created from ChemT, and a few others designed by Marvin Sketch were subjected to molecular structure curation and standardization since some were chemically or structurally wrong. Fortified with ten predefined checkers

alvaMolecule software ([www.alvascience.com](http://www.alvascience.com)) version 1.0.4, 2020, could successfully inspect and identify erroneous structures and conjointly filter specific structural features. In addition, the alvaMolecule was used to perform verification on features such as multiple structures, unusual valence, and aromaticity while standardizing on chirality, isotopes, conversion of unusual covalent bonds to ionic bonds, and the addition of charges to quaternary nitrogen atoms (N).

### 3.3 Structure-based Virtual Screening (SBVS) and ADMET analysis

The second objective was achieved through SBVS by molecular docking of the library compounds against the *Mtb*-DHFR enzyme. Under this objective, ADMET studies were also carried out for the exploration of the drug-like properties for the whole compound library. During execution of this objective, we initiated activities such as, macromolecular/protein structure preparation, ligand preparation, validation of the docking protocol, and molecular docking against both *Mtb*-DHFR and *human*-DHFR for the purposes of selectivity studies. Under all these investigations, every compound's attributes was bench marked against the chosen reference ligands INH and NSC-339679 whose structure is in figure 3.2.

### 3.4 Macromolecule Structure Preparation

It was imperative to utilize more than one crystal structure in the interim of virtual screening to maximize the probability of prequalifying a better or potential drug candidate since only the compounds with desired attributes against all three crystal structures will be promoted to the next stage. Three crystal structures of *Mtb*-DHFR enzyme proteins of PDB IDs: 4KNE, 4KL9, and 1DG8 with resolutions 2.0 Å, 1.39 Å and 2.0 Å respectively were retrieved from RCSB Protein Data Bank (PDB, [www.rcsb.org](http://www.rcsb.org)). For selectivity studies against human DHFR, another protein receptor PDB ID: 1OHJ with a resolution of 2.5 Å was used. The receptors were imported into Biovia Discovery 2021 (<https://3ds.com/products-services/biovia/products>) where the attributes of their binding sites e.g. the grid dimensions, were identified before the elimination of ligand groups. Subsequently, the water molecules were removed followed by the removal of heteroatoms, and the deletion of other chains (where there was more than one) to remain with the main chain. All receptor proteins were saved in the PDB format. The receptors were then imported into AutoDock Tools 4.2 (Morris et al., 2009) to complete this successive target preparation by adding polar



hydrogens, computation of Gasterger and Kollman charges, and assigning AD4 Type before saving all receptor proteins/targets in pdbqt format.

### 3.5 Preparation of Ligands

All compounds in the library were converted to the SDF format preferred by PyRx. Energy minimization was performed in PyRx v 0.8 (<http://pyrx.sourceforge.net>) (Dallakyan & Olson, 2015) initially using the universal force field (UFF) and subsequently using the Ghemical force field which was also responsible for geometry optimization (Hutchison et al, 2011). After the addition of polar hydrogens and charges, the ligands were converted to the pdbqt format with the help of the Open Babel toolkit in PyRx.

### 3.6 Reference Ligands

Hong et al. (2022), reported the discovery of a very potent novel inhibitor of *Mtb*DHFR enzyme, NSC-339579 (1,3-diamino-7H-pyrrol[3,2-f]quanzoline (PQZ)). The compound (figure 3.2) had a very good inhibitory activity possessing an IC<sub>50</sub> of 6 nM *in vitro* against *Mtb*DHFR. Therefore, this study employed NSC-339579 and isoniazid (INH) as reference ligands to serve as a blueprint for prequalification of potential candidate anti-TB compounds. We used isoniazid on the basis that it was an anti-TB approved drug, but we had no information that it target *Mtb*DHFR, therefore we decided to include a known potent *Mtb*DHFR inhibitor, NSC-339579. Following Structure Based Virtual Screening (SBVS), all ligands which had the binding affinity similar or greater than that of NSC-339579 could be regarded as good and promising compounds and would be promoted to the next stage of the study.

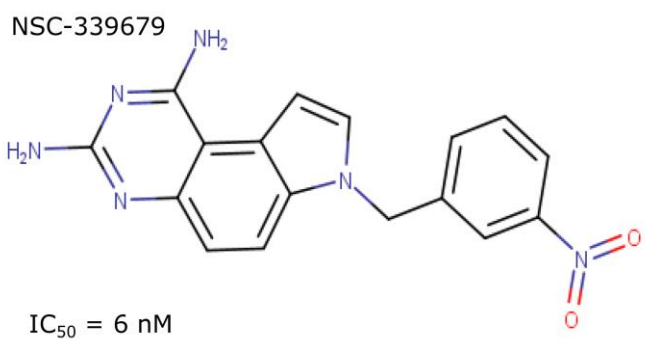


Figure 3. 2: Structure of NSC-339679 compound used as a reference ligand

### 3.7 Virtual Screening against *Mtb*-DHFR and *h*-DHFR

The services of AutoDock vina in PyRx software were prescribed at this juncture to perform virtual screening of 1 700 compounds against *Mtb*-DHFR (PDB ID: 4KNE, PDB ID: 4KL9, and PDB ID: 1DG8). Ultimately the compounds were subjected to filtration by Lipinski's rule of five to a total of 520 ligands. To identify selectivity, the ligands with the best affinities and activities against *Mtb*-DHFR were pre-qualified (50 candidate ligands) and screened against the *h*-DHFR (PDB ID: 1OHJ) receptor. Conversely, the task could determine those small molecules that favor inhibition of *Mtb*-DHFR contra to *h*-DHFR.

### 3.8 Validation of the Docking Protocol

We used the proteins PDBs of PDB ID: 4KNE, PDB ID: 4KL9, PDB ID: 1DG8, and PDB ID: 1OHJ, and their corresponding cocrystallized ligands in the validation of the docking protocol. The co-crystallized ligands were removed from their binding pockets and re-docked on the same grid parameters. Following re-docking, regeneration of their original interactions and poses confirms the reliability of the docking protocol. Ultimately superimposition of the extracted co-crystallized ligands and the docked poses should confirm validation (figure 4.6).

### 3.9 ADMET Studies

The pre-qualified ligands (potential candidates) were subjected to ADMET analysis using alvaDesc software from alvascience. This is a very important *in-silico* predictive study, which could reduce the costs and time spent on in-vivo experiments. The software alvaDesc tools calculated physicochemical properties and molecular descriptors such as molecular weight (Mwt), two LogP models which are according to Moriguchi and Ghose-Chippen octanol-water partition coefficient, Log S or ESOL (Estimated Solubility) relating to the water solubility of a drug, Lipinski rule of five (RO5) for an orally administered drug in humans, Verber's rule (Verber et al., 2002) of molecular bioavailability, and other indicatory lists of drug-like and lead-like alerts (Mauri, 2020). The parameter called the quantitative estimate of drug-likeness (QED) which is calculated by alvaDesc is of vital importance when selecting pre-qualified molecules in the early stage of drug discovery (Mauri, 2020). We also looked at other physicochemical properties such

as synthetic accessibility (SA), topological polar surface area using N and O atom polar contributions (TPSA N, O) for polarizability assessment, and Molar Refractivity (MRcons).

Moreover, the research also considered chirality studies determining the number of chiral centers of the designed compounds using alvaDesc program, and other toxicity assessment aspects such as the blood-brain barrier (BBB) and gastrointestinal absorptivity using the BOILED EGG technique via the SwissADME web tool.

### **3.10 Validation of the molecular docking results**

Objective three (3) sought to prove the validity and accuracy of the results obtained by molecular docking simulations.

#### **3.10.1 Molecular Dynamics Simulations**

Molecular Dynamics (MD) Simulations have been conducted through GROMACS 2022 software packages supported by NVIDIA GeForce GT 730 graphics card in Linux Ubuntu 22.10. Solvent molecular dynamics was executed to investigate molecular docking solutions further. The employed procedure for Molecular Dynamics (MD) Simulations has been recommended and practiced by many researchers including Keretsu, Bhujbal, & Cho (2020) research group.

Four of the top 20 prequalified ligands from molecular docking simulations and ADMET studies have been selected for Molecular Dynamics (MD) simulations. The subject of classical MD Simulations was so that it would be possible to study and understand the dynamic binding effects on the structural stability and conformational flexibilities of the selected triazine derivative DHFR-ligand complexes. The parameters of the ligands were set using the general amber force field (GAFF) (Wang et al., 2004) by the Acypye program (Da Silva & Vranken., 2012). The GROMACS CHARMM general force field (Vanommeslaeghe et al., 2010) and CHARMM36 force-field (Huang & MacKerell, 2013), were used for the generation of both the Protein topology and coordinate files. The protein–ligand complex was contained in a dodecahedron and solvated with TIP3P water. The solvated system was neutralized by the addition of counter ions i.e. chloride ions, subsequent rapid energy minimization was performed to the steepest decent at 1000 steps with position restraint on DHFR – ligand complexes. Next the two-phase ensemble 50000 ps equilibration for a restrained constant number of particles, volume, and temperature (NVT) was

executed together with a constant number of particles, pressure, and temperature (NPT) ensemble for one ns equilibration respectively. Ultimately, unrestrained 50 ns production simulations were performed for the systems with the temperature maintained at 310 K and 1 bar. Post MD 50ns production run, we used system trajectory to carry out structural analysis in which the root mean square deviation (RMSD), root mean square fluctuation (RMSF), radius of gyration (Rg), and hydrogen bonds analysis were determined. Plotting of individual graphs was performed in xmgrace (Turner, 2005), and also in Microsoft excel.

### 3.11 Synthesis

In the final objective (objective 4), two compounds from the prequalified ligand compounds were selected for synthesis based on their considerable drug-like properties and their synthetic accessibility (easy of synthesis).

#### 3.11.1 Synthesis of tetrahydro-1,3,5-triazine-2-amine derivatives

This objective was carried out in the Chinhoyi University of Technology chemistry laboratory. Materials and reagents which include synthesis glassware, silica gel G TLC plates of 2 mm thickness, chemicals (synthesis chemical scaffolds), and solvents were bought from Aldrich and Enamine respectively. Scheme 3 in figure 3.3 shows the general process used during synthesis.

Scheme 3: DCC-Mediated Amide Coupling

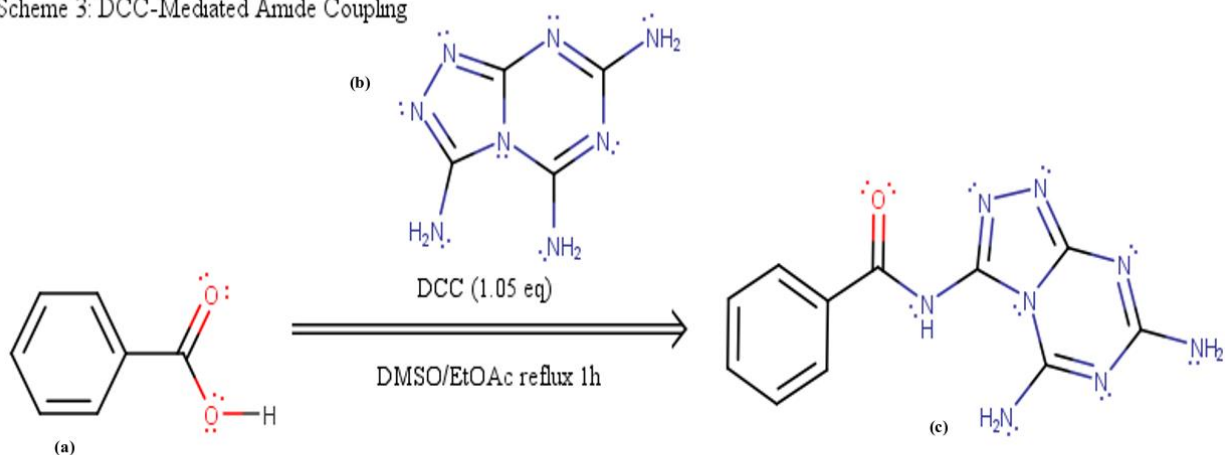


Figure 3. 3: DCC-Mediated Amide Coupling

### 3.11.2 Synthesis: DCC-Mediated Amide Coupling

Dunetz et al. (2016) have reported this method (figure 4.16) using ethyl-acetate (EtOAc). At this juncture, we tried to apply this method, but, the choice of solvent was challenging in this objective because triazine scaffold (a) could not dissolve in many solvents except DMSO, which was also problematic in the later stage of this reaction because of its higher boiling point (189°C).

Several solvent combination mixtures were tried in order to find the best solvent or solvent mixture that could dissolve triazine scaffolds. Consequently, triazine scaffold (a) was discovered to be a sparingly soluble solvent 1:4 solvent mixture of ethyl acetate (EtOAc), while triazine scaffold (b) was completely soluble in the same solvent mixture. However, continued permutations of trials were discouraged by limited resources because only one gram (1g) of each chemical scaffold was purchased. As a result, DMSO and nBuOH - EtOAc mixture (1:4) was used.

### 3.11.3 The general procedure for the carbodiimide coupling using DCC

Figure 3.4 below is the illustration of the reaction mechanism. The prepared triazine amine (b) was added to a prepared carboxylic acid (benzoic acid) (a) in a 100ml round-bottomed flask containing 40 ml DMSO as a solvent at 50°C. The formation of an ammonium salt was anticipated. The progress of the reaction was monitored using silica gel G TLC plates of 2 mm thickness. After 15min a solution of DCC was added to the reaction matrix, and the temperature was raised to the range of 75-80°C during reflux. A sweet/fruit-smelling odor evolved and confirmed successful formation of an ester (shown in figure 4.10) which gave optimism for the successful progress of the reaction. After refluxing for 3h the solution was cooled at room temperature. Subsequently, 2HCl was prepared in a 25ml volumetric flask, and 5 drops were added to the cooled reaction matrix followed by gravity filtration to purge the by-product dicyclohexyl urea (DCU) using fluted filter paper.

Scheme 4: DCC-Mediated Amide coupling mechanism

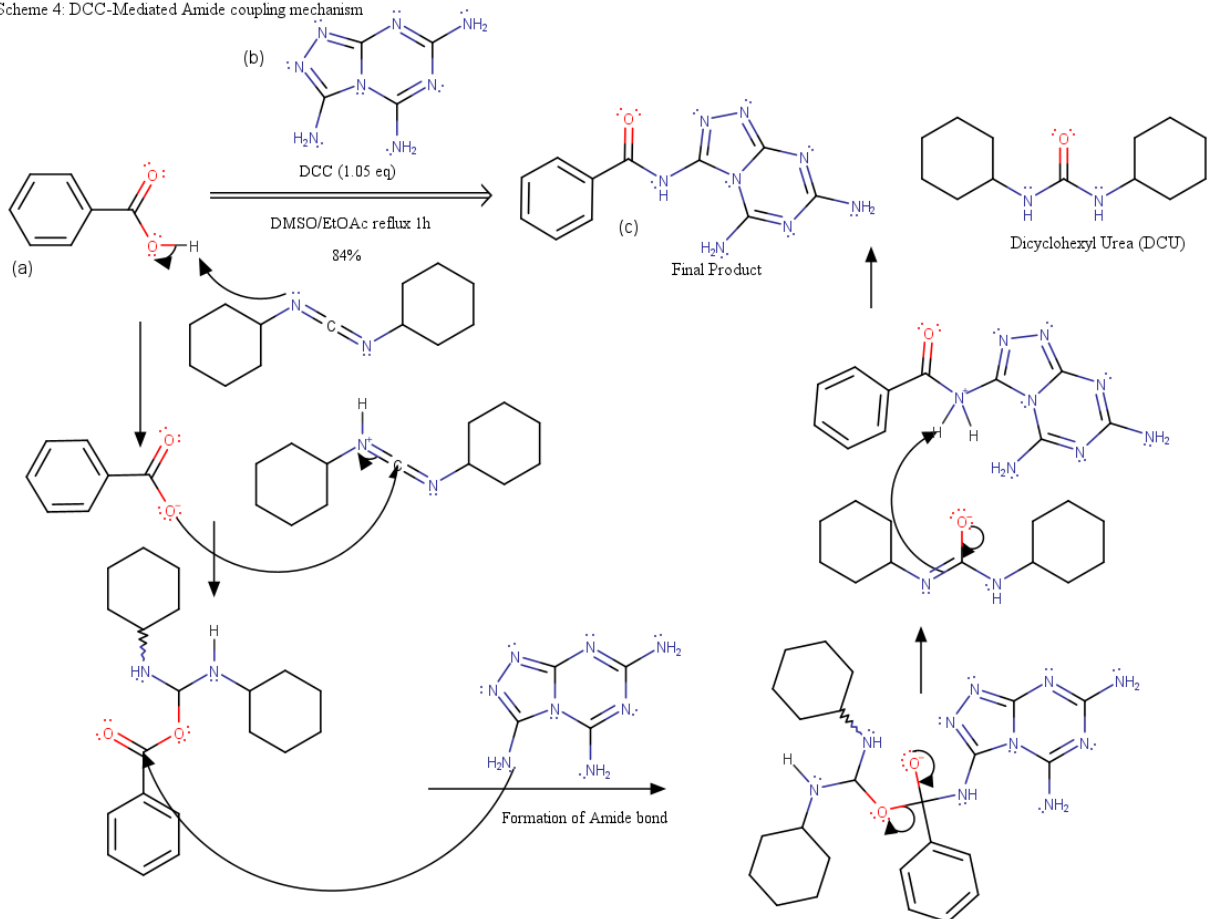


Figure 3. 4 Scheme for the DCC-Mediated Amide coupling reaction mechanism

### 3.11.4 Reaction Workup

At first, the crude product was washed with hexane in a separating funnel resulting in immediate separation into two distinct layers since hexane and DMSO are immiscible and have a wide gap in polarity and density. We avoided an aqueous workup because water and DMSO are miscible and polar solvents. Instead, DMSO and hexane were the chosen solvents during washing and extraction. The non-polar constituents would extract into hexane during constant shaking and venting leaving the polar (final product) in DMSO. The DMSO portion (bottom of the separatory funnel) was purged into a clean round bottom flask. Four (4) hour attempts to remove DMSO by concentrating in a rotary evaporator proved a futile exercise owing to the high boiling point of DMSO (189°C) regardless of the high-temperature (120°C) water bath. Alternatively, the DMSO extract was poured into a separatory funnel and washed with distilled water although DMSO and

water are miscible, polar, and both have high boiling points. This was a valid scientific application because most organic compounds do not dissolve in water. As a result, the organic compound formed a precipitate in water, and excess was added to make the solution more anti-organic to facilitate further precipitation. The precipitate was filtered off by gravity filtration using fluted filter paper. Following this aqueous workup, the purified product, a white solid amide, was dried.

The reaction with DMSO as solvent was attempted several times (3 times) in an effort to form crystals until the realization that crystallization is difficult to form in DMSO (Wu et al., 2014), however, the needle-like shaped crystals eventually appeared in the Erlenmeyer flask after four days.

A similar reaction was carried out in the n-BuOH - EtOAc solvent mixture (1:4) in which 0.1g of the triazine solid was reacted with 0.037g of benzoic acid in 0.1g DCC catalysts. The reaction mixture was refluxed for 3 hours and after 1 hour the sweet-smelling odor filled the laboratory for a period of about 30 minutes. After refluxing, the reaction vessel was cooled and 5 drops of 2M HCl were added, followed by gravity filtration using a fluted filter paper to remove the DCU unwanted-product. However, TLC analysis showed 2 spots confirming the possibility of the presence of DCU in our desired product. As a result, we carried out column chromatography whereby TLC analysis was performed on the collected six fractions.

## CHAPTER 4

### RESULTS AND DISCUSSION

#### 4.1 Library Generation Results

Rational drug discovery methods were instrumental in the generation of a library of compounds, **2°hop** Scaffold hopping, and structure-activity relationship (SAR) were specifically used. The application of these two techniques i.e. **2°hop** Scaffold hopping, and structure-activity relationship depended on two known 1,3,5-triazine based bioactive molecules, THT1 and THT2 previously predicted and confirmed as antituberculosis phenotypic hits. Table 4.1 presents the compounds that were designed using ChemT software. Data curation was implemented on the generated compounds datasets and subsequently, alarms were raised by the alvaMolecule software program on 37 erroneous chemical structures on the basis of aromaticity and unusual valence (Figure 4.1) 37 erroneous structures detected by checkers in alvaMolecule software.

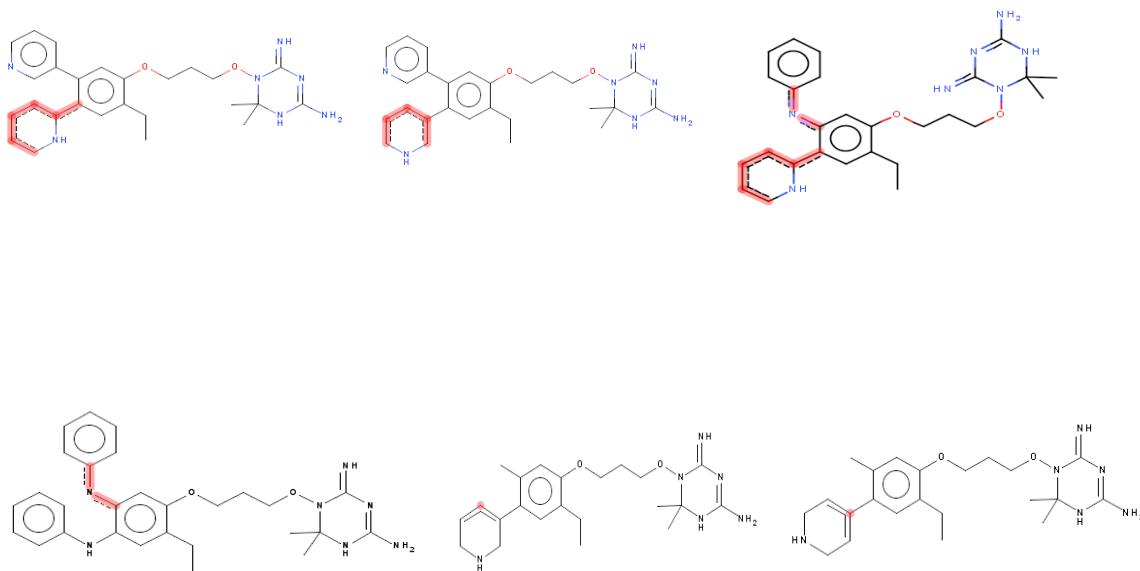
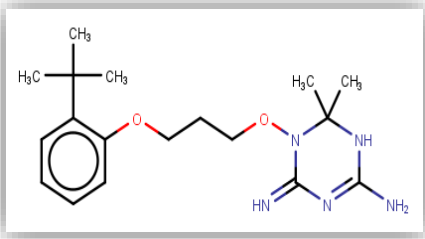
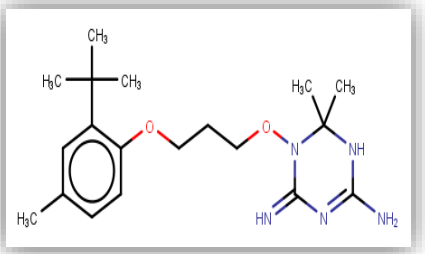
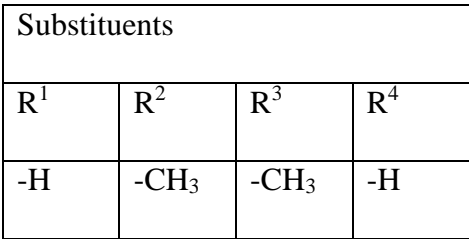
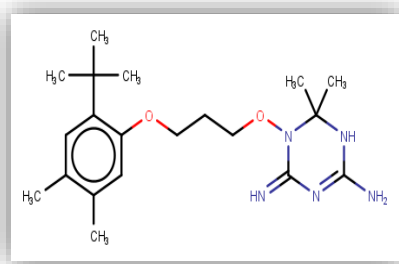


Figure 4. 1: The illustration of typical erroneous issues resolved by molecular structure curation.



Table 4. 1: Structure-Activity Relationship studies

#	Name	Analog Structure	Receptor-Ligand Binding Energy ( $\Delta G$ , Kcal/mol)		
			4kne	4kl9	1dg8
1	THT1	Substituents	-7.8	-8.4	-8.5
		R <sup>1</sup>			
		R <sup>2</sup>			
		R <sup>3</sup>			
					
2	BTHT1	Substituents	-7.7	-8.4	-8.8
		R <sup>1</sup>			
		R <sup>2</sup>			
		R <sup>3</sup>			
					
3	CTHT1	Substituents	-8.4	-9.0	-8.8
		R <sup>1</sup>			
		R <sup>2</sup>			
		R <sup>3</sup>			
					



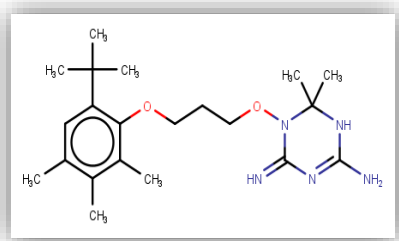
Substituents			
R <sup>1</sup>	R <sup>2</sup>	R <sup>3</sup>	R <sup>4</sup>
-CH <sub>3</sub>	-CH <sub>3</sub>	-CH <sub>3</sub>	-H

-8.3

-9.2

-9.1

#### 4 DTHT1



Structure-activity relationship studies were conducted to identify analogs with higher binding affinities i.e. lower binding energies for the DHFR receptor. This concept of the Structure-Activity Relationship was able to promptly establish positions on THT1 and THT2 structures where judicious structural modifications can translate to changes in various properties such as in particular binding affinity. As compared to electron-donating groups the electron-withdrawing groups such as  $-\text{COCH}_3$  substituents located on phenyl rings are known to be proficiently contributing to antibacterial and or antimicrobial activity (Yadav & Ganguly, 2015).

Results in figure 4.1 showed that introducing a  $-\text{COCH}_3$  group on compound FTHT1 significantly improved binding energy. The electronegative oxygen atom in a  $-\text{COCH}_3$  was involved in two convectional hydrogen bonds with GLY A: 18 and ASP A: 19. The triazine moiety was also involved in four hydrogen bond interactions, i.e. two H-bonds between ASP A:27 with the  $-\text{NH}$  on the para and meta position, and the other two on ILE A:5 and ILE A:94. It was also observed that the substitution of a  $-\text{CH}_3$  functional group on the meta position of BTHT1 had adverse effects

in terms of binding energy for both 4kne and 4kl9 where a decline in binding affinity was prominent. This, therefore, means that substitution for  $-CH_3$  on that ring position should be disregarded because electron-donating groups are associated with poor inhibition and poor activity. In their study, Yadav & Ganguly (2015) postulated that electron-withdrawing groups might be involved in lowering MIC values. Based on the similarity property principle, we can consider the similarity of two compounds based on their shape and ability to form the same interactions (Silakari & Singh, 2021). Using the same principle on compounds THT1 and BTHT1, substituting only one  $-CH_3$  group led to a complete change in conformation and formed no common interactions in the process.

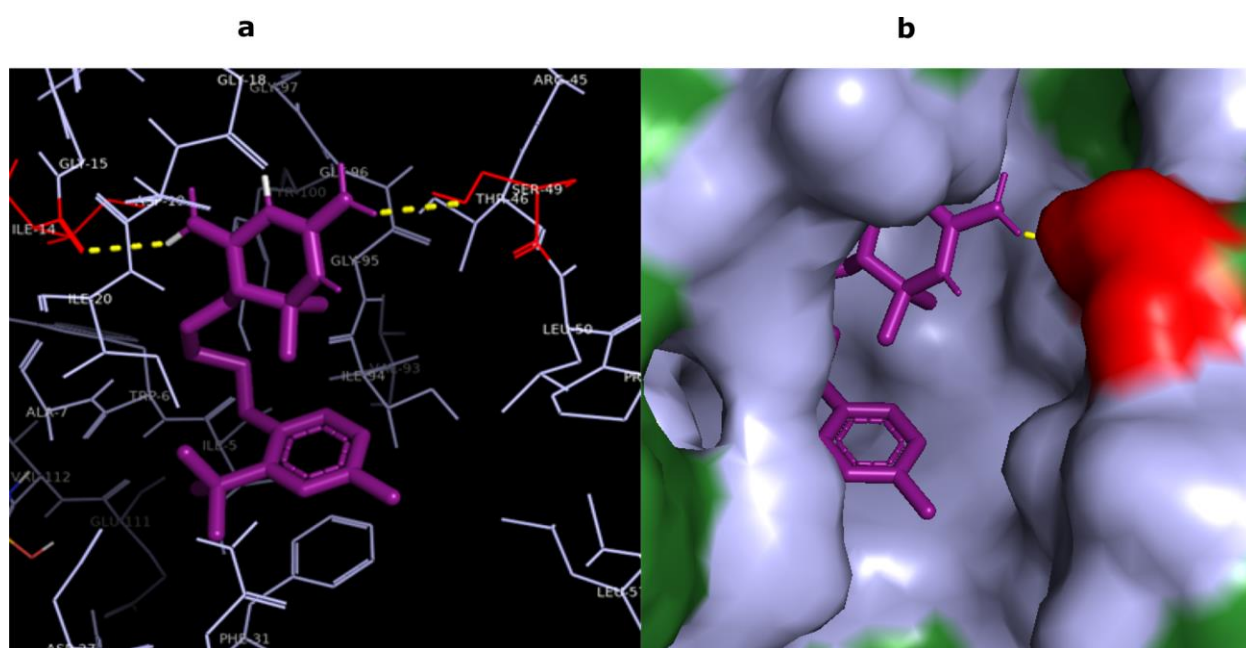


Figure 4. 2: 4kne-BTHT1 interactions with amino acids of the binding pocket. (a) 3D- interactions (b) 3D surface representation, ligand (purple), polar interactions (ILE: 14 & SER: 49), polar contacts (red), non-polar contacts (light green),

It was observed that generally, there was complete independence between chemical structure and the corresponding receptor-ligand interactions. At the end of our structure-activity relationship studies, we realized that many compound structures in the library had to violate the Lipinski rule of five to acquire a considerable boost in binding energies. This was observed in compounds OTHT2, PTHT2, QTHT2, and RTHT2 (Table 4.1) that had molecular weight greater than 500.

## 4.2 Compounds designed by Scaffold Hopping

Using 1° and 2° scaffold hopping concepts (Sun et al., 2012), we generated compounds that constituted 1587 of the 1700 library capacity. We initiated 1° hop presented in figure 4.3 which is characterized by minor modifications i.e., swapping of carbon atoms with nitrogen atoms on the aromatic ring or replacement with other heteroatoms, in particular oxygen atom(s).

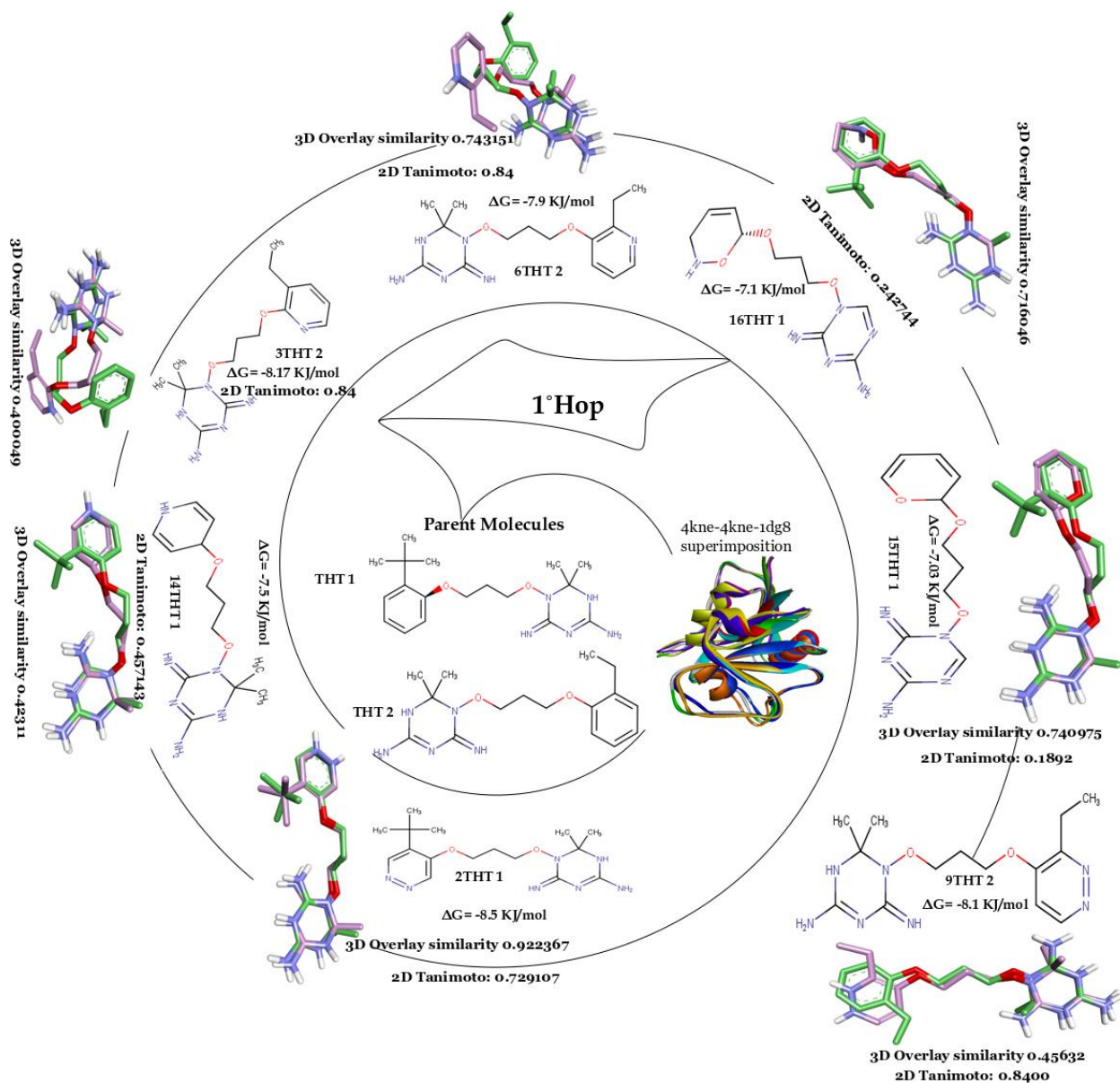


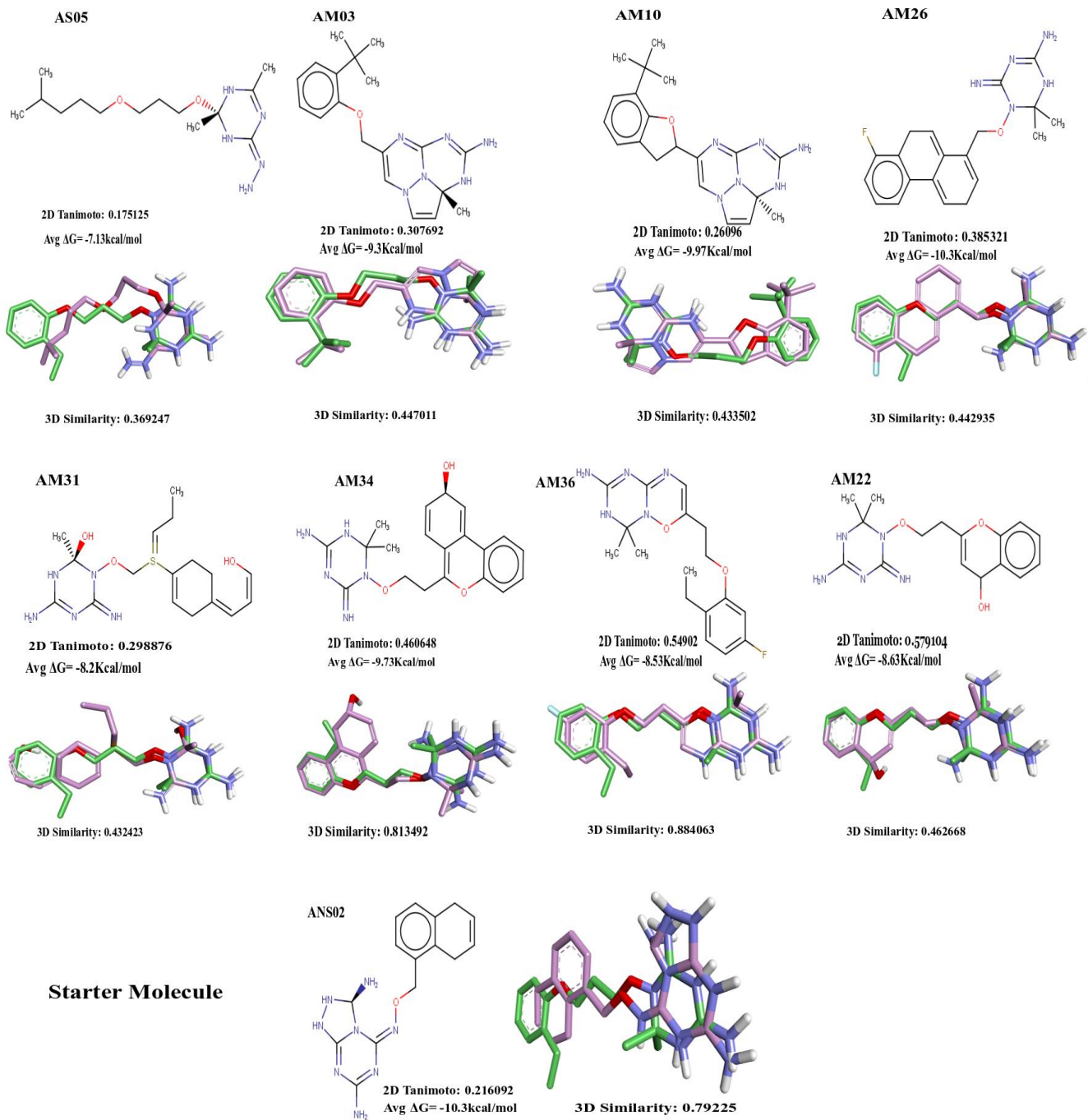
Figure 4. 3: 1° target-based Scaffold Hopping technique using THT1 and THT2 as the starter molecules, 2D/3D similarities of the starter molecules to the product molecules, and virtual screening of the daughter analogs to determine the binding energies imparted by alterations on each scaffold. The displayed  $\Delta G$ -value represents the average docking score obtained against Mtb-DHFR macromolecular receptors PDB ID: 4kne, 4kl9, & 1dg8.

The variations in similarities in terms of 2D & 3D structural forms of all ligands to their parent/starter molecules suggest that there are some catalytic features in 3D terrain that a molecule cannot possess or show in 2D form. This observation was in agreement with the study by Gohlke et al. (2015) in which they reflected the presence of some untraceable similarities in the 3D landscape but can be absent or difficult to detect in 2D similarity comparisons. A small dataset of 19 compound analogs in figure 4.3 is the product of 1° scaffold hopping. The assigned values of changes in Gibbs free energies ( $\Delta G$  (Kcal/mol)) are the average binding energies yielded by subsequent molecular docking during virtual screening against reportedly chosen three crystal structures of the *Mtb*-DHFR enzyme target. The most significant docking score from the entire dataset was found to be -8.5 kcal/mol held by compound 2THT1. Regarding similarity, 2THT1 was similar to its parent molecule THT1 in 3D (0.922367) compared to its 2D Tanimoto similarity (0.729107). Judging on the similarity scores and docking scores from figure 4.3, the greater the similarity, the greater the binding energy, hence biological activity. We can deduce that the activity landscape was linear to the compound similarity, especially in 2D. Relevant examples include compounds 3THT2, 2THT1, and 9THT2, etc.

Similarly on the other hand, compounds that were dissimilar to their parent molecules in either 2D or 3D showed poor activity to *Mtb*-DHFR i.e., low binding energies. In this judicious task of scaffold hopping, we were not much concerned about the activity of an individual scaffold. Still, meticulous attention was paid to the change in biological activity imparted by the entire compound. During virtual screening with three different macromolecular crystal structures, it was imperatively observed that the DHFR enzyme protein could handle and feasibly interact with structurally diverse molecules.

#### **4.2.1 Two Degree (2°) Scaffold-Hopping**

To minimize and curtail the deficiencies of heterocycle replacement i.e., 1° Scaffold-Hopping in figure 4.3, we implemented 2° scaffold-hopping, a technique characterized by extensive ring closure and opening on the non-triazine moiety. Figure 4.4 shows examples of molecules generated by ring closure and opening from across the least to the top-predicted chemotypes.



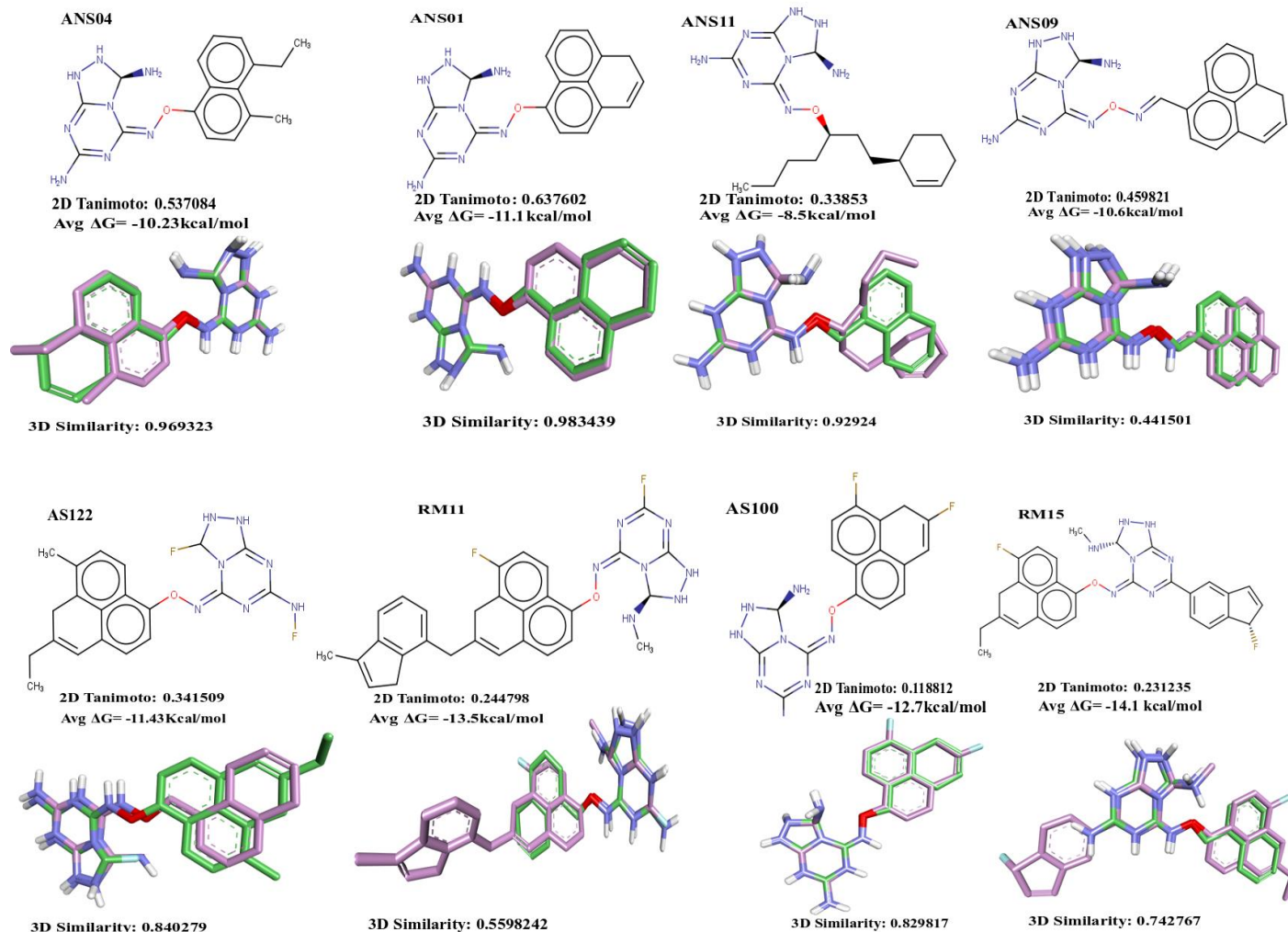


Figure 4. 4: Two degree, 2° Scaffold-Hopping product molecules, 2D and 3D Similarities (dark green=starter molecule, pink = product molecule), and Virtual Screening of 1-3-5-Triazine derivative molecules.

From molecule AS05 to AM22, we used THT1 & THT2 as starter molecules to compare the 2D & 3D of the generated compounds. For the rest of the compounds in figure 4.4, compound ANS02 was employed as the starter molecule to replace THT1 and THT2 because of its simple structure and good binding affinity, to generate and fetch better compounds as the study journey through the 2° scaffold hopping expedition. Resultantly, after ANS02 was introduced as the starter molecule, the library gained vast of new compounds with improved binding affinities (figure 4.4). These new molecules were in the range between  $-10.3 \text{ kcal mol}^{-1}$  to  $-14.1 \text{ kcal mol}^{-1}$  in terms of average binding energies after virtual screening against PDB ID: 4kne, 4kl9, and 1dg8 of the *Mtb*DHFR enzyme. Ring-opening and closure were employed as facets and features of the 2° scaffold hopping (see figure 4.4). The observation was that ring-opening led to a loss in binding affinity or reduction in binding energies regardless of the starter molecule used. Examples of such

phenomena are on compound AS05 ( $\Delta G = -7.13 \text{ kcal mol}^{-1}$ ), AM31 ( $\Delta G = -8.2 \text{ kcal mol}^{-1}$ ), and ANS11 ( $\Delta G = -8.5 \text{ kcal mol}^{-1}$ ), which had the lowest binding affinities among all compounds.

Based on observations in figure 4.4, we acknowledged a possibility of structural dissimilarity among molecules in terms of their 2D when they are so similar with regards to their 3D. Therefore it was discernible that the 3D form of a molecule offers a striking unique blueprint for determining structural similarity among molecules.

Below is figure 4.5 which shows the optimum superimposition of structural protein receptors used in virtual screening. In this aspect, we sought to determine structural similarity among these three macromolecules, and this similarity is significant because it is often correlated with evolutionary relatedness.

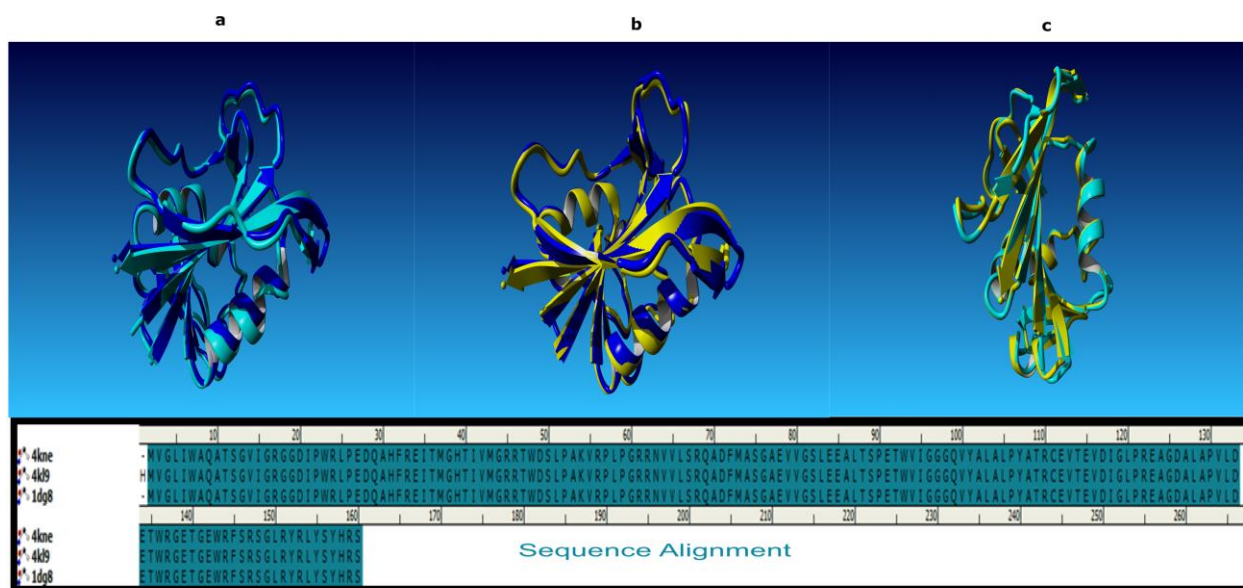


Figure 4. 5: Superimposition/Sequence alignment of (a) PDB ID: 4kne and 4kl9, (b) PDB ID: 4kne and 1dg8, (c) PDB ID: 4kl9 and 1dg8, PDB ID 4kne (blue), PDB ID 4kl9 (cyan), PDB ID 1dg8 (yellow).

The above structural alignment between 4KNE and 4KL9 has a C (alpha) RMSD of 1.237Å over 159 aligned residues with 100% sequence identity. The above structural alignment between 4KNE and 1DG8 has a C (alpha) RMSD of 1.111Å over 159 aligned residues with 100% sequence identity. The above structural alignment between 1DG8 and 4KL9 has a C (alpha) RMSD of 0,620 Å over 159 aligned residues with 100% sequence identity. For good efficiency, RMSD values should be at most < 2 Å (Silakari & Singh, 2021).

Table 4. 2: RMSD Calculation of all aligned receptor molecules against each other



Receptor molecules	Reference	Main-chain
<b>4kl9</b>	<b>4kne</b>	<b>1.237</b>
<b>1dg8</b>	<b>4kne</b>	<b>1.111</b>
<b>1dg8</b>	<b>4kl9</b>	<b>0.620</b>

### 4.3 Validation of the docking protocol

In this section, we initially re-generated the co-crystallized ligands from their respective macromolecules and re-docked them in their original active sites to validate the docking protocol (figure 4.6).

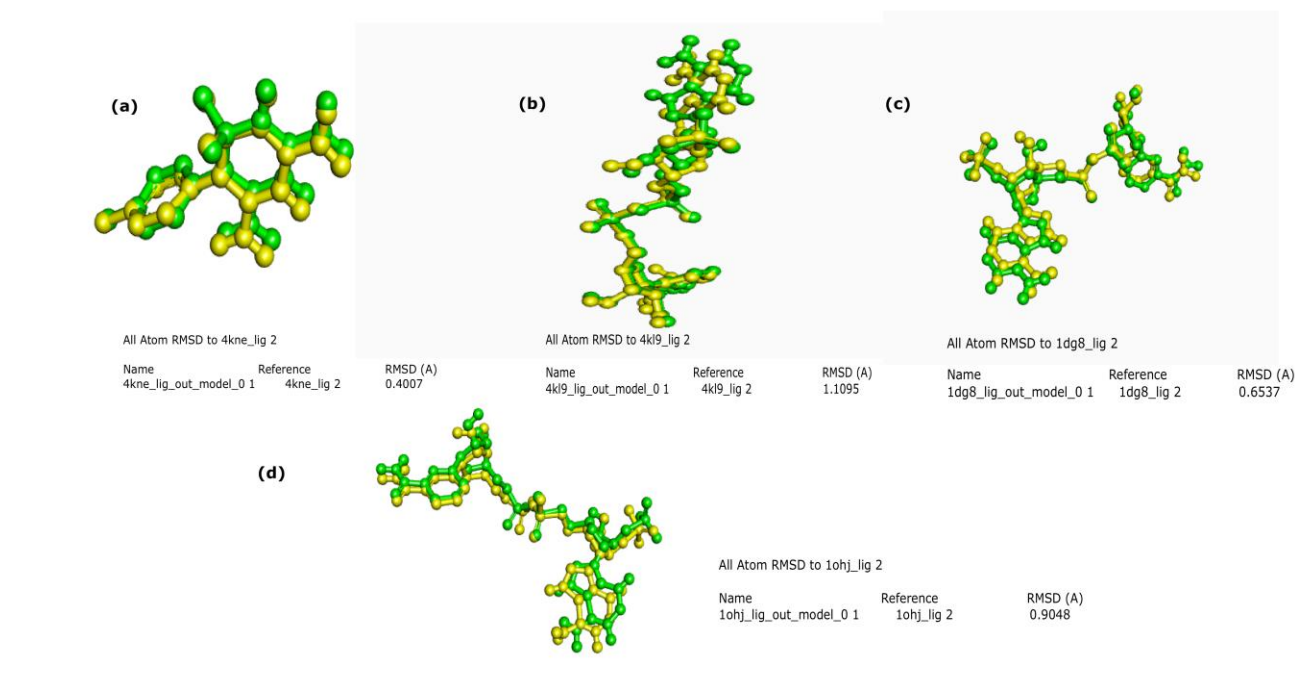


Figure 4. 6: Co-crystallized ligands (green) superimposed with predicted ligands (yellow), presented for validation of the docking protocol [a]. 4kne in complex with cycloguanil, b). 4kl9 in complex with NADPH, c). 1dg8 complexed with NADPH d). 1ohj complexed with PT523].

We substantiated the robustness of the docking protocol by matching and correlating the co-crystallized cycloguanil of the *Mtb*-DHFR (PDB ID: 4KNE), NADPH (dihydro-nicotinamide-adenine-dinucleotide phosphate) of PDB ID: 4KL9 & PDB ID: 1DG8 of the *Mtb*-DHFR, and N-

(4-Carboxy-4-{3,5-dichloro-4-[(2,4-diamino-pteridin-6-ylmethyl)-amino]-benzoylamino}-butyl)-phthalamic acid (ligand 2) of human-DHFR (PDB ID: 1OHJ) with their docked equivalents. Eventually, all their subsequent RMSD values were calculated over all atoms. The reported RMSD value that can validate a docking protocol's success is  $< 2\text{\AA}$  (Taha et al, 2011), which aligns or agrees with the results in figure 4.6. Following this exercise, the RMSD for all used macromolecular PDB IDs was  $0.4007\text{\AA} < \text{RMSD} < 1.1095\text{\AA}$ , meaning that the docking protocol worked successfully.

#### 4.4 *In-silico* ADMET Studies

In this section, we investigated the drug-likeness of the 23 compounds with good docking scores (Table 4.3). With the aid of alvaDesc software, four molecular descriptors were chosen to investigate the physicochemical properties of the compounds and these were: constitutional indices, functional group counts, molecular properties, and drug-like indices. On constitutional indices, the study focused on molecular weight (Mwt). Only four compounds had molecular weight above 500 and compound RM11 had the highest Mwt of 525.61. The hydrogen bond donor and acceptors calculated under functional group counts were found to obey the Lipsnki rule of 5 perfectly across all selected compounds.

Table 4. 3: 1-3-5-triazine-2-amine derivative compounds along with their Lipinski rule, drug-like score consensus (DLScons), synthetic accessibility (SAscore), Quantitative Estimate of Drug-Likeness (QED), Aqueous Solubility, Cytochrome 450 inhibition prediction of 5 isoforms (1a2, 2c9, 2c19, 2d6, and 3a4), and binding affinity against DHFR enzyme receptors PDB ID: 4kne, 4kl9 and 1dg8.

Name	Lipinski Rule of Five		Cytochrome P450 (CYP450) Inhibition Isoforms					Aqueous Solubility (Log S)	Synthetic Accessibility (SAscore)	Quantitative Estimate of Drug-Likeness (QED)	Binding Affinities (kcal mol <sup>-1</sup> ) ΔG		
			1a2	2c9	2c19	2d6	3a4				Binding		
											4kne	4kl9	1dg8
AS05	Molecular Weight	299.48	No	No	No	No	No	-2.372	4.4229	0.3923	-7.19	-7.2	-7.0

	(<500Da)												
	Log P(<5)	2.0478											
	H-Bond donor (5)	4											
	H-bond acceptor (<10)	7											
	Violations	0											
	Drug-Like Score (DLScore)	0.9761											
AS122	Molecular Weight (<500Da)	411.46	No	Yes	Yes	No	Yes	-5.7443	5.3332	0.3975	-10.3	-11.3	-12.7
	Log P(<5)	4.8885											
	H-Bond donor (5)	3											
	H-bond acceptor (<10)	10											

	Violations	0											
	Drug-Like Score (DLScore)	0.7785											
RM11	Molecular Weight (<500Da)	525.61	No	No	No	No	No	-7.4482	5.4330	0.3371	-12.5	-13.1	-13.0
	Log P(<5)	4.3514											
	H-Bond donor (5)	3											
	H-bond acceptor (<10)	10											
	Violations	1											
	Drug-Like Score (DLScore)	0.6333											
RM15	Molecular Weight	525.61	No	No	No	No	Yes	-7.4061	5.5361	0.4153	-12.0	-11.8	-14.1

	(<500D a)												
	Log P(<5)	5.124 6											
	H-Bond donor (5)	3											
	H-bond accepto r (<10)	10											
	Violatio ns	2											
	Drug- Like Score (DLSco ns)	0.633 3											
RF43	Molecul ar Weight (<500D a)	493.5 9	No	Ye s	Yes	No	Ye s	-7.2911	5.2639	0.4239	-11.0	-12.1	- 13.1
	Log P(<5)	5.287 5											
	H-Bond donor (5)	3											
	H-bond accepto r (<10)	9											

Violations	1									
Drug-Like Score (DLScons)	0.702 3									

Under molecular properties, although alvaDesc inclusively calculated on three octanol-water partition coefficients (log P) models, the study concentrated much on the log P consensus (Log Pcons). Table 4.3 indicates that only RF02, RF15, and RF43 had log P values exceeding the optimal value of 5. All the compounds achieved better synthetic accessibility scores (i.e. SAScore  $\leq 6$ ), indicating that all selected compounds can be easily synthesizable. Looking at the calculated drug-like indices across all molecules, the Lipinski rule of five was evaluated to be obeyed satisfactorily because not more than 3 of its molecular descriptors were violated. Also calculated was the drug-likeness score consensus (DLScons) which evaluates the potential bioavailability of the chosen molecules. On this parameter high scores were prevalent among all compounds, best scores were achieved on compounds AM34 and AS05 with DLScons values of 0.9761 and 0.9285, respectively.

On the other hand, molecules AM22 (appendix 2) and AM34 attained perfect DLS values of 1, indicating that they are potentially suitable *Mtb-DHFR* inhibitors. All compounds possess good aqueous solubility (LogS) suggesting good pharmacological action powered by sufficient blood concentration. The other parameter is called the quantitative estimate of drug-likeness (QED) which is calculated based on the concept of desirability (Bickerton et al, 2012). A QED score greater than 0.3 indicates that a molecule has better drug-like properties, discerning that most compounds in table 4.3 had a considerable QED scores. In its computation QED incorporates the information derived from FDA-approved drugs. Therefore, it expresses and validates the ADME properties (Kosugi & Ohue 2021). Lastly, the calculated binding energy values saw compounds RF02, RM11, and RM15 emerging as the most significant drug candidates due to their highest docking scores. All compounds in table 4.3 possess considerable binding affinities proving

inhibitory against *Mtb-DHFR* hence anti-TB drugs. However, despite having the perfect DLS value, molecule AS05 had the lowest binding energy which is even lower than that of THT1 and THT2 the starter molecules of this study.

Also incorporated within table 4.3 are the results for metabolism properties displaying the inhibition capabilities of compounds to cytochrome P450 (CYP450) isoforms 1a2, 2ac9, 2c19, 2d6, and 3a4. Generally, many compounds show no inhibition. However, a few compounds proved to inhibit not all but some CYP450 isoforms. This investigation was of tremendous importance in predicting the possibilities of drug-drug interaction due to CYP450 enzyme inhibition (Montanha et al, 2022; Uehara et al., 2020), therefore, for all the compounds that could not inhibit CYP450 isoforms infers low risk of the drug-drug interaction phenomena. Failure of the compounds to inhibit the mentioned CYP450 enzymes means the CYP450 enzymes will be able to perform their drug metabolism action for excretion since the drug molecule should not stay in the body after it has performed its intended purpose.

#### 4.4.1 Computational Quantitative Characterization of Physicochemical Properties

An *In-silico* quantitative characterization in reliance on calculated physicochemical property profiles such as molecular weight (MW), number of rotatable bonds (RBN), H-bond donors and acceptors (nHDon and nHAcc), Chirality (chiral centers), molar refractivity consensus (MRcons), Topology polar surface area (TPSA) and synthetic accessibility (SAscore) was accomplished in this section (Table 4.4).

Table 4. 4: Univariate statistical analysis of *In-silico* predicted physicochemical properties of selected 16 compounds

<b>Molecular Descriptor</b>	<b>Average</b>	<b>Std. Deviation</b>	<b>Maximum</b>	<b>Minimum</b>
<b>Molecular Weight (MW)</b>	413.326	114.36435	525.610	137.160
<b>TPSA(NO)</b>	107.454	33.39606	209.320	68.010
<b>RBN</b>	4.313	2.44182	10	1

<b>nHDon</b>	3.125	1.09364	7	1
<b>nHAcc</b>	5.188	1.19754	10	4
<b>SAscore</b>	4.799	0.78191	5.686	3.023
<b>Estimated Solubility (ESOL)</b>	-4.968	2.13027	-0.683	-7.448
<b>Molar Refractivity consensus (MRcons)</b>	114.107	32.37337	148.196	35.891
<b>Chiral Center</b>	0.875	0.88506	3.000	0.000

---

*Note:* Molecular weight MW, Topological polar surface area using N, O polar contributions TPSA(N,O), Estimated solubility ESOL, Number of rotatable bonds RBN, Number of hydrogen bond donors, nHDon, Number of hydrogen bond acceptors nHAcc, Molar Refractivity Consensus MRcons, Synthetic accessibility score, SAscore, and Chiral centers.

ADMET studies remain indispensable in evaluating the most suitable route of administration for the drugs. Figure 4.7 displays four physicochemical properties such as molecular weight, Log P, number of hydrogen bond donors, and number of hydrogen bond acceptors, that are considered for the determination of the Lipinski rule of five (Ro5).



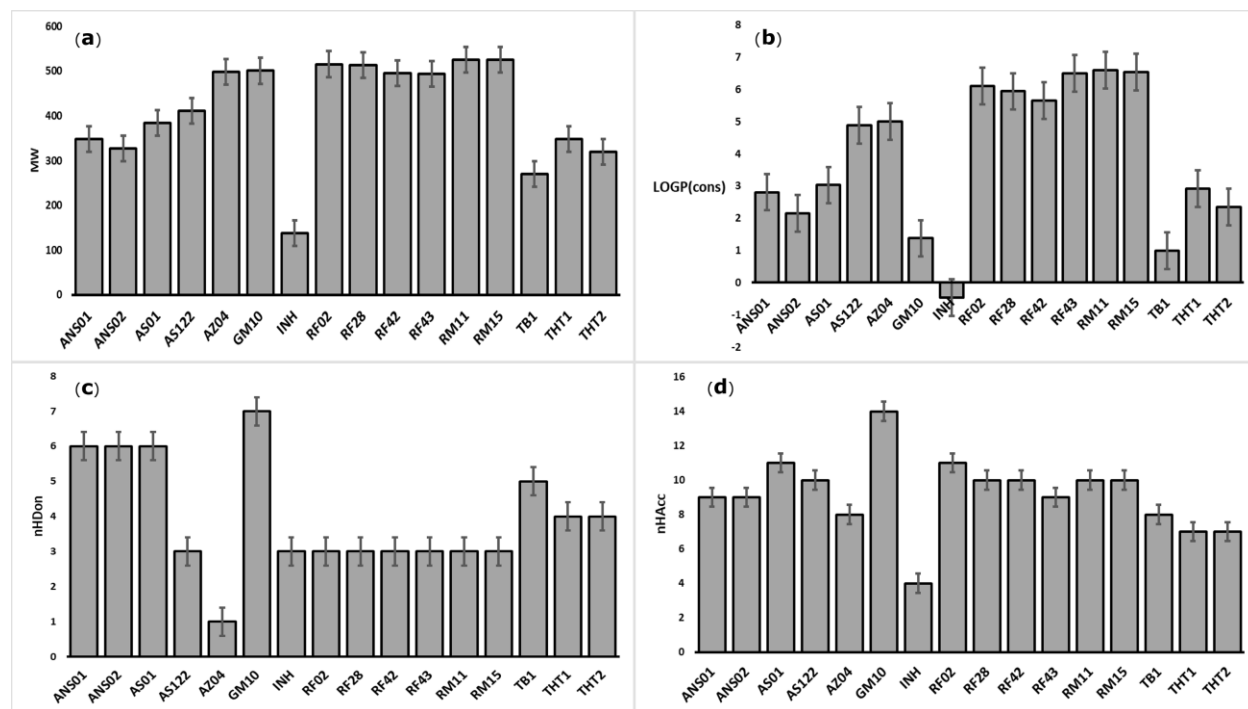


Figure 4. 7: Assessment of the Lipinski rule of five, (a) Molecular weight (MW), (b) LOGP (consensus), (c) number of hydrogen bond donors (nHDon), (d) number of hydrogen bond acceptors (nHAcc).

As shown in figure 4.7, it was observed from that compounds that had a log P greater than the commended (five) were found in the acceptable range with regard to other physicochemical properties like, MW, nHDon, and nHAcc. Similarly, GM10 had 7 nHDon and 14 nHAcc but fell in range in relation to MW and LOGP. Furthermore, the compounds did not violate at least three physicochemical properties indicating that they obeyed the Lipinski rule of five. Therefore the compounds suggested significant drug-like properties and can be considered better candidates for further studies.

Figure 4.8 summarizes the distribution of physicochemical properties in relation to Verber's rule, and other crucial drug-like properties such as chirality, molar refractivity MRcons, estimated solubility and synthetic accessibility SAscore.

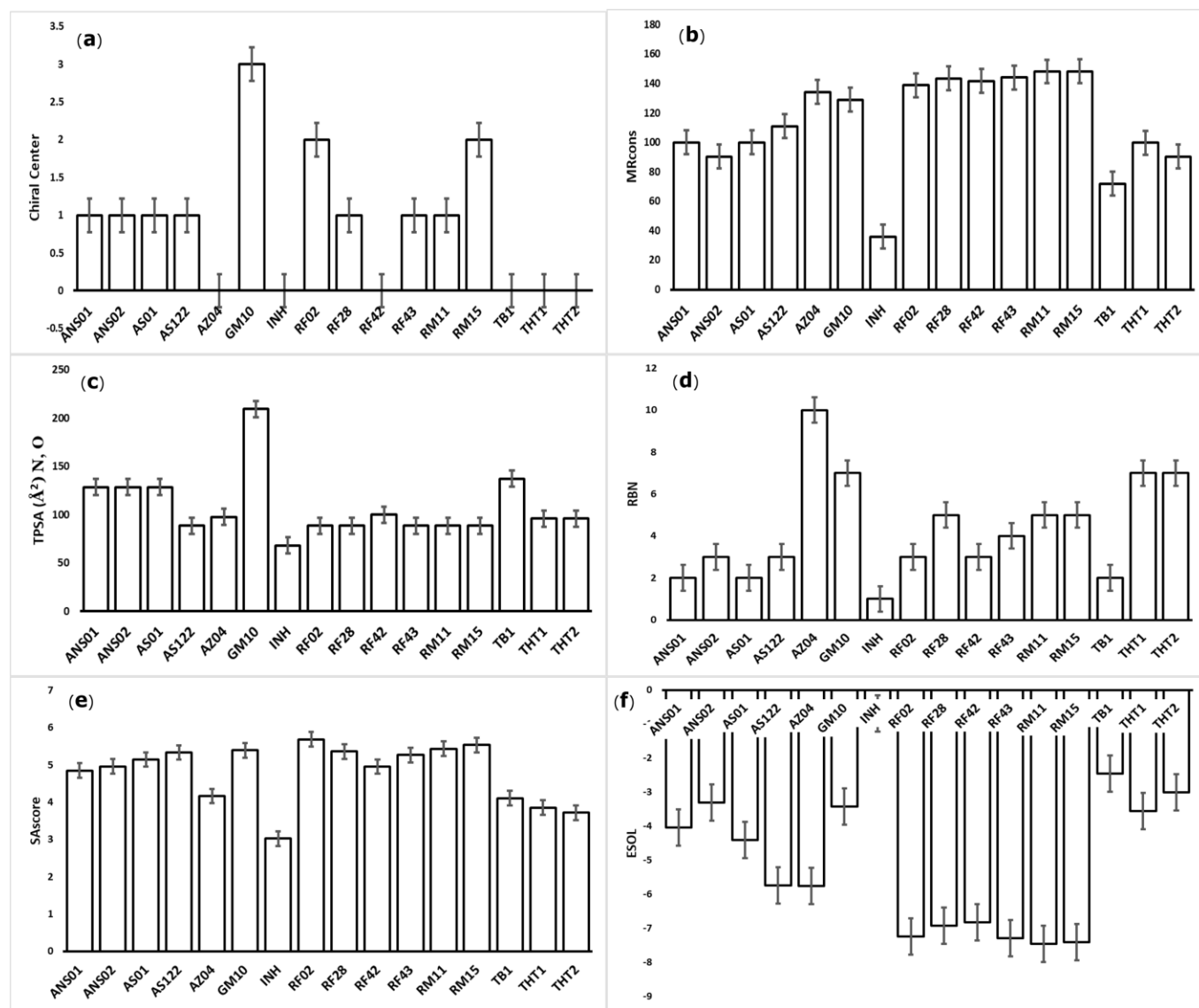


Figure 4. 8: Computational quantitative characterization of compounds' physicochemical properties, (a) Chiral centers, Molar refractivity consensus (MRcons), Topological polar surface area using N and O polar contributions, (d) number of rotatable bonds (RBN), (e) Synthetic accessibility score (SAscore) and (f) Estimated solubility (ESOL).

**Topological Polar Surface Area (TPSA):** All the designed 1,3,5-triazine derivative molecules in Figure 4.8 (c) were observed to fall within the permissible range i.e.  $TPSA \leq 140 \text{ \AA}^2$ , except for GM10 with a value of  $203.8 \text{ \AA}^2$ . The compounds' TPSA had an average of 107.45 with a standard deviation of 33.39. This implies that compound GM10 can potentially pose gastrointestinal absorption problems.

**Verber's Rule:** Verber et al. (2002) proposed the following for a drug with good bioavailability and these include  $\leq 10$  rotatable bonds (RBN),  $\leq 12$  H-bond donors plus acceptors in total (i.e.  $nHDon + nHAcc \leq 12$ ), and topological polar surface area (TPSA)  $\leq 140 \text{ \AA}^2$ . The compounds'

maximum RBN as in figure 4.8 (d) was 10 with an average of 4.31 and a standard deviation of 2.44. The nHDon displayed in figure 4.7 (c) for all compounds was 4.12 on average with a standard deviation of 2.09, nHAcc (figure 4.7 (d) 9.18 on average, and a standard deviation of 2.19. If more than three of these are violated then the drug molecule is rejected for the next stage of studies in the drug discovery pipeline. Nonetheless, all the selected 16 compounds were found within the acceptable range obeying Verber's rule. The Verber's rule excludes molecular weight MW.

**Molar refractivity (MR):** In this study, it was observed that the majority of the compounds fell within the MR qualifying range which is between 40 and 130, (figure 4.8 (b)) and the mean molar refractivity was 114.11 with a standard deviation of 32.37. According to Ghose et al. (1999) compounds with such an MR range are considered drug-like as they have good drug polarizability.

**Synthetic accessibility (SAscore):** We considered the ease of synthesis of which all compounds were predictively falling within the acceptable qualifying range of SAscore  $\leq 6$ . This suggests that it is possible for all these compounds to be synthesized in the laboratory.

**Chirality:** In terms of chirality, compounds AZ04, INH, TB1, TH1, and THT2 (figure 4.8 (a)) were observed with no chiral center which implies that the compounds were free of toxicity problems arising from stereoselectivity or enantiopurity issues that exist when a molecule is chiral. While the rest of are asymmetrical and chiral, compound GM10 had the highest number of chiral centers 3, followed by RF02 and RM10 with 2 chiral centers, and the rest of the compounds had only 1 chiral center. According to the US FDA guidelines, chirality determination is very crucial and should be addressed early like at this stage of drug discovery and development. The more the number of chiral centers in a compound the more the number of enantiomers from a single compound. This, therefore, means for the most optically active GM10 compound, ADMET studies must be meticulously executed to determine the biological activity and adverse effects associated with each possible isomer. However, the chirality of a compound structure could confer target (in this case *MtbDHFR*) binding specificity and selectivity and infer scaffold novelty (Brooks et al., 2011; Pelay-Gimeno et al., 2015). Furthermore, pelay-Gimeno et al. (2015) highlighted that chirality can enhance biological activity underlining that chiral scaffolds may confer high mycobacterial or inhibitory effects.

#### 4.4.2 Brain or Intestinal Estimated (BOILED EGG)

We analyzed other drug-likeness properties of some selected designed compounds using SwissADME ([www.swissadme.ch](http://www.swissadme.ch)) web tool from the Swiss institute of Bioinformatics (SIB Swiss Institute of Bioinformatics Members, 2016; Daina & Zoete, 2016). The server display a molecular sketcher on the left-hand side and the ChemoAxon's Marvin JS window on the right hand side where a data set of selected 16 compounds was inserted in SMILE (simplified molecular input line entry system) format. A graph called an egg plot (figure 4.9) was plotted showing the TPSA (the surface sum over all polar atoms or molecules) on the x-axis against WLOGP (lipophilicity of the drug) on the y-axis (Daina et al., 2017). The characteristics property of a molecule to cross or penetrate through the blood-brain barrier (BBB) is denoted by the yellow party of an egg i.e. egg yolk. Alternatively, the properties of molecules with a better chance of favoring passive absorption by the gastrointestinal tract (GIT) are represented by the white portion of the egg. Also, the molecules that had a higher probability of getting effluxed from the central nervous system (CNS) by P-glycoprotein (P-gp; PGP+), are colored blue dots, while the red dots represent molecules that are predictively non-substrates of P-gp (PGP-).

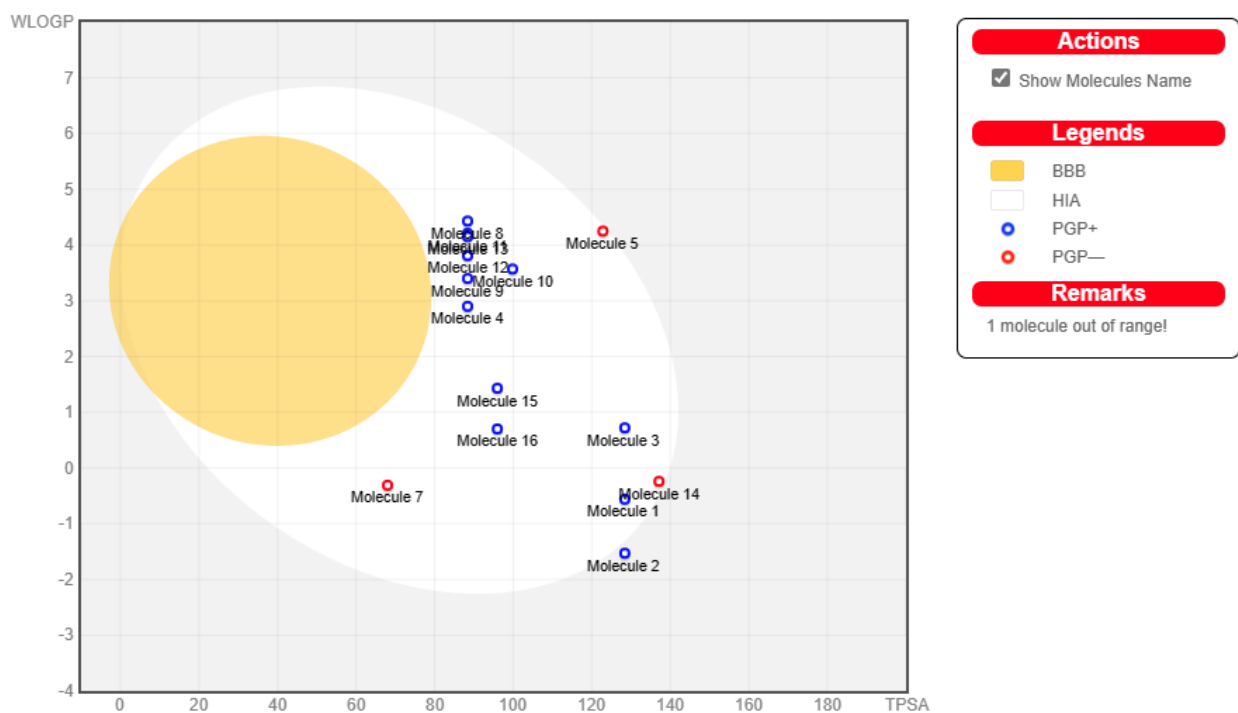


Figure 4. 9: Predicted boiled egg representation of the selected designed 1,3,5-triazine based derivatives using the Swiss ADME web tool.

As on figure 4.9, none of the molecules were found occupying the Boiled Egg’s yolk meaning that all molecules cannot passively permeate through the blood–brain barrier (BBB) therefore protecting the brain from unwanted or harmful substances if the *Mycobacterium tuberculosis* is not in the brain. Concurrently, 15 molecules were located within the Boiled Egg’s white area which is an indication that they were predicted to be passively absorbed by the gastrointestinal tract. However, only molecule 2 (ANS02) was found slightly out of the range because of its WLOGP which was -1.53 thus violating one of the Ghose et al. (1999) rules which require molecules in range  $-0.4 \leq \text{WLOGP} \leq 5.6$  to be considered drug-like, however, ANS02 satisfied on other molecular descriptors. The 14 molecules in green dots inferred that they can be potentially eluted from the central nervous system (CNS) by P-glycoprotein, and conversely, only three molecules, AZ04, INH, and TB1 represented in red dots were predictively non-substrates of P-gp (PGP–) hence they cannot be eluted from the central nervous system (CNS) by P-glycoprotein.

The study proceeded to look at the ADME and toxicity of the drug candidate molecules in Table 4.5.

All compounds in table 4.5 exhibited excellent gastrointestinal absorption, and good examples include compounds RM11, RF56, and RF28, etc., scoring 98.613, 97,342, and 95,656 respectively; overall, RF56 stood right on the podium with a perfect score of 100%. The beauty of these best scores lies in their compounds' excellent intestinal absorption capacity, which in turn results in adequate oral bioavailability (Othman et al., 2021).

Table 4. 5: ADME properties and Toxicity predictions among selected 24 compounds

Compound	Ames Toxicity	Max. Tolerated dose (Human) Log (mg/kg/day)	hERG 1	Oral Rate Acute Toxicity (LD50)	Oral Rate Chronic Toxicity (LOAEL)	Verhaar Daphnia base-line toxicity from MLOGP (mmol/l)	Intestinal Absorption
AS05	Yes	0.206	No	2.395	1.339	-3.7659	66.998
AM03	No	0.149	No	2.494	3.159	-4.6336	80.785

AM10	No	0.061	No	2.549	2.1	-4.8498	92.693
AM22	No	-0.006	No	2.334	0.986	-3.0664	73.988
AM26	No	0.01	No	2.374	0.712	-5.3491	95.162
AM31	No	0.034	No	2.421	0.999	-3.8143	91.118
AM34	Yes	0.097	No	2.519	1.931	-3.556	92.527
AM36	No	0.313	No	2.21	1.718	-4.6311	66.425
ANS01	No	0.075	No	2.557	0.862	-5.8378	66.322
ANS02	No	0.059	No	2.575	0.665	-5.2608	67.856
ANS04	No	0.524	No	2.937	2.944	-5.9097	75.377
ANS11	No	0.168	No	2.535	0.958	-5.9645	70.68
AS122	No	0.147	No	3.016	2.127	-6.6429	94.827
AS01	No	0.084	No	2.412	1.95	-6.0635	77.292
RM11	No	0.36	No	3.022	3.246	-8.5076	98.613
RM15	No	0.209	No	2.739	2.041	-8.5076	95.341
RF02	No	0.355	No	3.002	0.76	-7.8463	92.034
RF18	No	0.294	No	3.185	3.453	-7.8258	95.916
RF20	No	0.311	No	3.195	2.984	-7.027	83.287
RF28	Yes	0.283	No	3.022	1.747	-8.0053	95.656
RF42	No	0.178	No	2.962	2.208	-6.9572	91.786
RF43	No	0.311	No	3.195	2.984	-7.8463	83.287
RF48	Yes	0.013	No	3.027	3.53	-7.1442	100
RF56	Yes	0.282	No	3.01	1.297	-7.7653	97.342
THT1	Yes	0.108	No	2.467	2.713	-4.3125	74.74
THT2	Yes	0.038	No	2.489	2.6828	-3.8557	73.372
Isoniazid	Yes	0.282	No	2.364	2.824	-1.0512	75.651

It is shown in table 4.5 that five compounds have positive Ames toxicity implying that they can be potentially mutagenic. Contrarily, the rest of the compounds tested negative for Ames denoting

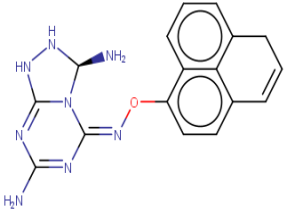
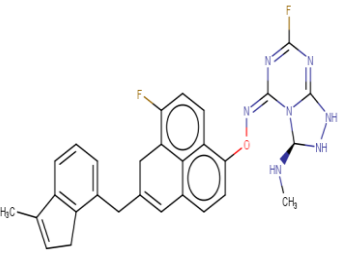
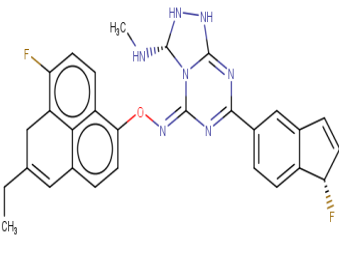
that they are less likely to be toxic in terms of mutagenicity. The lower the LD50 score of a compound the more lethal the compound. Juxtaposing the compound toxicity profile in terms of the oral rate acute toxicity (LD50 doses) of all the compounds ranging from 2.21 - 3.195 mol kg<sup>-1</sup>, all molecules had LD50 scores greater than that of isoniazid (2.364) the reference except compound AM22 AND AM36. This assessment deduces that most of the newly designed compounds in the constructed database are less toxic and are highly potential TB-Drug candidates.

#### 4.5 Analysis of interactions between 1,3,5-triazine-derivative ligands and *Mtb*-DHFR receptor

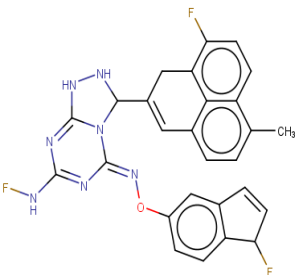
Through virtual screening using AutoDock Vina, we searched every nook and cranny of the newly designed compounds library to find molecules with optimized interactions in parallel with better binding energies. Ten (10) Molecules with high docking scores, good drug-like scores, and optimum interactions were shortlisted for synthesis and further studies. The binding energies across all 1700 molecules ranged from -6.3 to -14.1 kcal mol<sup>-1</sup>. The binding affinities to the macromolecules were in the order 4kne < 4kl9 < 1dg8 meaning in general, that molecules demonstrated the highest affinity for DHFR receptor PDB ID: 1DG8 1. However the anomalies were found for which the example was molecule RM11 which peculiarly had higher affinity for the PDB ID: 4KL9 than any other receptor present. Since the library contained hundreds of small molecules with best but similar binding affinities, ADMET, and drug-like molecules, we randomly selected among the best, ten compounds which are displayed in table 4.6.

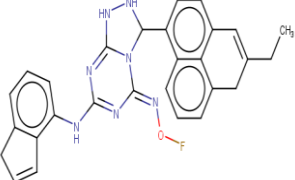
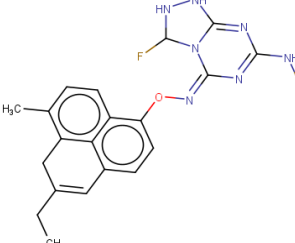
Table 4. 6: 2D -Structures, molecular formula, amino acid residues per each macromolecule, common amino acid residue interacting across all receptors, and binding affinities conjoined to three docked macromolecules (4kne, 4kl9, 1dg8), of 10 pre-qualified ligands.

Name	Structure	Molecular Formula	Amino Acid Residues			Common Residues Interacting across all receptors	Binding Affinities		
			PDB IDs				PDB IDs		
			4kne	4kl9	1dg8		4kne	4kl9	1dg8

ANS 01		$C_{28}H_{24}FN_7O$	ALA:7 ILE:14 ILE:94 LEU:57 PHE:31 TYR:1 00	ASP:27 GLN:2 8 HIS:30 ILE:5 ILE:14 ILE20 TRP:6	ALA:7 ILE:14 ILE:94 LEU:57 PHE:31 THR:4 6	ILE:14	-9.8	- 11. 1	- 12.4
RM1 1		$C_{29}H_{25}F_2N_7O$	ASP:27 GLN:2 8 GLY:9 6 GLY:9 7 ILE:14 ILE:94 LEU:57 PHE:31 PRO:58 TYR:1 00 VAL:5 4	ALA:7 GLY:1 8 GLY:9 7 ILE:14 LEU:24 THR:4 6 TRP:22	ALA:7 ARG:3 7 GLN:2 8 GLY:9 7 ILE:14 ILE:94 PHE:31 THR:4 6 VAL:5 4	ILE:14	- 12. 5	- 13. 1	- 13.0
RM1 5		$C_{29}H_{25}F_2N_7O$	ALA:1 26 ARG:4 5 GLN:2 8 ILE:14	ARG:4 5 GLY:1 8 ILE:20 ILE:94 LEU:50	ALA:7 ALA:1 26 ARG:4 5 ASP:27 GLN:2	ARG:45 ILE:94	- 12. 0	- 11. 8	- 14.1

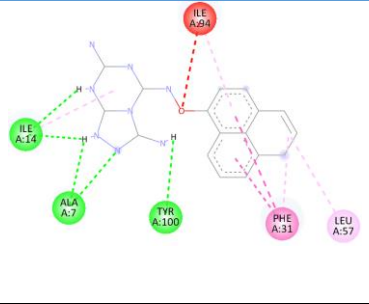
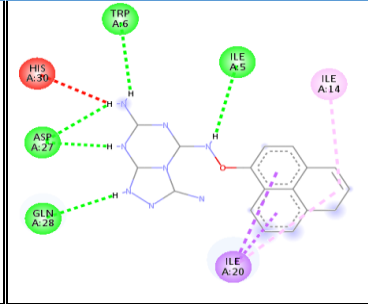
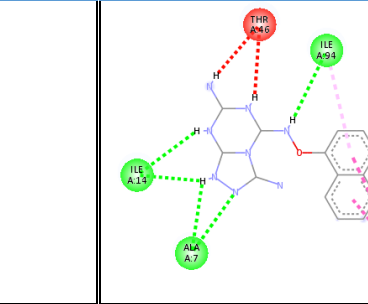
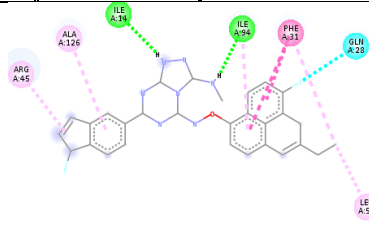
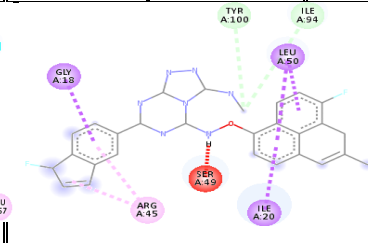
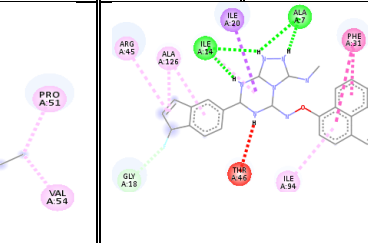


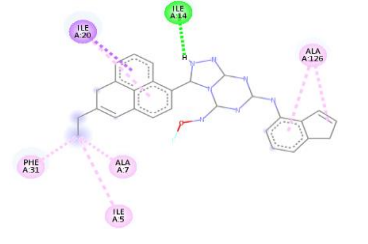
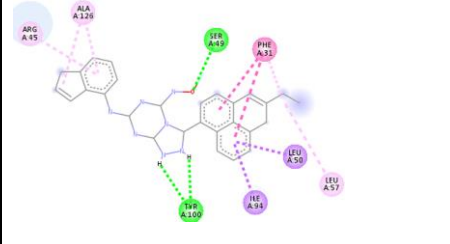
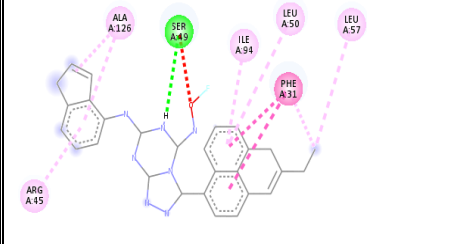
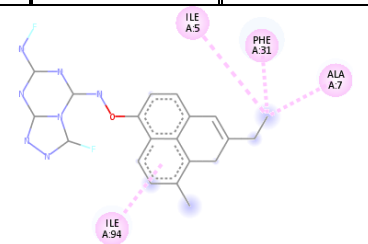
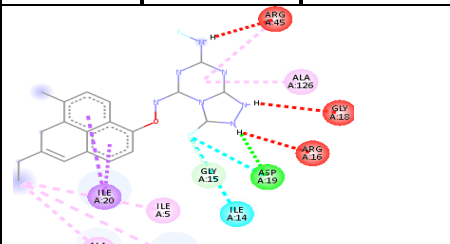
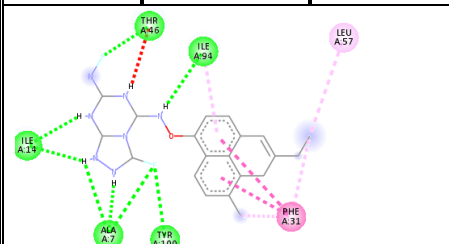
			ILE:94 LEU:54 PHE:31	PRO:51 SER:49 TRY10 0 VAL:5 4	8 GLY:1 8 ILE:14 ILE:20 ILE:94 PHE:31 THR:4 6 VAL:5 4				
RF02		$C_{27}H_{20}F_3N_7O$	ALA:7 ASP:27 GLN:2 8 GLY18 ILE:5 ILE:20 LEU50 TRP:6	ALA:1 26 ARG:2 3 ASP:19 GLY:1 8 GLY:9 5 GLY:9 6 ILE14 ILE:20 PHE:31 PRO:41 SER:45	ASP:27 ILE:20 PHE:31 PRO:51 SER:46 THR:4 6	ILE:20	11. 4	- 12. 9	- 14.0

RF43		C <sub>28</sub> H <sub>24</sub> FN <sub>7</sub> O	ALA:7 ALA:1 26 ILE:5 ILE:14 ILE:20 PHE:31	ALA:1 26 ARG:4 5 ILE:94 LEU:50 LEU:57 PHE:31 SER:49 TYR:1 00	ALA:1 26 ARG:4 5 ILE:94 LEU:50 LEU:57 PHE:31 SER:49	ALA:126 PHE:31	- 11. 0	- 12. 1	- 13.1
AS1 22		C <sub>20</sub> H <sub>19</sub> F <sub>2</sub> N <sub>7</sub> O	ALA:7 ILE:5 ILE:94 PHE:31	ALA:7 ALA:1 26 ARG:1 6 ARG:4 5 ASP:19 GLY:1 5 GLY18 ILE:5 ILE:14 ILE:20 PHE:31	ALA:7 ILE:14 ILE:94 LEU:57 PHE:31 THR:4 6 TRY:1 00	ALA:7 PHE:31	- 10. 3	- 11. 3	- 12.7

In this section, we also took note of the amino acids that were universally or commonly participating in interactions across all *Mtb-DHFR* receptors. In table 4.7, we contemplated the nature or type of interactions tangled between 10 ligands and each DHFR macromolecular receptor.

Table 4. 7: Ligand-target interactions of 10 best ligands for all three receptors (PDB ID: 4KNE, PDB ID: 4KL9, PDB ID: 1DG8) along with their type of interactions.

Name	4KNE-Ligand interaction			4KL9-Ligand interaction			1DG8-Ligand interaction		
ANS 01									
H-Bonding Interaction	Hydrophobic Interaction	Electrostatic Interaction	H-Bonding Interaction	Hydrophobic Interaction	Electrostatic Interactions	H-Bonding Interaction	Hydrophobic Interaction	Electrostatic Interactions	
ALA:7 ILE:14 TRY:100	PHE:31 LEU:57 ILE94	N/A	ASP:27 GLN:28 ILE:5 TRP:6	ILE:14 ILE:20	N/A	ALA:7 ILE:14 ILE:94	LEU:57 PHE:31	N/A	
RM1 5									
H-Bonding Interaction	Hydrophobic Interaction	Electrostatic Interaction	H-Bonding Interaction	Hydrophobic Interaction	Electrostatic interaction	H-Bonding Interaction	Hydrophobic Interaction	Electrostatic interaction	
ILE:14 ILE:94 GLN:28	ALA:126 ARG:45 PHE:31 LEU:57 ILE94	N/A	ILE:94 TYR:10 0	ARG:45 GLY:18 ILE:20 LEU:50	N/A	ALA:7 ASP:27 GLN:28 GLY:18 ILE:14	ALA:126 ARG:45 ILE:20 ILE:94	N/A	

				PRO:51 VAL:54			PHE:31 VAL54	
R43								
H-Bonding Interaction	Hydrophobic Interaction	Electrostatic Interaction	H-Bonding Interaction	Hydrophobic Interaction	Electrostatic interaction	H-Bonding Interaction	Hydrophobic Interaction	Electrostatic interaction
ILE:14	ALA:126 ALA:7 ILE:5 ILE:20 PHE:31	N/A	SER:40 TYR:100	ALA:126 ARG:45 ILE:94 LEU:50 LEU:57 PHE:31	N/A	SER:49	ALA:126 ARG:45 ILE:94 LEU:50 LEU:57 PHE:31	N/A
AS122								
H-Bonding Interaction	Hydrophobic Interaction	Electrostatic Interaction	H-Bonding Interaction	Hydrophobic Interaction	Electrostatic interaction	H-Bonding Interaction	Hydrophobic Interaction	Electrostatic interaction

Compound ANS01 formed five conventional hydrogen bonds against receptor PDB ID: 4KNE, which include two H-bonds between –NH and the nitrogen (N) atom on the 5-membered ring of the triazine moiety to the amino acid ALA:7, the same –NH formed another conventional H-bond with ILE:14 which is in-turned hydrogen-bonded to another –NH on the 6-membered ring of the

N/A	ALA:7 ILE:5 ILE:94 PHE:31	N/A	ASP:19 GLY:15 ILE:14	ALA:126 ARG:45 ALA:7 ILE:5 ILE:20	N/A	ALA:7 ILE:14 ILE:94 THR:46 TYR:10 0	LEU:57 PHE:31	N/A
-----	------------------------------------	-----	----------------------------	---	-----	--	------------------	-----

same triazine moiety. The final hydrogen bond is between the –CNH extending from the 5-membered ring of the triazine structure and the TYR: 100 residue. Other interactions include one unfavorable bump between ILE: 94 residue and oxygen atom on the linker of triazine and non-triazine moiety. Two pi-pi stacked between PHE:31 and the naphthalene part of the three fused benzene ring structure, three pi-alkyl interactions between i.e. LEU:57 and the third ring of the non-triazine moiety. The non-triazine moiety also formed pi-alkyl interactions with PHE:31 and ILE:94.

Contrasting with other receptors i.e., PDB ID:4KL9 and 1DG8, all their complexes with ANS01 bring forth five (5) convectional hydrogen bonds despite differences. With 4kl9, ANS01 formed convectional hydrogen bonds with ASP: 27, GLN: 28, TRP:6, and ILE:5. 1DG8 on the other hand 1DG8 and ANS01 had five hydrogen bonds formed between residues ALA:7 (2-H bonds), ILE:14 (2-H bonds), ILE:94 (1-H - bond), and also formed two pi-pi stacking interactions with the PHE:31 residue plus one pi-alkyl bond with LEU:57 residue. The second molecule, AS01 established four hydrogen bonds with receptor 4kne, two of which were convectional (with residues ASP: 27 and SER:49), and the other two (with residues GLY:15 and PHE:31) were carbon-hydrogen bonds. Again with 4kne, AS01 formed hydrophobic interactions comprising two pi-alkyl interactions by residues ALA: 126 and ILE: 14. Regarding PDB ID: 4KL9 and AS01, we see a total of seven H-bonds being formed, which include five convectional hydrogen bonds, one carbon-hydrogen bond, one hydrogen fluoride, and two types of hydrophobic interactions i.e., two pi-pi stacking both with the ILE:20 residues, and two pi-alkyl interactions with ILE:20 and ILE:14 residues. Two convectional H-bonds were formed between ASP:27 residue with two –NH groups on the 1,3,5-triazine moiety, and the third convectional H-bond is between the GLY:28 and 1,2,4-triazole ring that is fused with the triazine, and there also exists another convectional hydrogen bond between –NH on the linker of triazine and non-triazine moieties and the ILE:5 residue. Lastly, on the three fused non-triazine rings there was a convectional H-bond on the Fluorine atom and SER: 49

residue. Similarly, seven hydrogen bonds were observed concerning PDB ID: 1DG8, and five of them were H-bonds conventionally formed with amino acid residues ALA: 7, ILE: 14, and ILE: 94. AS01 had a very good docking score of  $-12.7 \text{ kcal mol}^{-1}$ , perhaps this was due to principally very strong H-F bonds and many other types of interactions.

Given the PDB ID:4KNE-RF02 complex, we observed four hydrogen bonds with ASP:27, TRP:6 (HF), GLY:18 (convectional H-bond) on the  $-\text{NH}$  of 1,2,4-triazole, carbon-hydrogen bond with GLN:28. The pi-pi stacking between the LEU:50 residue and 1-fluoro-4-methylphenalene ring, and between TRP:6 residue with the cyclopentadiene of the 3aH-indene moiety, two pi-alkyl interactions between two amino acid residues, i.e. ALA:7 ILE:5, and cyclopentadiene of the 3aH-indene moiety. ALA:7 and ILE:20 were also involved in pi-alkyl interactions with the benzene ring that is fused with the cyclopentadiene.

Among all RF02 complexes, PDB ID: 4KL9 formed 15 interactions with more than 4kne or 1dg8. 4KL9 was observed to participate in two convectional hydrogen bonds formed between two  $-\text{NH}$  groups of the 1,3,5-triazine moiety and the GLY:18 residue. The same triazine ring formed a pi-lone pair interaction with the SER:49 residue. The fluoro-cyclopentadiene that is involved in two carbon-hydrogen bonds with two amino acid residues, GLY:95 and GLY:96, also participated in pi-alkyl interaction with ALA:126 and ILE:14 residues. The pi-alkyl interactions between the  $-\text{CH}_3$  of the 1-fluoro-4-methylphenalene and PHE:31 were also confirmed, along with the pi-pi T-shaped bond between phenalene and PHE:31 residues ILE: 20 residues formed two pi-alkyl interactions with the phenalene ring and indene structures. The triazine structure formed pi-cationic interactions with both ARG: 23 and ASP:19, while the third pi-cationic bond was between ARG:23 residue and the 1,2,4-triazole moiety which had a pi-alkyl bond with the PRO:51 residue.

One of the study's best docking scores ( $\Delta G = -14.0 \text{ kcal mol}^{-1}$ ) was witnessed between RF02 and PDB ID: 1DG8, which was only supported by nine interactions. Against 1DG8, RF02 initiated one convectional hydrogen bond between the  $-\text{NH}$  of the triazine moiety and SER: 49 residues. The same triazine ring formed a carbon-hydrogen bond with THR: 46 residues. The ASP: 27 residues and the 1-fluoro-4-methylphenalene interacted through a hydrogen fluoride (HF) bond. Both the triazine ring and the benzene fused the 5-carbon membered ring formed pi-alkyl interactions with ILE: 20 residue, and similarly, a pi-alkyl interaction existed between the 5-carbon membered ring and PRO:51. The other pi-alkyl bond was the same as the one between the  $-\text{CH}_3$  of the 1-fluoro-

4-methylphenalene and PHE: 31 with PDB ID: 4KL9, and two pi-pi T-shaped bonds between PHE:31 residue and the phenalene structure were confirmed.

Another ligand with a very good binding affinity was RM11 ( $\Delta G = -13.1 \text{ kcal mol}^{-1}$  specifically with receptor 4kl9) which, in its interaction with PDB ID: 4KNE formed convectional hydrogen bonds with ILE: 94 and TYR:100 residues by the  $-\text{NH}$  group on the linker molecule. The fluorine atom on the 2-fluoro-1,3,5-triazine moiety of RM11 formed a convectional bond and a carbon-hydrogen bond with GLY:97 and GLY:96, respectively. The  $-\text{NH}$  functional group on the 1,2,4-triazole was conventionally hydrogen-bonded with ILE:14 residue, while the F atom on 1-fluoro-4-methylphenalene was involved in the formation of hydrogen fluoride (HF) bond with ASP:27 and GLN:28 residues. The phenalene ring was involved in the two types of hydrophobic interactions, i.e., one pi-alkyl with ILE: 94 and two pi-pi stacked interactions with PHE:31 residue. Other hydrophobic interactions were also present, including the alkyl bond between the  $-\text{CH}_3$  of the 3-methylidene and the VAL: 54 residue. In addition, the benzene and the cyclopentadiene rings of the 3-methylidene formed the pi-alkyl and pi-pi stacking interactions with the VAL:54 and LEU:50 residues respectively. Likewise, the cyclopentadiene ring also participated in pi-pi stacked interaction with PRO: 58 residue.

Regarding the complex PDB ID: 4KL9 – RM11 we observed the absence of conventional hydrogen bonds; instead there were unfavorable donor-donor interactions between  $-\text{NH}$  on the triazine moiety and the linker molecule, with the GLY:97 residue. The  $-\text{CH}_3$  of N-methyl-1,2,4-triazole-3-amine in R11 interacted with GLY:18 through carbon-hydrogen bonding. Also witnessed were the pi-alkyl interactions between the phenalene ring and the amino acid residues ILE:14 and ILE:20, additionally, the phenalene ring formed two pi-sigma bonds with ILE:20 and THR:46 residues. Table 3.5 indicated two alkyl bonds formed by the  $-\text{CH}_3$  group of the 3-methylidene and the LEU: 50 and TRP:22 residues. The pi-alkyl interaction between the benzene ring fused with methyl-cyclopentadiene and the ALA:7 residue is all driven by molecule RM11.

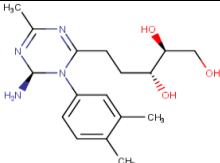
The interaction of compound RM11 with *Mtb-DHFR* PDB ID: 1DG8 receptor was meticulously considered in which ALA:7 and ILE:14 formed convectional hydrogen bonds with  $-\text{NH}$  groups on 1,2,4-triazole moiety. The third and fourth convectional hydrogen bonds were on the amine ( $-\text{NH}$ ) group of the N-methyl-1,2,4-triazole-3-amine bonded with the ILE:94 and on the F-atom attached to the 1,3,5-triazine moiety bonded with THR:46. The other hydrogen bonds included

one carbon-hydrogen bond on the F-atom attached to the 1,3,5-triazine moiety bonded with GLY:96 residue. The other was a hydrogen fluoride bond on fluoro-4-methylphenalene and GLN:28 residue. The two types of hydrophobic interactions comprised the two pi-pi stacked interactions between the phenalene and PHE:31. The phenalene ring also had pi-alkyl interaction with ILE:94 residue. The benzene ring fused with methyl-cyclopentadiene formed a pi-alkyl bond with VAL:54, and likewise, its adjacent cyclopentadiene was involved in another pi-alkyl bond with ARG:32 residue.

#### 4.6 Selectivity Studies

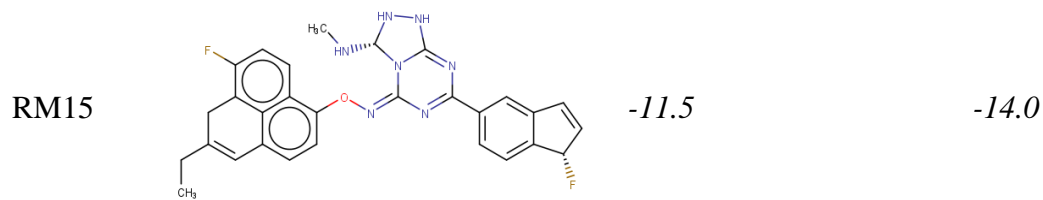
In this section, we looked at molecules designed to hypothetically mimic the binding of methotrexate inside the binding pocket of *Mtb*-DHFR. The 1,2,3-triol was attached to the non-triazine moiety in each of these molecules to optimize and amplify *Mtb*-DHFR selectivity. Due to their possession of the 1,2,3-triol group, these molecules are anticipated to favor the binding of *Mtb*-DHFR over h-DHFR since it is believed that the *Mtb*-DHFR also contains a glycerol binding pocket which is absent in h-DHFR. Finally, we displayed in table 4.8 the six newly designed molecules with a 1,2,3-triol attached to them, eleven (11) prequalified drug-like molecules, and the reference isoniazid together with the two starter designing molecules (THT1 & THT2).

Table 4. 8: Virtual screening of the glycerol mimicking molecules and the prequalified drug-like molecules to evaluate their selectivity properties towards h (human) DHFR (PDB ID: 1OHJ) and *Mtb*-DHFR (PDB ID: 1DG8)

Name	Structure	<i>h</i> -DHFR		<i>Mtb</i> -DHFR	
		Binding Affinity ( $\Delta G$ Kcal mol <sup>-1</sup> )	Binding Affinity ( $\Delta G$ Kcal/mol <sup>-1</sup> )	Binding Affinity ( $\Delta G$ Kcal/mol <sup>-1</sup> )	Binding Affinity ( $\Delta G$ Kcal/mol <sup>-1</sup> )
GM1		-8.4		-8.6	



GM6		-8.8	-9.7
GM12		-10.3	-10.3
RF02		-12.1	-14.0
RF28		-11.3	-14.1
RF43		-10.4	-13.1
RF56		-10.7	-13.2
RM11		13.0	-13.0



*Note:* A synergistic exploit of structural modification to improved affinity toward the target, and modification to disfavor or lower affinity toward off-target would greatly improve selectivity.

Many compounds in table 4.8 showed higher binding affinity towards *Mtb*-DHFR, suggesting that compounds will select *Mtb*-DHFR as their target over *h*-DHFR. Among all glycerol-mimicking compounds, GM10 (structure and interactions in figure 4.10) had the highest selectivity score marked by the big difference or gap in its binding energy between both *h*-DHFR and *Mtb*-DHFR. Compound RM11 and GM 13 showed similar binding affinity towards both *h*-DHFR and *Mtb*-DHFR, and this probably suggests similar selectivity to both targets. However it is possible to realize two different compounds have similar affinities but different selectivity profiles, owing to the fact that different forces can establish different thermodynamic profiles; therefore, it is imperative to master the reasons behind such peculiar discrepancies (Kawasaki, & Freire, 2011), and additionally *in vivo* selectivity studies are therefore crucial to validate these *in-silico* findings.

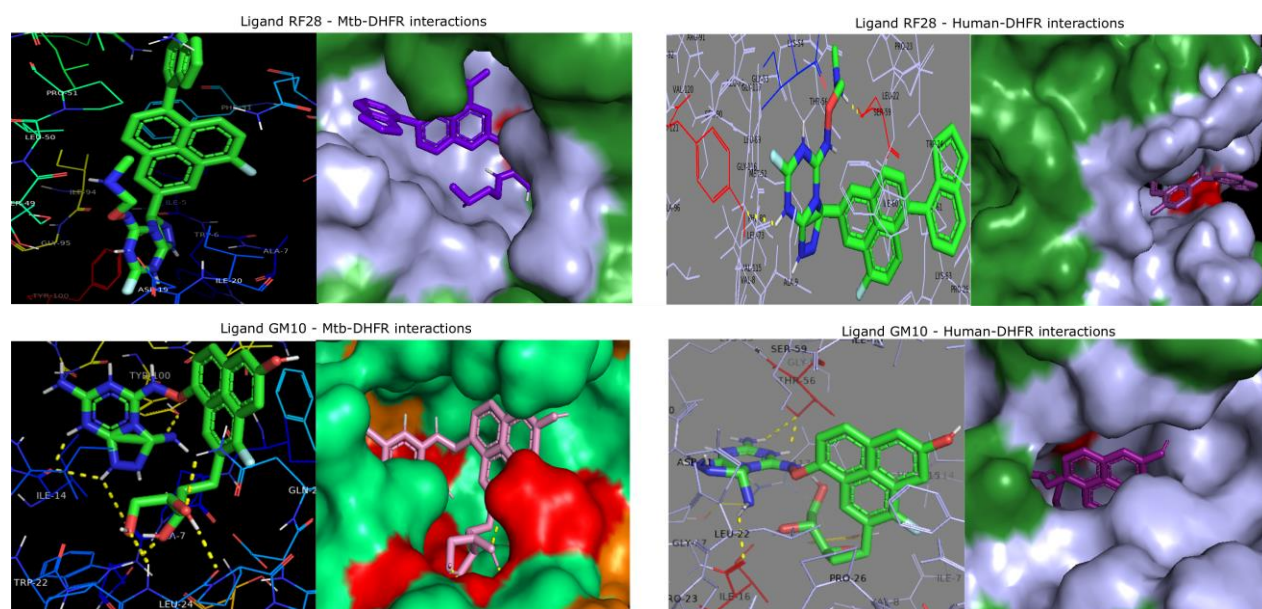


Figure 4. 10: Complex structures of MtbDhfr and humanDhfr with molecule (ligand) GM10 and RF28

Compound GM10 formed many interactions with *Mtb*-DHFR than with *h*-DHFR (figure 4.10) which contributed to its higher affinity for *Mtb*-DHFR even though the forces that contribute to binding affinity do not always contribute equally to selectivity. A tight fit between the ligand and its binding target not only maximizes van der Waals interactions but also reduces the probability that the ligand will be accommodated equally well in off-target molecules. Affinity gains with off-target proteins will not be as significant as with the target. In figure 4.10, we noticed molecule GM10 establishing more hydrogen bonds with *Mtb*-DHFR compared with *h*-DHFR, this observation can be attributable to an increase in selectivity since hydrogen bonds are also significant contributors to selectivity owing to their stringent distance and angle constraints. Ultimately, isoniazid, THT1 and THT2 confirmed greater affinity to *h*-DHFR suggesting that their interactions favored *h*-DHFR selectivity.

We also compared our designed compounds with the reference ligand in terms of the binding affinity and selectivity. From table 4.9, it can be seen the reference ligand used had good binding affinity. However, according to the observed docking scores, it can be inferred that NSC-339579 had slightly poor selectivity toward *Mtb*DHFR. Compared to the designed compounds of this research, NSC-339979 falls below compounds such as RF02, RM15, etc., which had excellent binding energy around -14.1 kcal/mol.

Table 4. 9: Binding affinity and some druglike properties of the reference ligand, NSC-339579

<i>Mtb</i> DHFR (kcal/mol)		Human-DHFR (kcal/mol)	
Macromolecule PDB IDs:			
4KNE	4KL9	1DG8	1OHJ
-9.1	-9.3	-10.1	-10.0
Some Druglike Properties			
TPSA	MRcons	CYP450 inhibition	Lipinski Rule of 5

		2 isoforms:	
128.57 Å <sup>2</sup>	98.41	CYP1A2	0 Violations
		CYP2D6	

---

NSC-339599 also exhibited excellent druglike properties, with its TPSA and MRcons values falling within the acceptable range. NSC-339599 also proved perfect obedience to the Lipinski rule of five, meaning it can be highly recommended for oral administration if developed into a drug. However, NSC-339599 was found inhibitory to the two CYP450 isoforms i.e. CYP1A2 and CYP2D6. Moreover, these good druglike properties (table 4.9) together with its reported IC<sub>50</sub> value (IC<sub>50</sub> = 6 nM, NSC-339599 can be justified in its use as a reference compound in this study.

#### 4.7 Molecular Dynamics

Molecular Dynamics (MD) Simulations were conducted through GROMACS 2022 software packages supported by NVIDIA GeForce GT 730 graphics card in Linux Ubuntu 22.10.

In Molecular Dynamics (MD) simulation in this study, atoms and molecules interacted as a function of time (ns) making MD an ideal computer-aided drug discovery (CADD) approach for the analysis of the dynamic behavior of complex systems. RMSD, RMSF, Rg, and the number of intermolecular Hydrogen bonds were the structural parameters used to evaluate the stability, flexibility, dynamic behavior and compactness of the ligand-protein complexes.

The protein-ligand complex of DHFR-AS100 was found in the range of 0.000578 nm – 0.243996 nm with an average of 0.173629 nm for the ligand (AS100) after least square fit to protein backbone, 0.000559 nm – 0.173629 nm with an average of 0.105358 nm for ligand AS100 alone and, 0.000596 nm – 1.485432 nm with an average of 0.994 nm for Dhfr-AS100 complex (Figure 4.11a). These observations have confirmed the stability of the *Mtb*Dhfr-AS100 complex without any major changes in orientation.

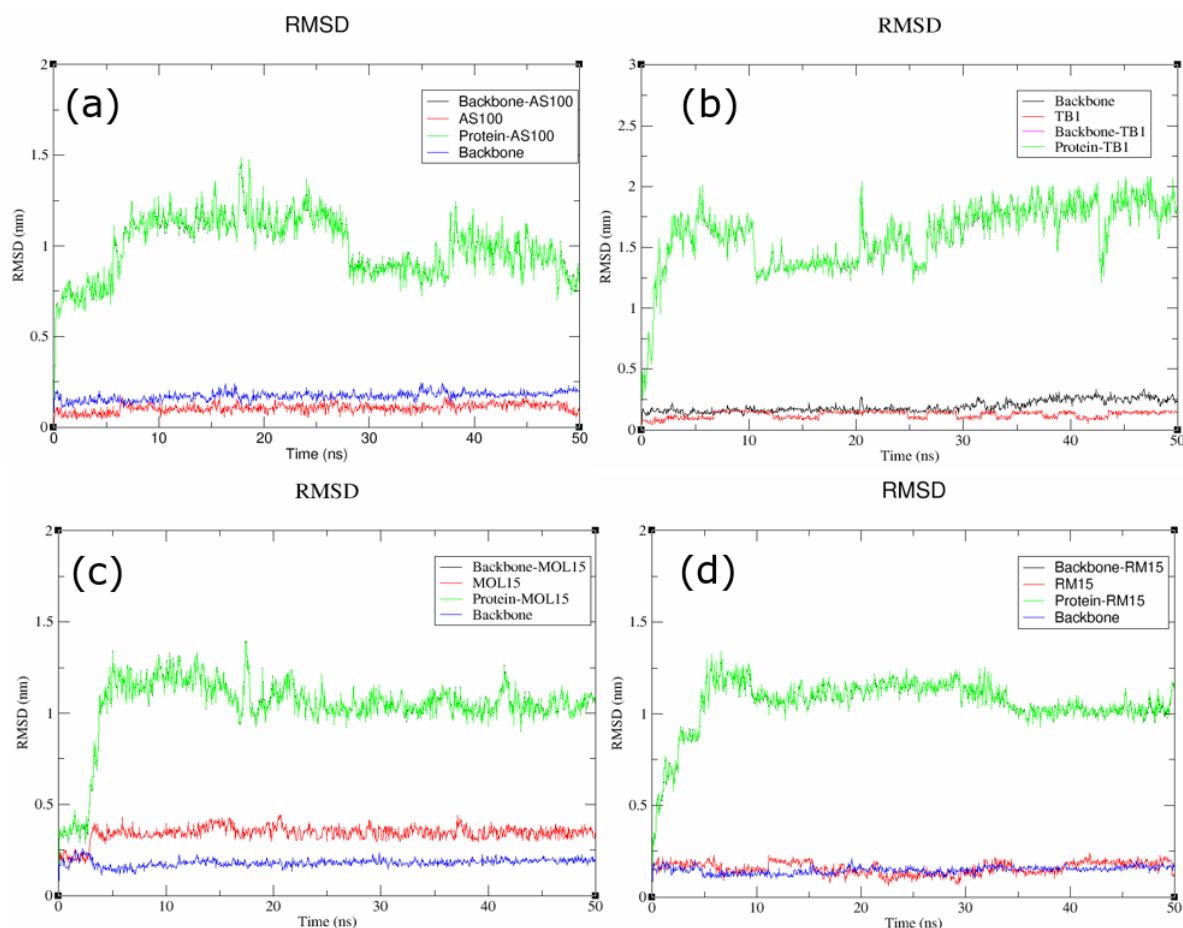


Figure 4.11: RMSD as a function of 50 ns MD simulation time of schematic plots for docked complexes (a) MtbDHFR-AS100, (b) MtbDHFR-MOL15, (c) MtbDHFR-TB1, and (d) MtbDHFR-RM15.

Figure 4.11(b) displays the least square fit RMSD of ligand (TB1)-backbone complex, and protein-TB1 complex for *MtbDhfr*-TB1 complex for a 50ns time-dependent MD simulation run. For the Backbone-TB1 complex, the RMSD ranged from 0.000513 nm – 2.107266 nm with an average of 1.596241 nm, while it ranged from 0.000472 nm – 0.162572 nm with an average of 0.124874 nm for ligand (TB1), and protein-TB1 range 0.000507 nm – 2.106764 nm with an average 1.599284 nm. Figure 4.11(c) considered the stability of the *MtbDhfr*-Mol15 complex during a 50ns simulation time in which the complex was found in the range of 0.000492 nm – 1.39455 nm with an average of 1.035366 nm for Backbone-MOL15, 0.000471 nm – 0.445705 nm with an average of 0.341571 nm for the ligand MOL15 itself, and protein-mol15 ranged from 0.000491nm – 0.13915 nm with an average of 1.035023 nm. The final protein-ligand complex (Figure 4.11(d)), *Mtb*:Dhfr-RM15 was found to range from 0.000518 nm – 0.211559 nm for Backbone-RM15, 0.000489 nm – 0.239329 nm with an average of 0.157472 nm for the ligand (RM15) alone, and

0.000512 nm – 1.338172 nm having an average of 1.059586 nm for protein-ligand (*MtbDhfr*-RM15) complex. The RMSD plots of compounds AS100 and RM15 overlay with their protein backbone, it is, therefore, apparent to infer stable complex formation.

For the complexes *MtbDhfr*-TB1 and *MtbDhfr*-MOL15 in figure 4.11(b) and 4.11(c) respectively, there is an overlaying or superimposition between the protein-ligand and backbone-ligand suggesting the two complexes have similar stabilities.

Considering the above mentioned average RMSD values for the selected four ligands, the ligands followed the following trend in terms of their stabilities: AS100 > TB1 RM15 > MOL15. This implies that ligand AS100 formed the most stable interactions in the active site of the *MtbDHFR* receptor target (PDB ID: 1DG8).

#### **4.7.1 Root mean square fluctuation (RMSF)**

Through the root mean square fluctuation (RMSF) (figure 4.12), we evaluated the structural integrity and atomic mobility of the four selected complexes. For the RMSF analysis, we calculated and plotted the RMSF value in nanometers and plotted against the residue number. The fluctuations of backbone-ligand complexes figure 4.12(b) and individual ligand figure 4.13 structures were assessed for 50 ns simulation trajectories. The Backbone-AS100 showed an average RMSF value of 0.090 nm, Mol15 had an average value of 0.0912nm, RM15 had an average value of 0.0911 nm, and 0.107 nm in the backbone RMSF. These lower fluctuation values indicate high or very significant stabilities when the lead compounds interact with the *MtbDHFR* receptor.

Again protein-ligand AS100 proved to be the most stable lead molecule over the simulation time as supported by its lowest average RMSF value of 0.090nm (Figure 4.12b) among other complexes. However high fluctuation up to 0.3277 nm was observed on AS100-Backbone but only during the initial stages around residue position 51 along the simulation period as the fluctuation turned minimal for the rest of the MD simulation time.

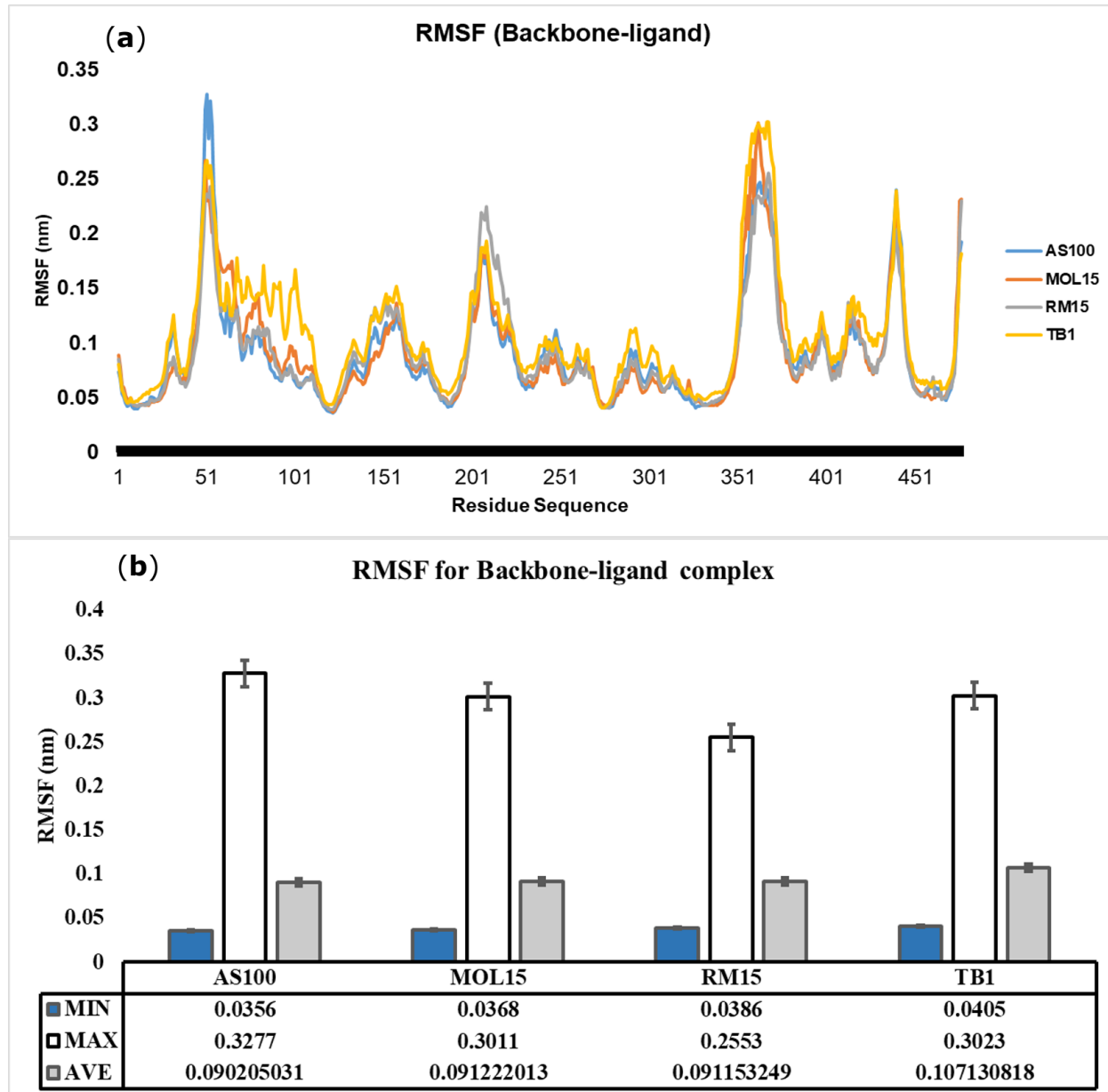


Figure 4. 12: Root mean square fluctuation (RMSF) graph (Fig 4.12a) showing minimum, maximum and average RMSF (Fig 4.12b) of Mtb-DHFR target when complexed with selected (4) ligands during a 50 ns Molecular dynamics (MD) simulation time.

In terms of atomic mobility and stability of the four complexes, the following trend can be inferred: AS100 > RM15 > MOL15 > TB1, suggesting that the TB1 complex is more flexible. The observed fluctuations can therefore be considered negligible since they fall in the permissible range of around 1 – 3Å. The RMSF plots in figure 4.12a seem to superimpose on one another, thereby inferring the high stability of the understudy complexes.

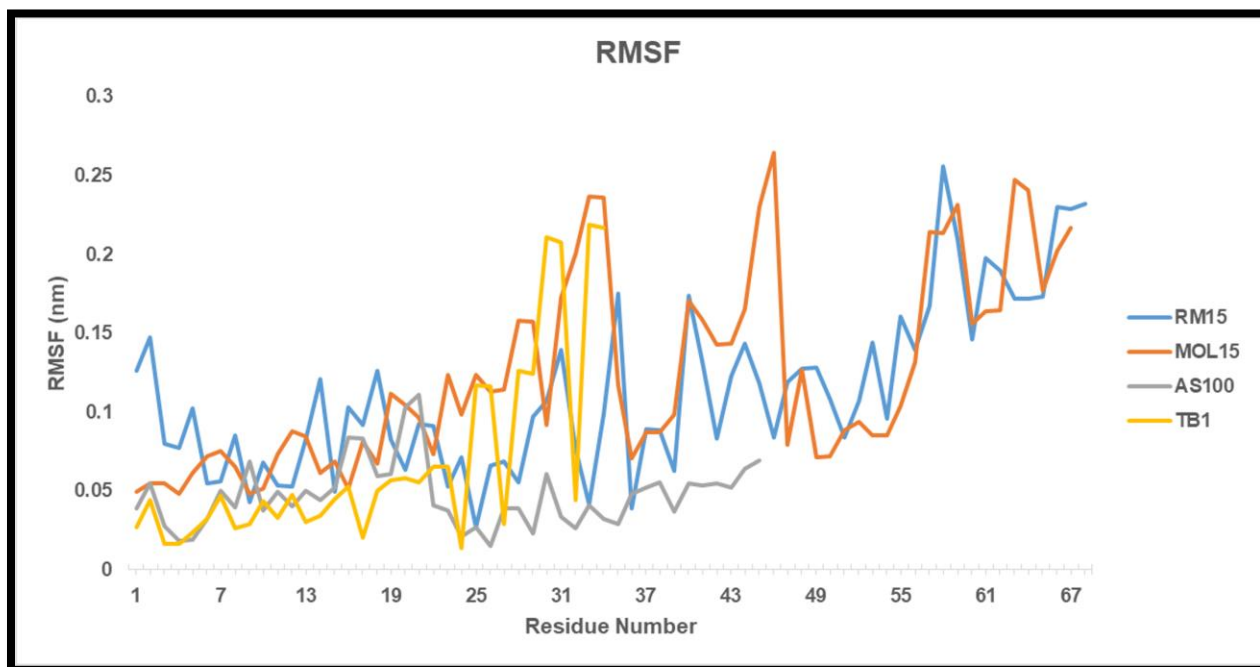


Figure 4. 13: Root mean square fluctuation (RMSF) for ligands

The root mean square fluctuation (RMSF) for the four ligands shown in figure 4.13 was calculated and plotted against the residue number. The average fluctuation for RM15, MOL15, AS100, and TB1 has been found in the range 0.112549, 0.123473, 0.047371, and 0.068926 nm. MOL15 had the highest fluctuation of 0.2646 nm around 43 – 49 residue number. In general, all ligands made minor fluctuations suggesting little to moderate flexibilities and high stabilities within their complexes in the active site of the *Mtb*-DHFR target.

#### 4.7.2 The radius of gyration, Rg

The radius of gyration was also evaluated to investigate the level of compactness of the *Mtb*-DHFR (PDB 1D: 1DG8) protein in the presence and absence of the prequalified ligands (leads). Here the radius of gyration (Rg) analysis reveals information about the folding and unfolding properties of the MtbDHFR protein receptor and also the MtbDHFR-ligand structure.

As shown in figure 4.14, all complexes formed a balanced and steady radius of gyration (Rg) with an average of approximately 0.3nm for Protein-RM15 which was the most compact over 50ns MD simulation. Complexes protein-AS100, Protein-TB1, and Protein-MOL15 were all stable at ~1.6 nm (figure 4.14b). These inferences confirm that the



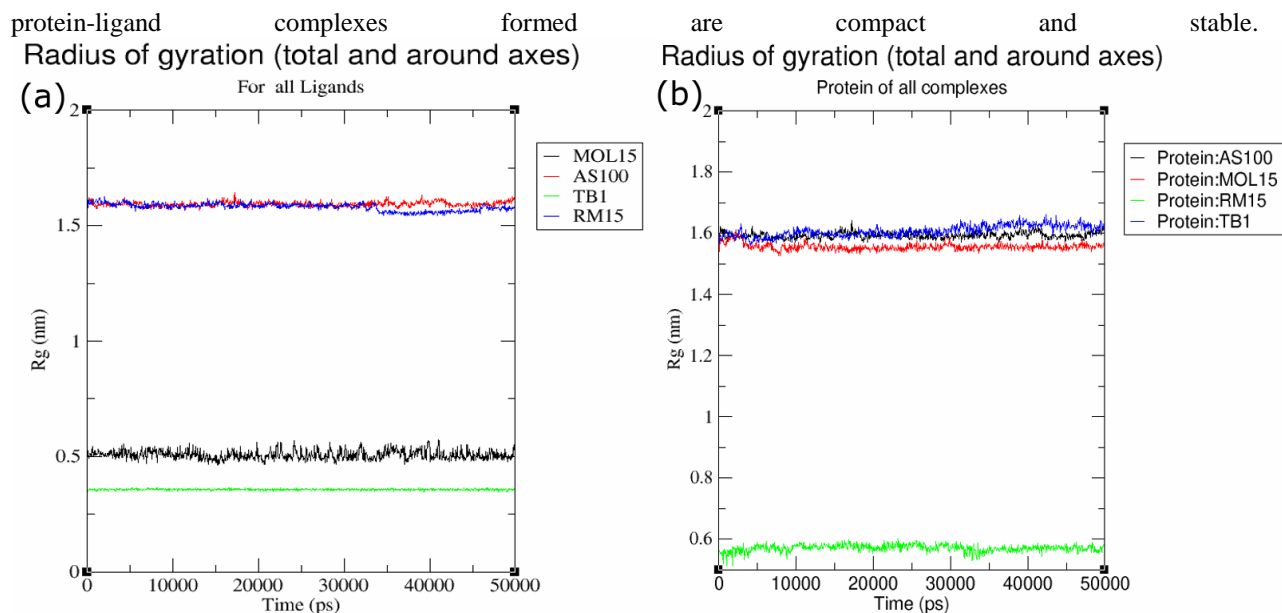


Figure 4. 14 : The radius of gyration (Rg) for ligands (a) and for protein (b) to which ligands bound during a 50 ns MD Simulation period.

In general, the observations proved protein stability boost upon binding of the ligands.

### 4.7.3 Hydrogen bonds Analysis

The stabilization of the secondary and tertiary structure of protein structure is provided and sustained hydrogen bonds. In molecular dynamics simulations, the binding affinity of the ligand to its target is well clarified or elucidated by the formed hydrogen bonds. This observation led to a statement generalized by Menendez et al. (2016) states that the more the number of hydrogen bonds formed, the stronger the binding affinity of the ligand to its target. Figure 4.15 showed the number of hydrogen bonds formed by all selected four ligands during a 50 ns MD Simulation time.

For ligand AS100, a maximum of five hydrogen bonds were formed during a molecular dynamic simulation of 50 ns. Ligand AS100 consistently formed two and three hydrogen bonds around 30 – 35 ns. Ligand MOL15 formed up to seven hydrogen bonds in the active site of DHFR protein. Moreover, MOL15 formed four hydrogen bonds more frequently for a very long time from around five ns to 50 ns dynamic simulation time. Up to three and two hydrogen bonds were formed (at the beginning of the dynamic simulation) at 0.0 and 0.2 ns, respectively by RM15 in the active site of *Mtb*DHFR protein target. Throughout the 50 ns simulation time, RM15 dominantly formed one

hydrogen bond. Ligand TB1 also formed three hydrogen bonds which appeared briefly around 42 ns, and one hydrogen bond frequently appeared during the 50 ns.

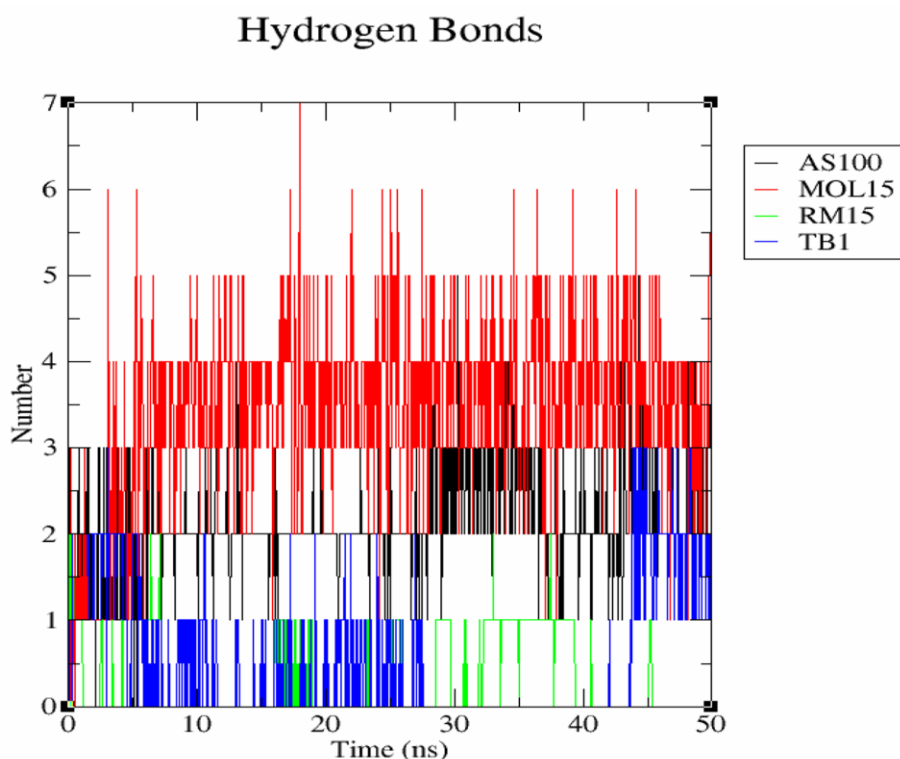


Figure 4. 15: The total number of hydrogen bonds between MtbDHFR protein and ligands AS100, MOL15, RM15, and TB1

The ligand MOL15 (figure 4.16) formed more hydrogen bonds (7) with an average of 3.443, AS100 formed an average of 2.1399 hydrogen bonds, while 0.5584 were formed by ligand TB1, and RM15 formed the least at an average of 0.2737.

In general, the complexes formed many hydrogen bonds, which explains the reasons behind the low fluctuations and high stability of the complexes. These results support excellent binding affinities of these four ligands as observed earlier by molecular docking.

#### 4.7.4 The outcomes of carbodiimide coupling using DCC

Figure 4.16 below is the illustration of the reaction mechanism. During synthesis as the reaction matrix was in reflux stage, a sweet/fruit-smelling odor evolved and confirmed successful formation

of an ester anticipated in figure 4.16. The persistent fruit smelling smell (pointing to the smell) gave optimism for the successful progress of the reaction.

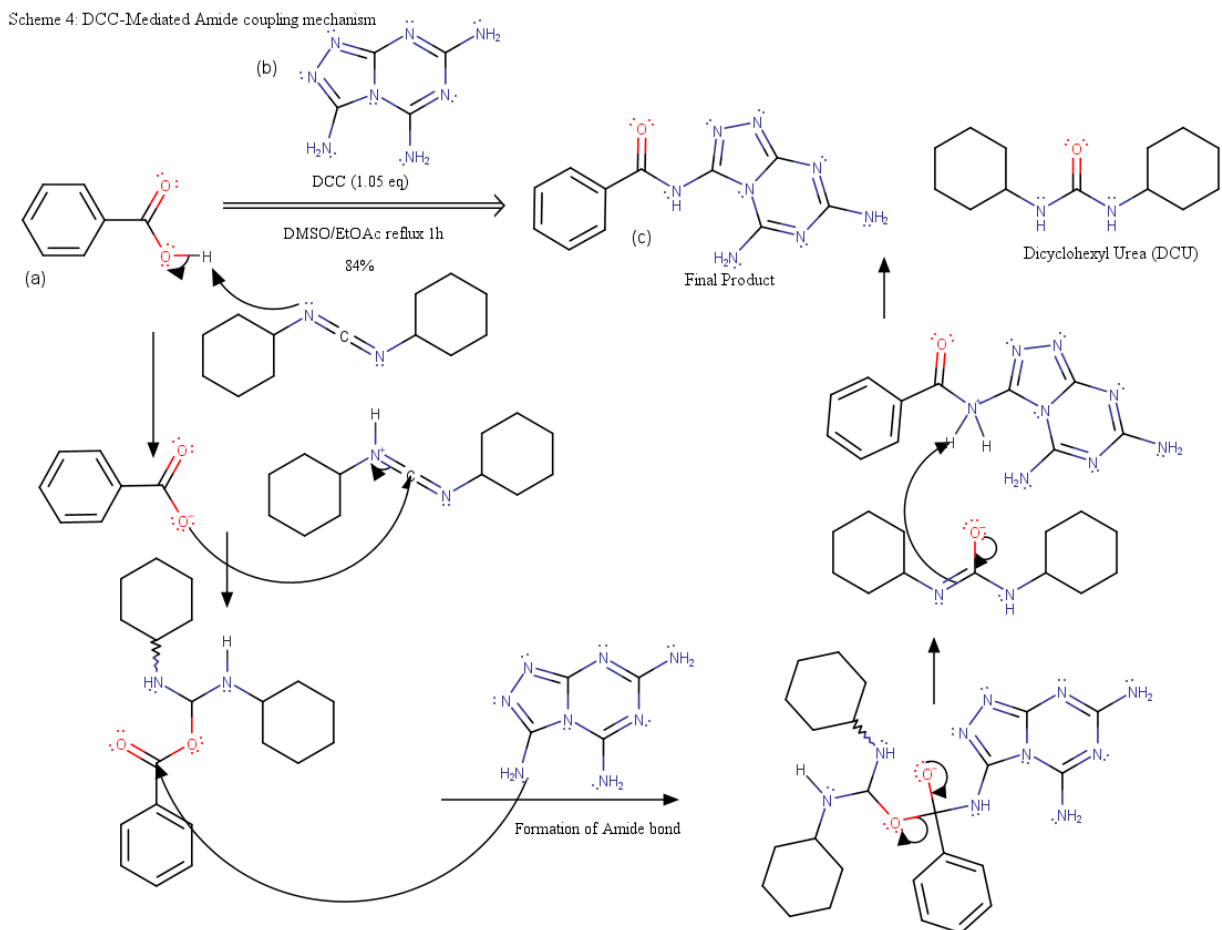


Figure 4. 16: Scheme for the DCC-Mediated Amide coupling reaction mechanism

It was also discovered that, a four (4) hour attempts to remove DMSO by concentrating in a rotary evaporator proved a futile exercise owing to the high boiling point of DMSO (189°C) regardless of the high-temperature (120°C) water bath. In several attempts to achieve crystallization it was also rediscovered that crystallization is difficult to form in DMSO (Wu et al., 2014), however, the needle-like shaped crystals eventually appeared in the Erlenmeyer flask after four days. We also realize that crystallization can occur and easier in n-BuOH - EtOAc solvent mixture when the product was left just for over a night. The mentioned observations were similar for both synthesized compounds, AZ01 and AZ02.

Table 4. 10: Characteristics of the compounds crystals

Compound	% Yield	Appearance
AZ_01	74	Uniform long needle-like transparent crystals
AZ_02	67	Uniform irregular crystals
UNK	46	Fine needle like transparent crystals

The distinction between the crystals in terms of shape was attributed to the different identities the synthesized compounds, with of AZ01 formed needle-shaped crystals while AZ02 produced irregular-shaped crystals. Each reaction process was performed in triplicate for each compound (i.e. AZ01 & AZ02) being synthesized, producing same and very consistent results including a percentage yield of 74% and 67% respectively conferring reproducibility and validation of the synthetic routes or protocols. However, for compound AZ01, crystallization proved difficult for the applied procedure promoting modification of the procedure by introducing column chromatography. After column chromatography, only two out of six collected fractions appeared with crystals but of different shape suggesting AZ01 coexisted with another compound (suspected to be DCU) before separation by column chromatography. As a result, all samples for the attempted synthesis were sent to the Holistic Drug Discovery and Development (H3D) center in Cape Town, South Africa for further experimentation such as for proton and carbon nuclear magnetic resonance (C/H-NMR) spectroscopy and also biological assays.

## CHAPTER 5

### CONCLUSION

Under the major deliverables of this study, we have managed to leverage suitable scientific knowledge, approaches, and techniques to generate a 1700-capacity compound library of 1,3,5-triazine derivatives. Among other attributes of a good drug, we reported in this study the exploitation of the key distinguishing features between the binding sites of *Mtb*DHFR and *human*DHFR enzymes in pursuit to address the question of selectivity against the two enzyme receptors. These selectivity studies enabled the design of compounds such as GM10 that were *Mtb*DHFR target specific or selective. In general, many compounds greatly favored *Mtb*DHFR inhibition than *human*DHFR and this predicted successful selectivity. Central to the optimization stage during design was the inclusion and linking of -C<sub>6</sub>H<sub>5</sub>NH<sub>2</sub> group to the non-triazine moiety of the starter molecules (THT1 & THT2) via Structure-Activity Relationship (SAR), which yielded compounds such as KTHT1 and MTHT1 which had better binding energies. Another designing strategy i.e. 1° and 2° scaffold hopping techniques yielded compounds with the most significant binding affinities across the whole library of which 2° scaffold-hopping generated compounds with novel scaffolds compared to 1° hop. Virtual screening across three macromolecular receptors of *Mtb*DHFR accomplished by AutoDock vina was successfully done with intense inquisitive to reveal the characteristics of the library in terms of biological activity, binding affinity, and selectivity. Another important factor that was considered was the synthetic accessibility (SA) and in this respect, all the prequalified shortlisted ligands had synthetic accessibility scores (SAscore) less than 6.5 denoting the feasibility and ease of synthesis of these ligands. In relation to selectivity, we saw ligands exhibit their selectivity towards *Mtb*-DHFR rather than human DHFR. *In-silico* ADMET prediction studies were successfully done where we were able to identify lead or drug-like compounds with an acceptable toxicity profile. The ADMET profile of the prequalified molecules showed that molecules can progress further in the TB drug-

discovery pipeline. The shortlisted compounds showed better drug-like and pharmacokinetic properties than the reference ligands (NSC-339579 and isoniazid) and starter molecules THT1 & THT2 hence potential anti-tubercular molecules. The stability verification of the *MtbDHFR* enzyme in complex four lead compounds was navigated and determined through the 50 ns MD simulations which also confirmed that the structure formed several hydrogen bonds with the amino acids in the binding site. Lastly, the final objective which required the synthesis of the prequalified molecule 1,3,5-triazine derivative was carried out, paving the way for further exploration and experimentation work such as biological assays and potentially preclinical testing.

This study is a stepping stone to the establishment of a validated and quintessential protocol for the design and synthesis of tetrahydro-1-3-5-triazine derivatives and a data-set for novel bioactive compounds that can be modified into anti-tuberculosis drugs. Furthermore, the inter-disciplinary project could advance basic science at CUT and boost molecule design and synthesis in addition to encouraging inter-disciplinary collaborations. Part of the research work was published in the *Frontiers in Molecular Biosciences Journal*. Two manuscripts have been submitted for publication and are currently under peer review. To further communicate the research findings, a poster presentation was done during the International Symposium at the H3D Organization (the pioneers of drug discovery in Africa) held at the Webersburg Estate, in the Stellenbosch winelands over the period 25-28 October 2022.

Conclusively it is imperative to mention that 1,3,5-triazine scaffolds holds a great promise to the design of novel effective anti-TB leads and certainly are a beacon of hope for the eradication of this global burdensome TB disease.

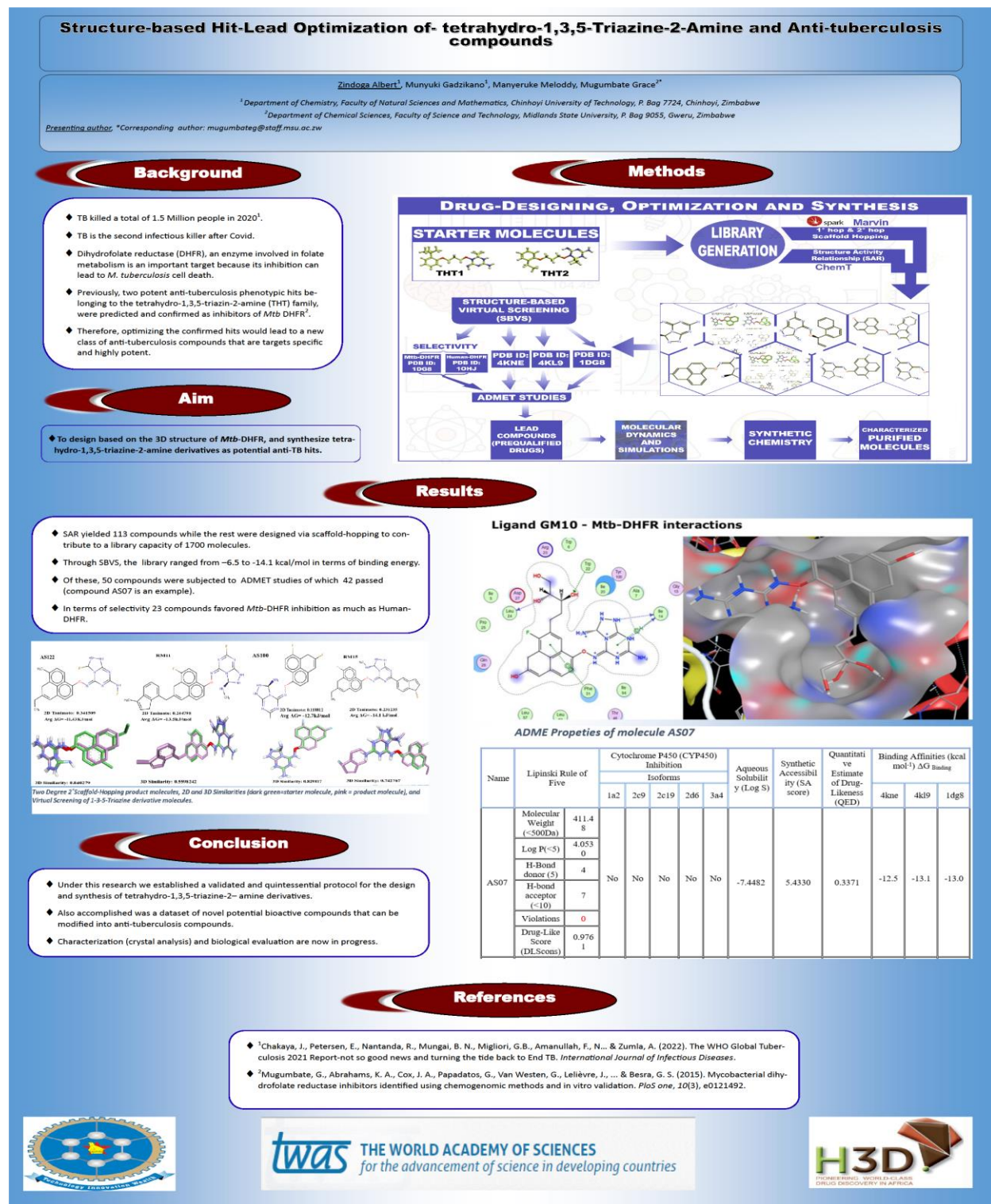
## **5.1 Recommendations and Future Work**

While the tetrahydro 1,3,5-triazine derivatives have presented excellent binding affinity against *MtbDHFR*, it can be recommended that medicinal chemists pay much attention and dedicate more time and efforts to developing of new series of tuberculosis drugs. Noticing the potential emanating from this research deliverables, Chinhoyi University of Technology should acknowledge and promote the arena of drug discovery and development since it is still new and foreign to many faculties and even to the school of natural sciences and mathematics at CUT. More interdisciplinary collaborations are also recommended across Africa and beyond, as this can make

wider strides in the direction of eradicating this burdensome tuberculosis. From the design point of view, it is imperative that we also consider other triazine-based scaffolds such as 1,2,3- triazine, and 1,2,4- triazine as this may also be another source of novel bioactive leads. While only two compounds were synthesized from a whole-generated library capacity of 1 700 compounds, we should as a matter of urgency consider as part of our future work to synthesize and carry out biological evaluations of many other promising compounds to maximize the probability of success in finding an improved and more safe TB drug. Alternatively other than structure-based techniques, our future research should embrace ligand-based drug design approaches such as pharmacophore modeling, quantitative structure-activity relationship, etc. We also recommend and propose as future work that more than 50 ns (e.g. 200ns) molecular dynamics be done to fully understand the bioactive stability of the compounds inside the binding site of the *MtbDhfr* target, and also molecular mechanics be carried out to understand actual binding energy of these ligands thus generating more accurate *in-silico* predictions in drug discovery research expedition.

# APPENDICES

## 5.2 Appendix A: Poster presentation









### 5.3 Appendix B: Research Paper

#### Application of Computational Methods in Understanding Mutations in Mycobacterium tuberculosis Drug Resistance

Full-text available

Article

Sep 2021

 Grace Mugumbate ·  Brilliant Nyathi ·  Albert Zindoga ·  Gadzikano Munyuki

The emergence of drug-resistant strains of Mycobacterium tuberculosis (Mtb) impedes the End TB Strategy by the World Health Organization aiming for zero deaths, disease, and suffering at the hands of tuberculosis (TB). Mutations with...

Download

Share

1 Recommendation · 139 Reads · 4 Citations

## 5.4 Appendix C: Manuscript

Structure-Based Hit-Lead optimization of Tetrahydro-1,3,5-Triazine-2-amine derivatives as inhibitors of *Mycobacterium tuberculosis* DHFR and anti-tuberculosis compounds.

Zindoga Albert<sup>1\*</sup>, Munyuki Gadzikano<sup>1</sup>, and Mugumbate Grace<sup>2</sup>

<sup>1</sup> Department of Chemistry, Faculty of Natural Sciences and Mathematics, Chinhoyi University of Technology, Chinhoyi, Zimbabwe

<sup>2</sup> Department of Chemical Sciences, Faculty of Science and Technology, Midlands State University, P. Bag 9055, Gweru, Zimbabwe

\*Corresponding Author: [chemialbert@gmail.com](mailto:chemialbert@gmail.com), [mugumbateg@stuff.msu.ac.zw](mailto:mugumbateg@stuff.msu.ac.zw)

### Abstract

Among several *Mycobacterium tuberculosis* potential drug targets, Dihydrofolate Reductase (DHFR) a key enzyme involved in folate metabolism is an important target in which its inhibition results in mycobacterial cell death. Several successful antifolates against infectious diseases exist, but none have been developed to combat tuberculosis. Previously, two potent anti-tuberculosis phenotypic hits belonging to the tetrahydro-1,3,5-triazine-2-amine (THT) family, were predicted and confirmed as inhibitors of *Mtb* DHFR. Therefore, optimizing the confirmed hits would lead to a new class of anti-tuberculosis compounds that are targets specific and highly potent.

**Aim:** To design based on the 3D structure of *Mtb*-DHFR, and synthesize tetrahydro-1,3,5-triazine-2-amine derivatives as potential anti-TB hits.

**Methods and Findings:** Structure-activity relationship (SAR) was applied to design 113 tetrahydro-1,3,5-triazine-2-amine based on the 3D structure of *Mtb*-DHFR, using the by ChemT

## 5.5 Appendix D: Book Chapter

### Structure-Based Hit-Lead optimization of Tetrahydro-1,3,5-Triazine-2-amine derivatives as inhibitors of *Mycobacterium tuberculosis* DHFR and anti-tuberculosis compounds

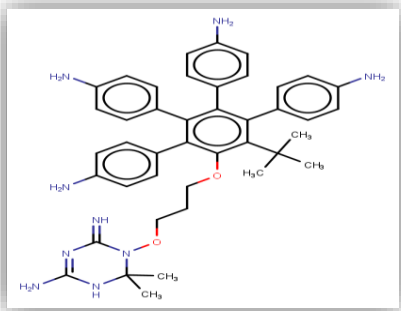
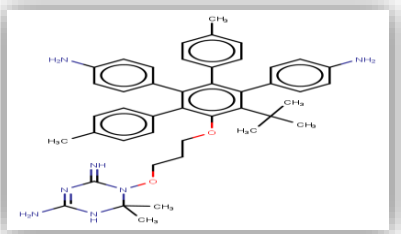
Zindoga Albert<sup>1\*</sup>, Munyuki Gadzikano<sup>1</sup>, and Mugumbate Grace<sup>2</sup>  
Chinhoyi University of Technology, azindoga@cut.ac.zw  
Midlands State University

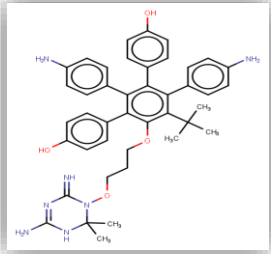
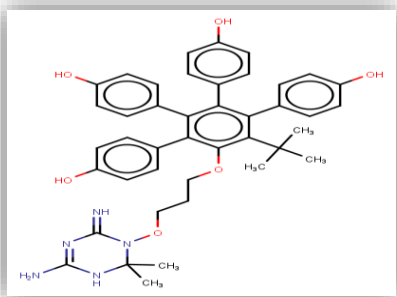
#### Abstract

Several successful antifolates against infectious diseases exist, but none have been developed to combat tuberculosis. Previously, two potent anti-tuberculosis phenotypic hits belonging to the tetrahydro-1,3,5-triazine-2-amine (THT) family, were predicted and confirmed as inhibitors of *MtbDHFR*. Therefore, optimizing the confirmed hits would lead to a new class of anti-tuberculosis compounds that are targets specific and highly potent. The study aims to design based on the 3D structure of *MtbDHFR*, and synthesize tetrahydro-1,3,5-triazine-2-amine derivatives as potential anti-TB hits. Structure-activity relationship (SAR) was applied to design 113 tetrahydro-1,3,5-triazine-2-amine based on the 3D structure of *MtbDHFR*. The rest of the compounds were designed by scaffold hopping to inflate the library to a capacity of 1700 compounds. By considering the key distinguishing features between human-DHFR and *MtbDHFR*, the matter of selectivity was well addressed. The compound library was subjected to virtual screening by Auto-Dock Vina determining binding affinity and best poses for each compound inside *MtbDHFR* binding site. Next, ADMET studies were performed. The carbodiimide, DCC-mediated coupling was used to synthesize two of the pre-qualified compounds. Furthermore, Molecular dynamics (MD) simulations were performed where selected four ligand complexes were confirmed stable. Pleasingly the study demonstrated a successful hit to lead optimization and all compounds were identified with, binding affinities ranging from -6.5 to -14.1 kcal/mol, improved drug-like, and ADMET properties. Two of the high-ranked compounds were synthesized.

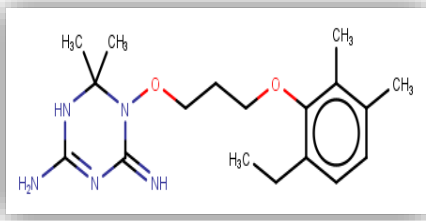
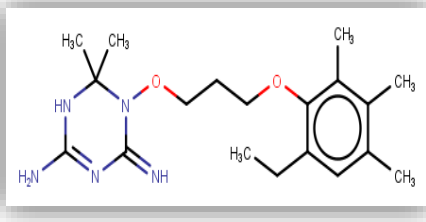
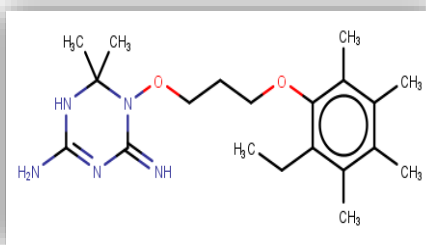
**Keywords:** Computer Aided Drug Design, SAR, Scaffold hopping, ADMET, Molecular Docking, Molecular Dynamics

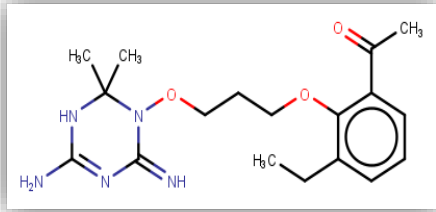
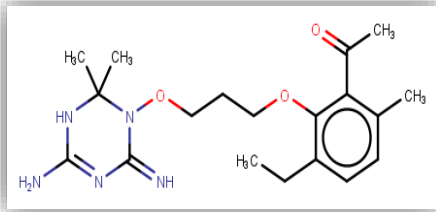
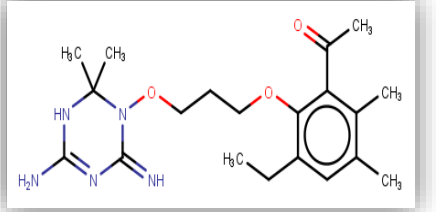
## 5.6 Appendix 1: Structure-Activity Studies

#	Name	Analog Structure	Receptor-Ligand Binding Energy ( $\Delta G$ , Kcal/mol)																		
			4kne	4kl9	1dg8																
			14	NTHT1	<table border="1"> <thead> <tr> <th colspan="4">Substituents</th> </tr> <tr> <th>R<sup>1</sup></th> <th>R<sup>2</sup></th> <th>R<sup>3</sup></th> <th>R<sup>4</sup></th> </tr> </thead> <tbody> <tr> <td>-</td> <td>-</td> <td>-</td> <td>-</td> </tr> <tr> <td>C<sub>6</sub>H<sub>5</sub>NH<sub>2</sub></td> <td>C<sub>6</sub>H<sub>5</sub>NH<sub>2</sub></td> <td>C<sub>6</sub>H<sub>5</sub>NH<sub>2</sub></td> <td>C<sub>6</sub>H<sub>5</sub>NH<sub>2</sub></td> </tr> </tbody> </table> 	Substituents				R <sup>1</sup>	R <sup>2</sup>	R <sup>3</sup>	R <sup>4</sup>	-	-	-	-	C <sub>6</sub> H <sub>5</sub> NH <sub>2</sub>	C <sub>6</sub> H <sub>5</sub> NH <sub>2</sub>	C <sub>6</sub> H <sub>5</sub> NH <sub>2</sub>	C <sub>6</sub> H <sub>5</sub> NH <sub>2</sub>
Substituents																					
R <sup>1</sup>	R <sup>2</sup>	R <sup>3</sup>	R <sup>4</sup>																		
-	-	-	-																		
C <sub>6</sub> H <sub>5</sub> NH <sub>2</sub>	C <sub>6</sub> H <sub>5</sub> NH <sub>2</sub>	C <sub>6</sub> H <sub>5</sub> NH <sub>2</sub>	C <sub>6</sub> H <sub>5</sub> NH <sub>2</sub>																		
15	OTHT1	<table border="1"> <thead> <tr> <th colspan="4">Substituents</th> </tr> <tr> <th>R<sup>1</sup></th> <th>R<sup>2</sup></th> <th>R<sup>3</sup></th> <th>R<sup>4</sup></th> </tr> </thead> <tbody> <tr> <td>-</td> <td>-</td> <td>-</td> <td>-</td> </tr> <tr> <td>C<sub>6</sub>H<sub>5</sub>CH<sub>3</sub></td> <td>C<sub>6</sub>H<sub>5</sub>NH<sub>2</sub></td> <td>C<sub>6</sub>H<sub>5</sub>CH<sub>3</sub></td> <td>C<sub>6</sub>H<sub>5</sub>NH<sub>2</sub></td> </tr> </tbody> </table> 	Substituents				R <sup>1</sup>	R <sup>2</sup>	R <sup>3</sup>	R <sup>4</sup>	-	-	-	-	C <sub>6</sub> H <sub>5</sub> CH <sub>3</sub>	C <sub>6</sub> H <sub>5</sub> NH <sub>2</sub>	C <sub>6</sub> H <sub>5</sub> CH <sub>3</sub>	C <sub>6</sub> H <sub>5</sub> NH <sub>2</sub>	-9.6	-8.2	-7.4
Substituents																					
R <sup>1</sup>	R <sup>2</sup>	R <sup>3</sup>	R <sup>4</sup>																		
-	-	-	-																		
C <sub>6</sub> H <sub>5</sub> CH <sub>3</sub>	C <sub>6</sub> H <sub>5</sub> NH <sub>2</sub>	C <sub>6</sub> H <sub>5</sub> CH <sub>3</sub>	C <sub>6</sub> H <sub>5</sub> NH <sub>2</sub>																		

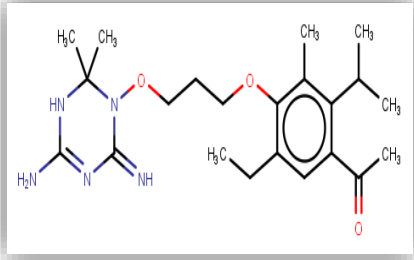
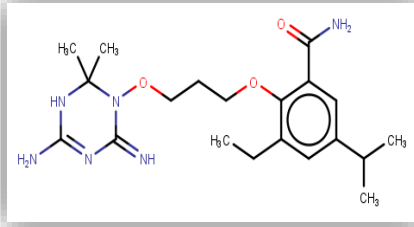
16	PTHT1	<table border="1"> <thead> <tr> <th colspan="4">Substituents</th> </tr> <tr> <th>R<sup>1</sup></th> <th>R<sup>2</sup></th> <th>R<sup>3</sup></th> <th>R<sup>4</sup></th> </tr> </thead> <tbody> <tr> <td>-</td> <td>-</td> <td>-</td> <td>-</td> </tr> <tr> <td>C<sub>6</sub>H<sub>5</sub>OH</td> <td>C<sub>6</sub>H<sub>5</sub>NH<sub>2</sub></td> <td>C<sub>6</sub>H<sub>5</sub>OH</td> <td>C<sub>6</sub>H<sub>5</sub>NH<sub>2</sub></td> </tr> </tbody> </table> 	Substituents				R <sup>1</sup>	R <sup>2</sup>	R <sup>3</sup>	R <sup>4</sup>	-	-	-	-	C <sub>6</sub> H <sub>5</sub> OH	C <sub>6</sub> H <sub>5</sub> NH <sub>2</sub>	C <sub>6</sub> H <sub>5</sub> OH	C <sub>6</sub> H <sub>5</sub> NH <sub>2</sub>	-9.3	-8.8	-7.7
Substituents																					
R <sup>1</sup>	R <sup>2</sup>	R <sup>3</sup>	R <sup>4</sup>																		
-	-	-	-																		
C <sub>6</sub> H <sub>5</sub> OH	C <sub>6</sub> H <sub>5</sub> NH <sub>2</sub>	C <sub>6</sub> H <sub>5</sub> OH	C <sub>6</sub> H <sub>5</sub> NH <sub>2</sub>																		
17	QTHT1	<table border="1"> <thead> <tr> <th colspan="4">Substituents</th> </tr> <tr> <th>R<sup>1</sup></th> <th>R<sup>2</sup></th> <th>R<sup>3</sup></th> <th>R<sup>4</sup></th> </tr> </thead> <tbody> <tr> <td>-</td> <td>-</td> <td>-</td> <td>-</td> </tr> <tr> <td>C<sub>6</sub>H<sub>5</sub>OH</td> <td>C<sub>6</sub>H<sub>5</sub>OH</td> <td>C<sub>6</sub>H<sub>5</sub>OH</td> <td>C<sub>6</sub>H<sub>5</sub>OH</td> </tr> </tbody> </table> 	Substituents				R <sup>1</sup>	R <sup>2</sup>	R <sup>3</sup>	R <sup>4</sup>	-	-	-	-	C <sub>6</sub> H <sub>5</sub> OH	C <sub>6</sub> H <sub>5</sub> OH	C <sub>6</sub> H <sub>5</sub> OH	C <sub>6</sub> H <sub>5</sub> OH	-9.6	-8.7	-7.5
Substituents																					
R <sup>1</sup>	R <sup>2</sup>	R <sup>3</sup>	R <sup>4</sup>																		
-	-	-	-																		
C <sub>6</sub> H <sub>5</sub> OH	C <sub>6</sub> H <sub>5</sub> OH	C <sub>6</sub> H <sub>5</sub> OH	C <sub>6</sub> H <sub>5</sub> OH																		
18	RTHT1	<table border="1"> <thead> <tr> <th colspan="4">Substituents</th> </tr> <tr> <th>R<sup>1</sup></th> <th>R<sup>2</sup></th> <th>R<sup>3</sup></th> <th>R<sup>4</sup></th> </tr> </thead> <tbody> <tr> <td>-</td> <td>-</td> <td>-</td> <td>-</td> </tr> <tr> <td>-</td> <td>C<sub>6</sub>H<sub>5</sub>CH<sub>3</sub> (fused)</td> <td>-</td> <td>C<sub>6</sub>H<sub>5</sub>CH<sub>3</sub> (fused)</td> </tr> </tbody> </table>	Substituents				R <sup>1</sup>	R <sup>2</sup>	R <sup>3</sup>	R <sup>4</sup>	-	-	-	-	-	C <sub>6</sub> H <sub>5</sub> CH <sub>3</sub> (fused)	-	C <sub>6</sub> H <sub>5</sub> CH <sub>3</sub> (fused)	-9.9	-9.6	-10.3
Substituents																					
R <sup>1</sup>	R <sup>2</sup>	R <sup>3</sup>	R <sup>4</sup>																		
-	-	-	-																		
-	C <sub>6</sub> H <sub>5</sub> CH <sub>3</sub> (fused)	-	C <sub>6</sub> H <sub>5</sub> CH <sub>3</sub> (fused)																		

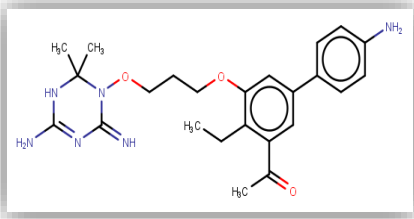
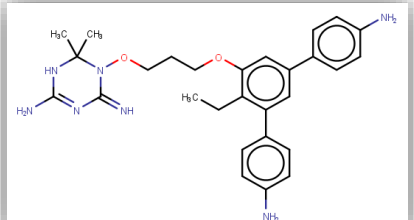
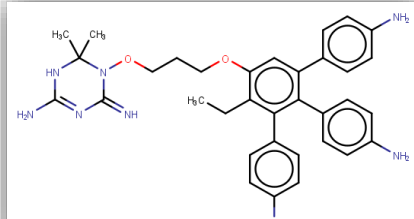
19	ATHT2	<table border="1"> <thead> <tr> <th colspan="4">Substituents</th> </tr> <tr> <th>R<sup>1</sup></th> <th>R<sup>2</sup></th> <th>R<sup>3</sup></th> <th>R<sup>4</sup></th> </tr> </thead> <tbody> <tr> <td>H</td> <td>H</td> <td>H</td> <td>H</td> </tr> </tbody> </table> 	Substituents				R <sup>1</sup>	R <sup>2</sup>	R <sup>3</sup>	R <sup>4</sup>	H	H	H	H	-7.4	-8.1	-8.2
Substituents																	
R <sup>1</sup>	R <sup>2</sup>	R <sup>3</sup>	R <sup>4</sup>														
H	H	H	H														
20	BTHT2	<table border="1"> <thead> <tr> <th colspan="4">Substituents</th> </tr> <tr> <th>R<sup>1</sup></th> <th>R<sup>2</sup></th> <th>R<sup>3</sup></th> <th>R<sup>4</sup></th> </tr> </thead> <tbody> <tr> <td>-CH<sub>3</sub></td> <td>-H</td> <td>-H</td> <td>-H</td> </tr> </tbody> </table> 	Substituents				R <sup>1</sup>	R <sup>2</sup>	R <sup>3</sup>	R <sup>4</sup>	-CH <sub>3</sub>	-H	-H	-H	-8.1	-8.1	-8.1
Substituents																	
R <sup>1</sup>	R <sup>2</sup>	R <sup>3</sup>	R <sup>4</sup>														
-CH <sub>3</sub>	-H	-H	-H														
21	CTHT2	<table border="1"> <thead> <tr> <th colspan="4">Substituents</th> </tr> <tr> <th>R<sup>1</sup></th> <th>R<sup>2</sup></th> <th>R<sup>3</sup></th> <th>R<sup>4</sup></th> </tr> </thead> <tbody> <tr> <td>-CH<sub>3</sub></td> <td>-CH<sub>3</sub></td> <td>-H</td> <td>-H</td> </tr> </tbody> </table> 	Substituents				R <sup>1</sup>	R <sup>2</sup>	R <sup>3</sup>	R <sup>4</sup>	-CH <sub>3</sub>	-CH <sub>3</sub>	-H	-H	-7.6	-8.4	-8.6
Substituents																	
R <sup>1</sup>	R <sup>2</sup>	R <sup>3</sup>	R <sup>4</sup>														
-CH <sub>3</sub>	-CH <sub>3</sub>	-H	-H														

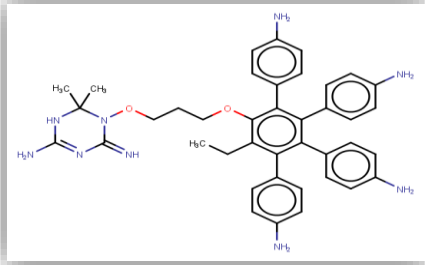
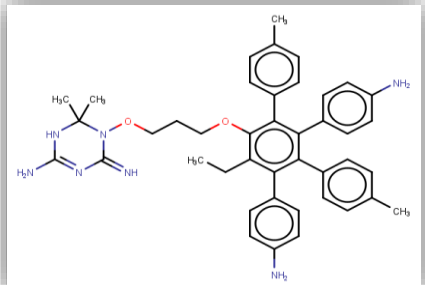
																	
22	DTHT2	<table border="1"> <thead> <tr> <th colspan="4">Substituents</th> </tr> <tr> <th>R<sup>1</sup></th> <th>R<sup>2</sup></th> <th>R<sup>3</sup></th> <th>R<sup>4</sup></th> </tr> </thead> <tbody> <tr> <td>-CH<sub>3</sub></td> <td>-CH<sub>3</sub></td> <td>-CH<sub>3</sub></td> <td>-H</td> </tr> </tbody> </table> 	Substituents				R <sup>1</sup>	R <sup>2</sup>	R <sup>3</sup>	R <sup>4</sup>	-CH <sub>3</sub>	-CH <sub>3</sub>	-CH <sub>3</sub>	-H	-8.3	-8.7	-9.0
Substituents																	
R <sup>1</sup>	R <sup>2</sup>	R <sup>3</sup>	R <sup>4</sup>														
-CH <sub>3</sub>	-CH <sub>3</sub>	-CH <sub>3</sub>	-H														
23	ETHT2	<table border="1"> <thead> <tr> <th colspan="4">Substituents</th> </tr> <tr> <th>R<sup>1</sup></th> <th>R<sup>2</sup></th> <th>R<sup>3</sup></th> <th>R<sup>4</sup></th> </tr> </thead> <tbody> <tr> <td>-CH<sub>3</sub></td> <td>-CH<sub>3</sub></td> <td>-CH<sub>3</sub></td> <td>-CH<sub>3</sub></td> </tr> </tbody> </table> 	Substituents				R <sup>1</sup>	R <sup>2</sup>	R <sup>3</sup>	R <sup>4</sup>	-CH <sub>3</sub>	-CH <sub>3</sub>	-CH <sub>3</sub>	-CH <sub>3</sub>	-8.4	-8.4	-9.1
Substituents																	
R <sup>1</sup>	R <sup>2</sup>	R <sup>3</sup>	R <sup>4</sup>														
-CH <sub>3</sub>	-CH <sub>3</sub>	-CH <sub>3</sub>	-CH <sub>3</sub>														

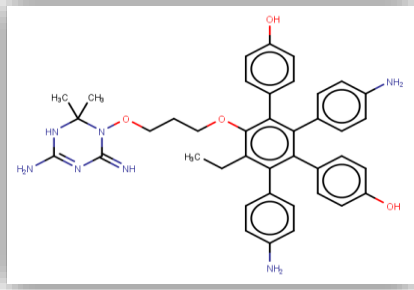
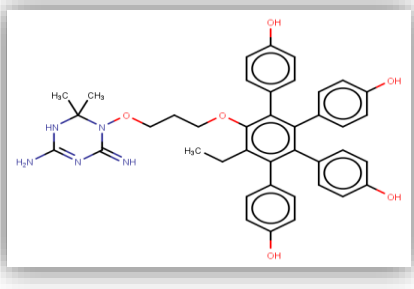
24	FTHT2	<table border="1" data-bbox="488 201 1003 426"> <thead> <tr> <th colspan="4">Substituents</th> </tr> <tr> <th>R<sup>1</sup></th> <th>R<sup>2</sup></th> <th>R<sup>3</sup></th> <th>R<sup>4</sup></th> </tr> </thead> <tbody> <tr> <td>-</td> <td>-H</td> <td>-H</td> <td>-H</td> </tr> <tr> <td>COCH<sub>3</sub></td> <td></td> <td></td> <td></td> </tr> </tbody> </table> 	Substituents				R <sup>1</sup>	R <sup>2</sup>	R <sup>3</sup>	R <sup>4</sup>	-	-H	-H	-H	COCH <sub>3</sub>				-7.9	-8.0	-8.2
Substituents																					
R <sup>1</sup>	R <sup>2</sup>	R <sup>3</sup>	R <sup>4</sup>																		
-	-H	-H	-H																		
COCH <sub>3</sub>																					
25	GTHT2	<table border="1" data-bbox="488 737 1003 961"> <thead> <tr> <th colspan="4">Substituents</th> </tr> <tr> <th>R<sup>1</sup></th> <th>R<sup>2</sup></th> <th>R<sup>3</sup></th> <th>R<sup>4</sup></th> </tr> </thead> <tbody> <tr> <td>-</td> <td>-CH<sub>3</sub></td> <td>-H</td> <td>-H</td> </tr> <tr> <td>COCH<sub>3</sub></td> <td></td> <td></td> <td></td> </tr> </tbody> </table> 	Substituents				R <sup>1</sup>	R <sup>2</sup>	R <sup>3</sup>	R <sup>4</sup>	-	-CH <sub>3</sub>	-H	-H	COCH <sub>3</sub>				-8.5	-8.2	-8.4
Substituents																					
R <sup>1</sup>	R <sup>2</sup>	R <sup>3</sup>	R <sup>4</sup>																		
-	-CH <sub>3</sub>	-H	-H																		
COCH <sub>3</sub>																					
26	HTHT2	<table border="1" data-bbox="488 1272 1003 1497"> <thead> <tr> <th colspan="4">Substituents</th> </tr> <tr> <th>R<sup>1</sup></th> <th>R<sup>2</sup></th> <th>R<sup>3</sup></th> <th>R<sup>4</sup></th> </tr> </thead> <tbody> <tr> <td>-CH<sub>3</sub></td> <td>-CH<sub>3</sub></td> <td>-</td> <td>-H</td> </tr> <tr> <td></td> <td></td> <td>COCH<sub>3</sub></td> <td></td> </tr> </tbody> </table> 	Substituents				R <sup>1</sup>	R <sup>2</sup>	R <sup>3</sup>	R <sup>4</sup>	-CH <sub>3</sub>	-CH <sub>3</sub>	-	-H			COCH <sub>3</sub>		-8.0	-8.5	-8.7
Substituents																					
R <sup>1</sup>	R <sup>2</sup>	R <sup>3</sup>	R <sup>4</sup>																		
-CH <sub>3</sub>	-CH <sub>3</sub>	-	-H																		
		COCH <sub>3</sub>																			



27	ITHT2	<table border="1" data-bbox="488 201 984 426"> <thead> <tr> <th colspan="4">Substituents</th> </tr> <tr> <th>R<sup>1</sup></th> <th>R<sup>2</sup></th> <th>R<sup>3</sup></th> <th>R<sup>4</sup></th> </tr> </thead> <tbody> <tr> <td>-CH<sub>3</sub></td> <td>-C<sub>3</sub>H<sub>7</sub></td> <td>-</td> <td>-H</td> </tr> <tr> <td></td> <td></td> <td>COCH<sub>3</sub></td> <td></td> </tr> </tbody> </table> 	Substituents				R <sup>1</sup>	R <sup>2</sup>	R <sup>3</sup>	R <sup>4</sup>	-CH <sub>3</sub>	-C <sub>3</sub> H <sub>7</sub>	-	-H			COCH <sub>3</sub>		-7.8	-8.3	-8.9
Substituents																					
R <sup>1</sup>	R <sup>2</sup>	R <sup>3</sup>	R <sup>4</sup>																		
-CH <sub>3</sub>	-C <sub>3</sub> H <sub>7</sub>	-	-H																		
		COCH <sub>3</sub>																			
28	JTHT2	<table border="1" data-bbox="488 783 1032 1008"> <thead> <tr> <th colspan="4">Substituents</th> </tr> <tr> <th>R<sup>1</sup></th> <th>R<sup>2</sup></th> <th>R<sup>3</sup></th> <th>R<sup>4</sup></th> </tr> </thead> <tbody> <tr> <td>-</td> <td>-H</td> <td>-C<sub>3</sub>H<sub>7</sub></td> <td>-H</td> </tr> <tr> <td>COCH<sub>3</sub></td> <td></td> <td></td> <td></td> </tr> </tbody> </table> 	Substituents				R <sup>1</sup>	R <sup>2</sup>	R <sup>3</sup>	R <sup>4</sup>	-	-H	-C <sub>3</sub> H <sub>7</sub>	-H	COCH <sub>3</sub>				-8.1	-8.8	-9.4
Substituents																					
R <sup>1</sup>	R <sup>2</sup>	R <sup>3</sup>	R <sup>4</sup>																		
-	-H	-C <sub>3</sub> H <sub>7</sub>	-H																		
COCH <sub>3</sub>																					
29	KTHT2	<table border="1" data-bbox="488 1339 1032 1627"> <thead> <tr> <th colspan="4">Substituents</th> </tr> <tr> <th>R<sup>1</sup></th> <th>R<sup>2</sup></th> <th>R<sup>3</sup></th> <th>R<sup>4</sup></th> </tr> </thead> <tbody> <tr> <td>-H</td> <td>-</td> <td>-H</td> <td>-</td> </tr> <tr> <td></td> <td>C<sub>6</sub>H<sub>5</sub>NH<sub>2</sub></td> <td></td> <td>COCH<sub>3</sub></td> </tr> </tbody> </table>	Substituents				R <sup>1</sup>	R <sup>2</sup>	R <sup>3</sup>	R <sup>4</sup>	-H	-	-H	-		C <sub>6</sub> H <sub>5</sub> NH <sub>2</sub>		COCH <sub>3</sub>	-8.9	-9.2	-8.9
Substituents																					
R <sup>1</sup>	R <sup>2</sup>	R <sup>3</sup>	R <sup>4</sup>																		
-H	-	-H	-																		
	C <sub>6</sub> H <sub>5</sub> NH <sub>2</sub>		COCH <sub>3</sub>																		

																					
30	LTHT2	<table border="1" data-bbox="488 499 1078 795"> <thead> <tr> <th colspan="4">Substituents</th> </tr> <tr> <th>R<sup>1</sup></th> <th>R<sup>2</sup></th> <th>R<sup>3</sup></th> <th>R<sup>4</sup></th> </tr> </thead> <tbody> <tr> <td>H</td> <td>-</td> <td>H</td> <td>-</td> </tr> <tr> <td></td> <td>C<sub>6</sub>H<sub>5</sub>NH<sub>2</sub></td> <td></td> <td>C<sub>6</sub>H<sub>5</sub>NH<sub>2</sub></td> </tr> </tbody> </table> 	Substituents				R <sup>1</sup>	R <sup>2</sup>	R <sup>3</sup>	R <sup>4</sup>	H	-	H	-		C <sub>6</sub> H <sub>5</sub> NH <sub>2</sub>		C <sub>6</sub> H <sub>5</sub> NH <sub>2</sub>	-9.2	-9.7	-9.2
Substituents																					
R <sup>1</sup>	R <sup>2</sup>	R <sup>3</sup>	R <sup>4</sup>																		
H	-	H	-																		
	C <sub>6</sub> H <sub>5</sub> NH <sub>2</sub>		C <sub>6</sub> H <sub>5</sub> NH <sub>2</sub>																		
31	MTHT2	<table border="1" data-bbox="488 1129 1078 1425"> <thead> <tr> <th colspan="4">Substituents</th> </tr> <tr> <th>R<sup>1</sup></th> <th>R<sup>2</sup></th> <th>R<sup>3</sup></th> <th>R<sup>4</sup></th> </tr> </thead> <tbody> <tr> <td>H</td> <td>-</td> <td>-</td> <td>-</td> </tr> <tr> <td></td> <td>C<sub>6</sub>H<sub>5</sub>NH<sub>2</sub></td> <td>C<sub>6</sub>H<sub>5</sub>NH<sub>2</sub></td> <td>C<sub>6</sub>H<sub>5</sub>NH<sub>2</sub></td> </tr> </tbody> </table> 	Substituents				R <sup>1</sup>	R <sup>2</sup>	R <sup>3</sup>	R <sup>4</sup>	H	-	-	-		C <sub>6</sub> H <sub>5</sub> NH <sub>2</sub>	C <sub>6</sub> H <sub>5</sub> NH <sub>2</sub>	C <sub>6</sub> H <sub>5</sub> NH <sub>2</sub>	-9.4	-9.0	-8.6
Substituents																					
R <sup>1</sup>	R <sup>2</sup>	R <sup>3</sup>	R <sup>4</sup>																		
H	-	-	-																		
	C <sub>6</sub> H <sub>5</sub> NH <sub>2</sub>	C <sub>6</sub> H <sub>5</sub> NH <sub>2</sub>	C <sub>6</sub> H <sub>5</sub> NH <sub>2</sub>																		

32	NTHT2	<table border="1"> <thead> <tr> <th colspan="4">Substituents</th> </tr> <tr> <th>R<sup>1</sup></th> <th>R<sup>2</sup></th> <th>R<sup>3</sup></th> <th>R<sup>4</sup></th> </tr> </thead> <tbody> <tr> <td>-</td> <td>-</td> <td>-</td> <td>-</td> </tr> <tr> <td>C<sub>6</sub>H<sub>5</sub>NH<sub>2</sub></td> <td>C<sub>6</sub>H<sub>5</sub>NH<sub>2</sub></td> <td>C<sub>6</sub>H<sub>5</sub>NH<sub>2</sub></td> <td>C<sub>6</sub>H<sub>5</sub>NH<sub>2</sub></td> </tr> </tbody> </table> 	Substituents				R <sup>1</sup>	R <sup>2</sup>	R <sup>3</sup>	R <sup>4</sup>	-	-	-	-	C <sub>6</sub> H <sub>5</sub> NH <sub>2</sub>	C <sub>6</sub> H <sub>5</sub> NH <sub>2</sub>	C <sub>6</sub> H <sub>5</sub> NH <sub>2</sub>	C <sub>6</sub> H <sub>5</sub> NH <sub>2</sub>	-9.3	-7.9	-8.2
Substituents																					
R <sup>1</sup>	R <sup>2</sup>	R <sup>3</sup>	R <sup>4</sup>																		
-	-	-	-																		
C <sub>6</sub> H <sub>5</sub> NH <sub>2</sub>	C <sub>6</sub> H <sub>5</sub> NH <sub>2</sub>	C <sub>6</sub> H <sub>5</sub> NH <sub>2</sub>	C <sub>6</sub> H <sub>5</sub> NH <sub>2</sub>																		
33	OTHT2	<table border="1"> <thead> <tr> <th colspan="4">Substituents</th> </tr> <tr> <th>R<sup>1</sup></th> <th>R<sup>2</sup></th> <th>R<sup>3</sup></th> <th>R<sup>4</sup></th> </tr> </thead> <tbody> <tr> <td>-</td> <td>-</td> <td>-</td> <td>-</td> </tr> <tr> <td>C<sub>6</sub>H<sub>5</sub>CH<sub>3</sub></td> <td>C<sub>6</sub>H<sub>5</sub>NH<sub>2</sub></td> <td>C<sub>6</sub>H<sub>5</sub>CH<sub>3</sub></td> <td>C<sub>6</sub>H<sub>5</sub>NH<sub>2</sub></td> </tr> </tbody> </table> 	Substituents				R <sup>1</sup>	R <sup>2</sup>	R <sup>3</sup>	R <sup>4</sup>	-	-	-	-	C <sub>6</sub> H <sub>5</sub> CH <sub>3</sub>	C <sub>6</sub> H <sub>5</sub> NH <sub>2</sub>	C <sub>6</sub> H <sub>5</sub> CH <sub>3</sub>	C <sub>6</sub> H <sub>5</sub> NH <sub>2</sub>	-9.7	-7.9	-8.5
Substituents																					
R <sup>1</sup>	R <sup>2</sup>	R <sup>3</sup>	R <sup>4</sup>																		
-	-	-	-																		
C <sub>6</sub> H <sub>5</sub> CH <sub>3</sub>	C <sub>6</sub> H <sub>5</sub> NH <sub>2</sub>	C <sub>6</sub> H <sub>5</sub> CH <sub>3</sub>	C <sub>6</sub> H <sub>5</sub> NH <sub>2</sub>																		

34	PTHT2	<table border="1"> <thead> <tr> <th colspan="4">Substituents</th> </tr> <tr> <th>R<sup>1</sup></th> <th>R<sup>2</sup></th> <th>R<sup>3</sup></th> <th>R<sup>4</sup></th> </tr> </thead> <tbody> <tr> <td>-</td> <td>-</td> <td>-</td> <td>-</td> </tr> <tr> <td>C<sub>6</sub>H<sub>5</sub>OH</td> <td>C<sub>6</sub>H<sub>5</sub>NH<sub>2</sub></td> <td>C<sub>6</sub>H<sub>5</sub>OH</td> <td>C<sub>6</sub>H<sub>5</sub>NH<sub>2</sub></td> </tr> </tbody> </table> 	Substituents				R <sup>1</sup>	R <sup>2</sup>	R <sup>3</sup>	R <sup>4</sup>	-	-	-	-	C <sub>6</sub> H <sub>5</sub> OH	C <sub>6</sub> H <sub>5</sub> NH <sub>2</sub>	C <sub>6</sub> H <sub>5</sub> OH	C <sub>6</sub> H <sub>5</sub> NH <sub>2</sub>	-9.3	-8.1	-7.8
Substituents																					
R <sup>1</sup>	R <sup>2</sup>	R <sup>3</sup>	R <sup>4</sup>																		
-	-	-	-																		
C <sub>6</sub> H <sub>5</sub> OH	C <sub>6</sub> H <sub>5</sub> NH <sub>2</sub>	C <sub>6</sub> H <sub>5</sub> OH	C <sub>6</sub> H <sub>5</sub> NH <sub>2</sub>																		
35	QTHT2	<table border="1"> <thead> <tr> <th colspan="4">Substituents</th> </tr> <tr> <th>R<sup>1</sup></th> <th>R<sup>2</sup></th> <th>R<sup>3</sup></th> <th>R<sup>4</sup></th> </tr> </thead> <tbody> <tr> <td>-</td> <td>-</td> <td>-</td> <td>-</td> </tr> <tr> <td>C<sub>6</sub>H<sub>5</sub>OH</td> <td>C<sub>6</sub>H<sub>5</sub>OH</td> <td>C<sub>6</sub>H<sub>5</sub>OH</td> <td>C<sub>6</sub>H<sub>5</sub>OH</td> </tr> </tbody> </table> 	Substituents				R <sup>1</sup>	R <sup>2</sup>	R <sup>3</sup>	R <sup>4</sup>	-	-	-	-	C <sub>6</sub> H <sub>5</sub> OH	C <sub>6</sub> H <sub>5</sub> OH	C <sub>6</sub> H <sub>5</sub> OH	C <sub>6</sub> H <sub>5</sub> OH	-9.6	-8.3	-8.1
Substituents																					
R <sup>1</sup>	R <sup>2</sup>	R <sup>3</sup>	R <sup>4</sup>																		
-	-	-	-																		
C <sub>6</sub> H <sub>5</sub> OH	C <sub>6</sub> H <sub>5</sub> OH	C <sub>6</sub> H <sub>5</sub> OH	C <sub>6</sub> H <sub>5</sub> OH																		

36	RTHT2	Substituents					-9.6	-10.0	-10.3
		R <sup>1</sup>	R <sup>2</sup>	R <sup>3</sup>	R <sup>4</sup>				
		-	C <sub>6</sub> H <sub>5</sub> CH <sub>3</sub> (fused)	-	C <sub>6</sub> H <sub>5</sub> CH <sub>3</sub> (fused)				

### 5.7 Appendix 2: Lipinski rule of five, Synthetic Accessibility, and ADME Studies

Name	Lipinski Rule of Five		Cytochrome P450 (CYP450) Inhibition Isoforms					Aqueous Solubility (Log S)	Synthetic Accessibility (SA score)	Quantitative Estimate of Drug-Likeness (QED)	Binding Affinities (kcal mol <sup>-1</sup> ) ΔG		
			1a2	2c9	2c19	2d6	3a4				Binding		
											4kne	4kl9	1dg8
AS05	Molecular Weight (<500Da)	299.48	No	No	No	No	No	-2.372	4.4229	0.3923	-7.19	-7.2	-7.0
	Log P(<5)	2.0478											

	H-Bond donor (5)	4											
	H-bond acceptor (<10)	7											
	Violations	0											
	Drug-Like Score (DLScore)	0.9761											
AM03	Molecular Weight (<500Da)	411.46											
	Log P(<5)	4.8885											
	H-Bond donor (5)	3	No	No	No	No	No	-3.7889	4.7424	0.8520	-8.9	-9.6	-9.8
	H-bond acceptor (<10)	10											
	Violations	0											
	Drug-Like	0.7785											

	Score (DLScor ns)												
AM1 0	Molecular Weight (<500Da)	364.5	No	No	No	Yes	No	-4.1168	5.1215	0.8380	-9.5	-9.8	-
	Log P(<5)	2.867											
	H-Bond donor (5)	3											
	H-bond acceptor (<10)	7											
	Violations	0											
	Drug-Like Score (DLScor ns)	0.9											
AM2 6	Molecular Weight (<500Da)	367.47	No	Yes	No	Yes	Yes	-4.4423	4.3206	0.7454	-9.9	-10.8	-
	Log P(<5)	3.4545											

	H-Bond donor (5)	4												
	H-bond acceptor (<10)	7												
	Violations	0												
	Drug-Like Score (DLScores)	0.8642												
AM34	Molecular Weight (<500Da)	381.48												
	Log P(<5)	1.9038												
	H-Bond donor (5)	5	No	No	No	No	No	-3.3470	4.6246	0.5706	-9.5	-9.7	-	10.0
	H-bond acceptor (<10)	8												
	Violations	0												
	Drug-Like	0.9285												



	Score (DLScore)												
ANS 01	Molecular Weight (<500Da)	348.41	No	No	No	No	No	-4.0442	4.8504	0.5194	-9.8	-11.1	-12.4
	Log P(<5)	2.8111											
	H-Bond donor (5)	4											
	H-bond acceptor (<10)	9											
	Violations	0											
	Drug-Like Score (DLScore)	0.5952											
ANS 02	Molecular Weight (<500Da)	326.41	No	No	No	No	No	-3.3014	4.9594	0.3821	-10.1	-10.2	-10.6
	Log P(<5)	2.1502											

	H-Bond donor (5)	4												
	H-bond acceptor (<10)	9												
	Violations	0												
	Drug-Like Score (DLScores)	0.6833												
ANS 04	Molecular Weight (<500Da)	352.45	Yes	No	No	No	No	-4.2445	4.8429	0.5272	-9.0	-10.6	-	11.1
	Log P(<5)	3.2089												
	H-Bond donor (5)	4												
	H-bond acceptor (<10)	9												
	Violations	0												
	Drug-Like	0.6238												

	Score (DLScor ns)												
ANS 11	Molecular Weight (<500Da)	362.55	No	No	No	No	No	-3.9236	4.8271	0.3821	-7.9	-9.2	-8.4
	Log P(<5)	3.5941											
	H-Bond donor (5)	4											
	H-bond acceptor (<10)	9											
	Violations	0											
	Drug-Like Score (DLScor ns)	0.7952											
AS12 2	Molecular Weight (<500Da)	411.46	No	Yes	Yes	No	Yes	-5.7443	5.3332	0.3975	-10.3	-11.3	-12.7
	Log P(<5)	4.8885											

	H-Bond donor (5)	3											
	H-bond acceptor (<10)	10											
	Violations	0											
	Drug-Like Score (DLScores)	0.7785											
RM1 1	Molecular Weight (<500Da)	525.61											
	Log P(<5)	4.3514											
	H-Bond donor (5)	3	No	No	No	No	No	-7.4482	5.4330	0.3371	-12.5	-13.1	-13.0
	H-bond acceptor (<10)	10											
	Violations	1											
	Drug-Like	0.6333											

	Score (DLScores)												
R15	Molecular Weight (<500Da)	525.61	No	No	No	No	Yes	-7.4061	5.5361	0.4153	-12.0	-11.8	-14.1
	Log P(<5)	5.1246											
	H-Bond donor (5)	3											
	H-bond acceptor (<10)	10											
	Violations	2											
	Drug-Like Score (DLScores)	0.6333											
RF02	Molecular Weight (<500Da)	515.54	No	Yes	Yes	No	Yes	-7.2448	5.6862	0.3408	11.4	-12.9	-14.0
	Log P(<5)	5.1757											

	H-Bond donor (5)	3												
	H-bond acceptor (<10)	8												
	Violations	2												
	Drug-Like Score (DLScores)	0.5047												
RF28	Molecular Weight (<500Da)	513.6	No	Yes	No	No	No	-6.9221	5.3597	0.2062	-10.1	-11.2	-	13.9
	Log P(<5)	3.9428												
	H-Bond donor (5)	3												
	H-bond acceptor (<10)	10												
	Violations	1												
	Drug-Like	0.6333												

	Score (DLScor ns)												
RF42	Molecular Weight (<500Da)	495.56	No	Yes	Yes	No	Yes	-6.8248	4.9544	0.3500	-10.9	-12.1	-12.3
	Log P(<5)	4.6613											
	H-Bond donor (5)	3											
	H-bond acceptor (<10)	10											
	Violations	0											
	Drug-Like Score (DLScor ns)	0.6071											
RF43	Molecular Weight (<500Da)	493.59	No	Yes	Yes	No	Yes	-7.2911	5.2639	0.4239	-10.4	-12.1	-13.1
	Log P(<5)	6.4960											

	H-Bond donor (5)	3																		
	H-bond acceptor (<10)	9																		
	Violations	1																		
	Drug-Like Score (DLScores)	0.7																		
RF43	Molecular Weight (<500Da)	493.59	No	Yes	Yes	No	Yes	-7.2911	5.2639	0.4239	-11.0	-12.1	-	13.1						
	Log P(<5)	5.2875																		
	H-Bond donor (5)	3																		
	H-bond acceptor (<10)	9																		
	Violations	1																		
	Drug-Like Score	0.7023																		



	Score (DLScor ns)												
Isoniazid	Molecular Weight (<500Da)	137.16	Yes	No	No	No	Yes	-0.6834	3.7149	0.3362			-5.2
	Log P(<5)	-0.469											
	H-Bond donor (5)	3											
	H-bond acceptor (<10)	4											
	Violations	0											
	Drug-Like Score (DLScor ns)	0.7523											

THT 1	Molecular Weight (<500Da)	347.52	No	No	No	No	No	-3.5530	3.8547	0.6922	-7.8	-8.4	-8.5
-------	---------------------------	--------	----	----	----	----	----	---------	--------	--------	------	------	------

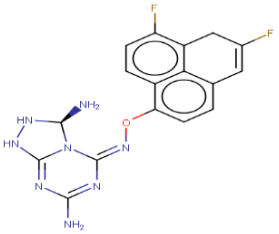
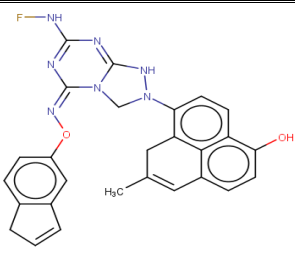
	Log P(<5)	2.91 22											
	H-Bond donor (5)	4											
	H-bond acceptor (<10)	7											
	Violations	0											
	Drug-Like Score (DLScore)	1											
	THT 2	Molecular Weight (<500Da)	319.46										
Log P(<5)		2.35 42											
H-Bond donor (5)		4	No	No	No	No	No	-3.0055	3.7149	0.7002	-7.4	-8.1	-8.2
H-bond acceptor (<10)		7											
Violations		0											

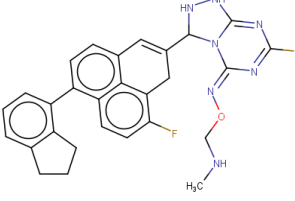
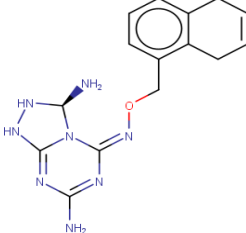
	Drug-Like Score (DLScor ns)	1											
RF56	Molecular Weight (<500Da)	458.51											
	Log P(<5)	5.7582											
	H-Bond donor (5)	2	Yes	Yes	Yes	No	Yes	-6.5834	5.0956	0.4538	-11.0	-11.0	-12.7
	H-bond acceptor (<10)	9	s	s									
	Violations	1											
	Drug-Like Score (DLScor ns)	0.7											
AM36	Molecular Weight (<500Da)	347.44	No	No	No	No	No	-3.6034	4.1401	0.8419	-8.1	-9.0	-8.5

	Log P(<5)	2.69 72											
	H-Bond donor (5)	3											
	H-bond acceptor (<10)	8											
	Violations	0											
	Drug-Like Score (DLScore)	1											
AM2 2	Molecular Weight (<500Da)	331.42											
	Log P(<5)	1.33 36											
	H-Bond donor (5)	5	No	No	No	No	No	-2.6648	4.4793	0.6021	-8.4	-8.9	-8.6
	H-bond acceptor (<10)	8											
	Violations	0											

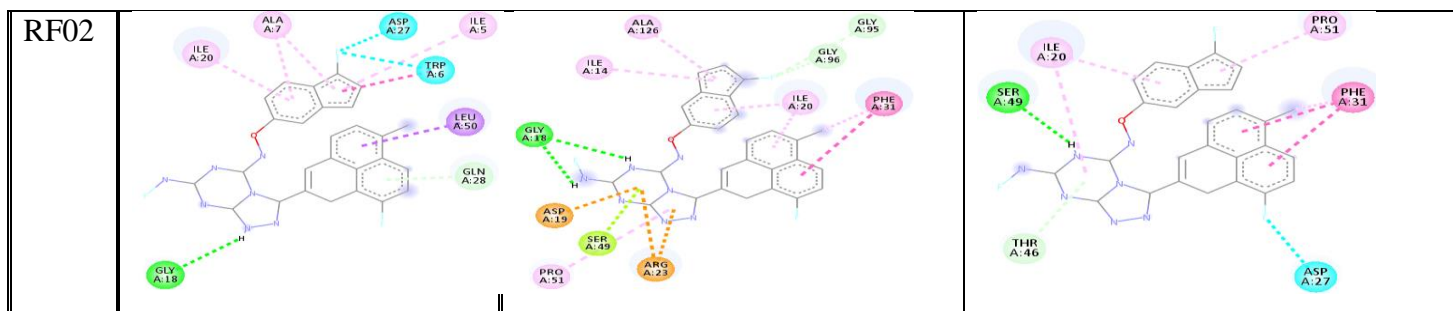
	Drug-Like Score (DLScore)	1											
AM3 1	Molecular Weight (<500Da)	381.56	No	No	No	Yes	No	-3.5226	5.1552	0.3048	-7.7	-8.3	-8.7
	Log P(<5)	2.5638											
	H-Bond donor (5)	5											
	H-bond acceptor (<10)	8											
	Violations	0											
	Drug-Like Score (DLScore)	0.7833											

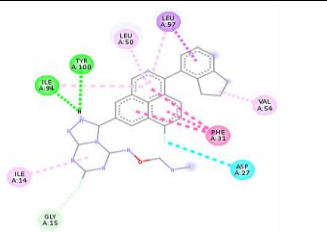
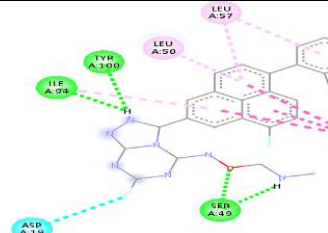
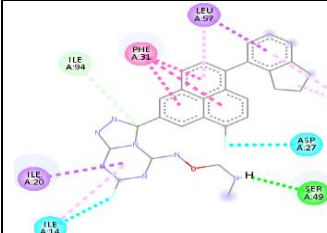
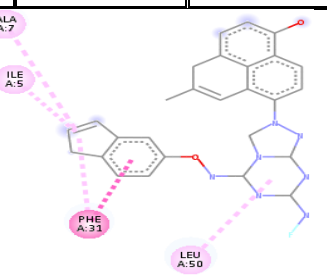
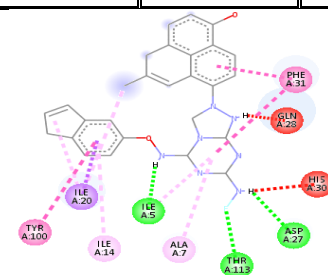
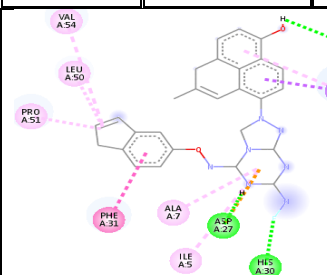
**5.8 Appendix 3: 2D -Structures, and common amino acid residue interacting across all receptors, and binding affinities conjoined to three docked macromolecules (4kne, 4kl9, 1dg8), of 10 pre-qualified ligands.**

Name	Structure	Molecular Formula	Amino Acid Residues			Common Residues Interacting across all receptors	Binding Affinities		
			PDB IDs				PDB IDs		
			4kne	4kl9	1dg8		4kne	4kl9	1dg8
ASO1		C <sub>17</sub> H <sub>14</sub> F <sub>2</sub> N <sub>8</sub> O	ASP:27 ALA:1 26 GLY:1 5 ILE:14 PHE:31 SER:49	ASP:27 GLN:2 8 GLY:1 5 HIS:30 ILE:5 ILE:14 ILE:20 PHE:31 SER:49	ALA:7 ASP:27 GLN:2 8 ILE:14 ILE:20 ILE:94 LEU:57 PHE:31 THR:4 6	ASP:27 ILE:14	- 10. 0	- 11. 3	- 12.7
RF42		C <sub>27</sub> H <sub>22</sub> FN <sub>7</sub> O <sub>2</sub>	ALA:7 ILE:5 LEU:50 PHE:31	ALA:7 ASP:27 HIS:30 ILE:5 ILE:14 ILE:20 GLN:2 8 PHE:31 THR:1 33 TYR:1 00	ALA:7 ASP:27 HIS:30 ILE:5 ILE:14 ILE:20 LEU:50 PHE:31 PRO:51 VAL:5 4	ALA:7 ILE5 PHE:31	- 10. 9	- 12. 1	- 12.3

RF28		C <sub>28</sub> H <sub>25</sub> F <sub>2</sub> N <sub>7</sub> O	ASP:27 GLY:1 5 ILE:14 ILE:94 LEU:50 LEU:57 PHE:31 TYR:1 00 VAL:5 4	ASP:19 ILE:94 LEU:50 ILE:20 PHE:31 SER:49 TYR:1 00 VAL:5 4	ASP:27 ILE:14 ILE:20 ILE:94 LEU:57 PHE:31 SER:49 VAL:5 4	ILE:94 LEU:57 PHE:31	- 10. 1	- 11. 2	- 13.9
AS0 2		C <sub>15</sub> H <sub>18</sub> N <sub>8</sub> O	ALA:7 ILE:5 ILE:14 ILE:94 PHE:31	ALA:7 ASP:27 GLN:2 8 ILE:14 ILE:20 LEU:24 TYR:1 00	GLY:1 8 ILE:14 LEU:57 PHE:31 SER:49 TYR:1 00	ILE:14	- 10. 1	- 10. 2	- 10.9

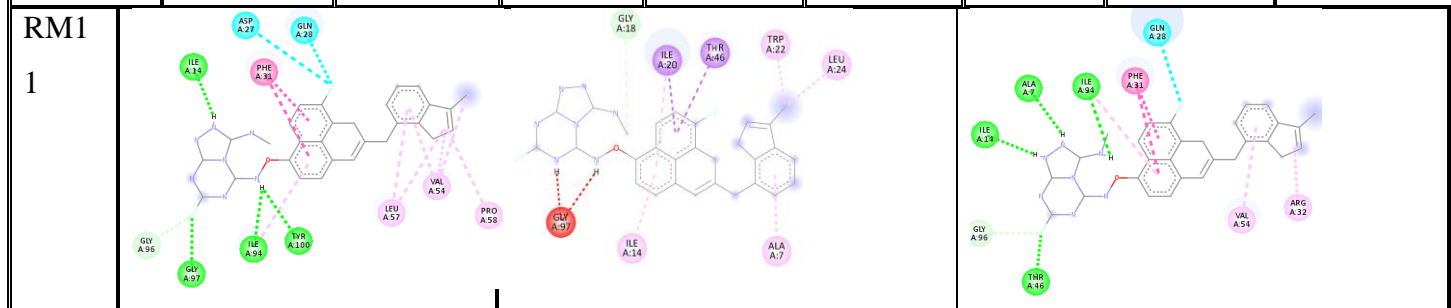
**5.9 Appendix 4: Ligand-target interactions of 10 best ligands for all three receptors (PDB ID: 4KNE, PDB ID: 4KL9, PDB ID: 1DG8) along with their type of interactions.**



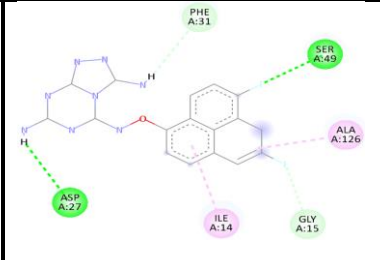
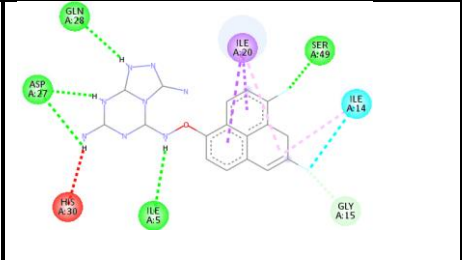
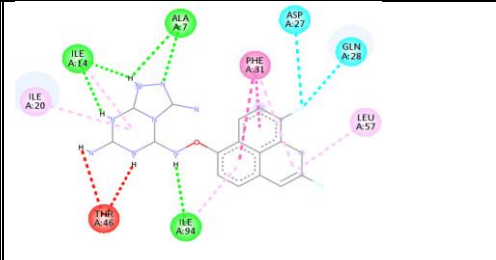
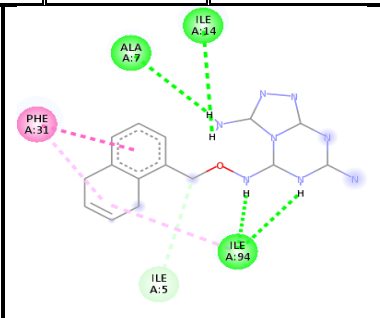
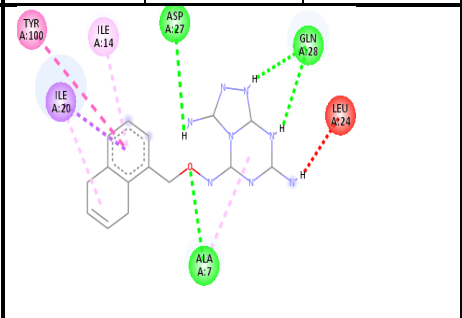
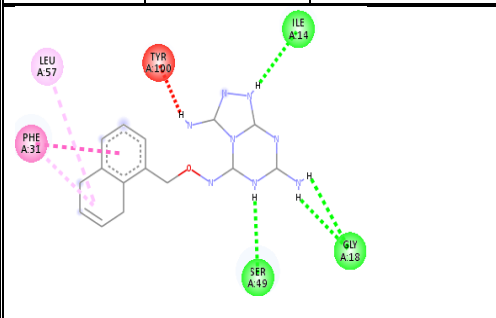
H-Bonding Interaction	Hydrophobic Interaction	Electrostatic Interaction	H-Bonding Interaction	Hydrophobic Interaction	Electrostatic interaction	H-Bonding Interaction	Hydrophobic Interaction	Electrostatic interaction
ASP:27 GLY:18 GLN:28 TRP:6	ALA:7 ILE:5 ILE:20 LEU:50	N/A	GLY:18 GLY:95 GLY:96 SER:49	ALA:126 ILE:14 ILE:20 PHE:31 PRO:51	ASP:19 ARG:23	ASP:27 AER:49 THR:46	ILE:20 PHE:31 PRO:51	N/A
RF28								
H-Bonding Interaction	Hydrophobic Interaction	Electrostatic Interaction	H-Bonding Interaction	Hydrophobic Interaction	Electrostatic interaction	H-Bonding Interaction	Hydrophobic Interaction	Electrostatic interaction
ASP:27 ILE:94 GLN: 15 TYR:100	ILE:14 LEU:50 LEU:57 PHE:31 VAL:54	N/A	ASP:19 ILE:94 SER:49 TYR:100	ILE:94 LEU:50 LEU:57 PHE:31	N/A	ASP:27 ILE:14 ILE:94 SER:49	ILE:14 ILE:20 LEU:57 PHE:31 VAL:54	N/A
RF42								



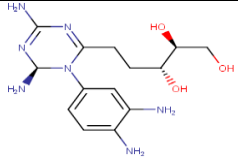
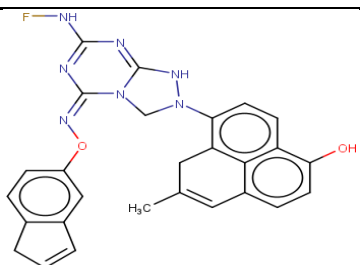
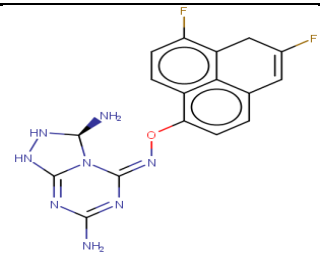
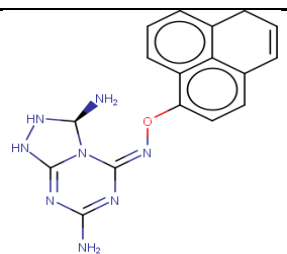
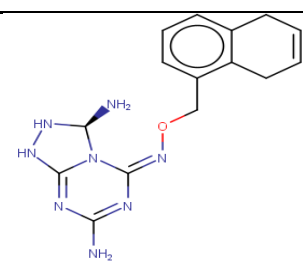
H-Bonding Interaction	Hydrophobic Interaction	Electrostatic Interaction	H-Bonding Interaction	Hydrophobic Interaction	Electrostatic interaction	H-Bonding Interaction	Hydrophobic Interaction	Electrostatic interaction
N/A	ALA:7 ILE:5 LEU:50 PHE:31	N/A	ASP:27 ILE:5 THR:113	ALA:7 ILE:14 ILE:20 PHE:31 TYR:100	N/A	ASP:27 HIS:30 ILE:14	ALA:7 ILE:5 ILE:20 LEU:50 PHE:31 PRO:51 VAL:54	ASP:27

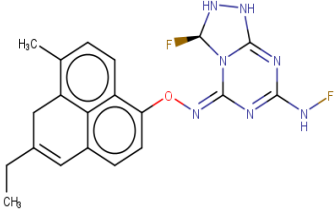
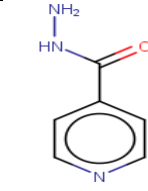
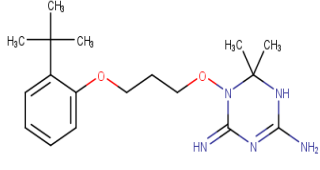
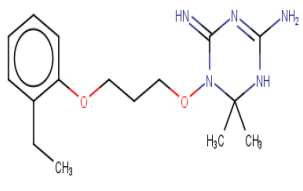
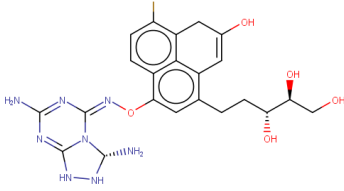
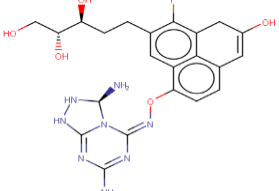


H-Bonding Interaction	Hydrophobic Interaction	Electrostatic Interaction	H-Bonding Interaction	Hydrophobic Interaction	Electrostatic interaction	H-Bonding Interaction	Hydrophobic Interaction	Electrostatic interaction
ASP:27 GLN:28 ILE:14 ILE:94 GLY:96 GLY:97 TYR:100	ILE:94 LEU:57 PHE:31 PRO:58 VAL:54	N/A	GLY:18	ALA:7 ILE:14 ILE:20 LEU:24 TRP:22 THR:46	N/A	ALA:7 ILE:14 ILE:94 GLN:28 GLY:96 THR:46	ARG:32 PHE:31 VAL:54	N/A

AS01								
H-Bonding Interaction	Hydrophobic Interaction	Electrostatic Interaction	H-Bonding Interaction	Hydrophobic Interaction	Electrostatic Interactions	H-Bonding Interaction	Hydrophobic Interaction	Electrostatic Interactions
ASP:27 SER:49 GLY:15 PHE:31	ALA:126 ILE:14	N/A	ASP:27 GLY:28 ILE:5 ILE14 SER:49 GLY:15	ILE:20 ILE14	N/A	ALA:7 ASP:27 GLN:28 ILE:14 ILE:94	ILE:20 LEU:57 PHE:31 ILE:94	N/A
ANS02								
H-Bonding Interaction	Hydrophobic Interaction	Electrostatic Interaction	H-Bonding Interaction	Hydrophobic Interaction	Electrostatic Interactions	H-Bonding Interaction	Hydrophobic Interaction	Electrostatic Interactions
ALA:7 ILE:5 ILE:14 ILE:94	PHE:31	N/A	ALA:7 ASP:27 GLN:28	ILE:14 ILE:20 TYR:100	N/A	ILE:14 GLY:18 SER:14	LEU:57 PHE:31	N/A

**5.10 Appendix 5: Virtual screening of the glycerol mimicking molecules and the prequalified drug-like molecules to evaluate their selectivity properties towards h (human) DHFR (PDB ID: 1OHJ) and Mtb-DHFR (PDB ID: 1DG8).**

Name	Structure	<i>h</i> -DHFR Binding Affinity ( $\Delta G$ Kcal mol <sup>-1</sup> )	<i>Mtb</i> -DHFR Binding Affinity ( $\Delta G$ Kcal/mol <sup>-1</sup> )
GM3		-7.2	-8.0
RF42		-11.3	-12.3
AS01		-11.1	-12.7
ANS01		-10.7	-12.4
ANS02		-9.8	-10.9

AS122		-10.5	-12.7
Isoniazid		-5.5	-5.2
THT1		-8.5	-8.4
THT2		-7.9	-7.7
GM8		-9.2	-10.4
GM10		-9.4	-11.5

## DISCLOSURE STATEMENT

The author(s) confirmed there was no conflict of interest.

Albert Zindoga; ORCID: <https://orcid.org/0000-0003-3846-986X>

## CHAPTER 6

### REFERENCES

- Abdelhameed, A. S., Alanazi, A. M., Bakheit, A. H., Hassan, E. S., Herqash, R. N., & Almutairi, F. M. (2019). Novel BTK inhibitor acalabrutinib (ACP-196) tightly binds to site of the human serum albumin as observed by spectroscopic and computational studies. *International journal of biological macromolecules*, 127, 536-543.
- Abreu, R. M. V., Froufe, H. J., Daniel, P. O., Queiroz, M. J. R., & Ferreira, I. C. (2011). ChemT, an open-source software for building template-based chemical libraries. *SAR and QSAR in Environmental Research*, 22(5-6), 603-610.
- Adessi, C. and Soto, C. (2002) Converting a peptide into a drug: strategies to improve stability and bioavailability. *Curr. Med. Chem.* 9, 963–978
- Agarwal, P. K., Billeter, S. R., Rajagopalan, P. R., Benkovic, S. J., & Hammes-Schiffer, S. (2002). Network of coupled promoting motions in enzyme catalysis. *Proceedings of the National Academy of Sciences*, 99(5), 2794-2799.
- Agranat, I., Caner, H., & Caldwell, J. (2002). Putting chirality to work: the strategy of chiral switches. *Nature Reviews Drug Discovery*, 1(10), 753-768.
- Agrawal, H., Kumar, A., Bal, N. C., Siddiqi, M. I., & Arora, A. (2007). Ligand based virtual screening and biological evaluation of inhibitors of chorismate mutase (Rv1885c) from *Mycobacterium tuberculosis* H37Rv. *Bioorganic & medicinal chemistry letters*, 17(11), 3053-3058.
- Allen, F. H. (2002). The Cambridge Structural Database: a quarter of a million crystal structures and rising. *Acta Crystallographica Section B: Structural Science*, 58(3), 380-388.
- Allué-Guardia, A., García, J. I., & Torrelles, J. B. (2021). Evolution of drug-resistant *Mycobacterium tuberculosis* strains and their adaptation to the human lung environment. *Frontiers in Microbiology*, 137.

Alvarez, L., Espaillat, A., Hermoso, J. A., de Pedro, M. A., & Cava, F. (2014). Peptidoglycan remodeling by the coordinated action of multispecific enzymes. *Microbial drug resistance*, 20(3), 190-198.

Alvascience. alvaModel (Software to Model QSAR Data) Version 2.0.0. 2021. Available online: <https://www.alvascience.com> (accessed on).

Alvascience. alvaMolecule (Software to View and Prepare Chemical Datasets) Version 1.0.4. 2020. Available online: <https://www.alvascience.com> (accessed on).

Al-Zoubi, R. M., Marion, O., & Hall, D. G. (2008). Direct and waste-free amidations and cycloadditions by organocatalytic activation of carboxylic acids at room temperature. *Angewandte Chemie International Edition*, 47(15), 2876-2879.

Amouri, H., & Gruselle, M. (2008). *Chirality in transition metal chemistry: molecules, supramolecular assemblies and materials*. John Wiley & Sons.

Antolín, A. I. (2021). Applications of Machine Learning in drug discovery and development.

Ariens, E. J. (1984). Stereochemistry, a basis for sophisticated nonsense in pharmacokinetics and clinical pharmacology. *European journal of clinical pharmacology*, 26, 663-668.

Bajorath, J. (2017). Computational scaffold hopping: cornerstone for the future of drug design?. *Future Medicinal Chemistry*, 9(7), 629-631.

Baker, J. J., Dechow, S. J., & Abramovitch, R. B. (2019). Acid fasting: modulation of *Mycobacterium tuberculosis* metabolism at acidic pH. *Trends in microbiology*, 27(11), 942-953.

Barf, T., Covey, T., Izumi, R., van de Kar, B., Gulrajani, M., van Lith, B., ... & Kaptein, A. (2017). Acalabrutinib (ACP-196): a covalent Bruton tyrosine kinase inhibitor with a differentiated selectivity and in vivo potency profile. *Journal of Pharmacology and Experimental Therapeutics*, 363(2), 240-252.

Beno, B. R., & Langley, D. R. (2010). MORPH: a new tool for ligand design. *Journal of chemical information and modeling*, 50(6), 1159-1164.

- Bergmann, R., Liljefors, T., Sørensen, M. D., & Zamora, I. (2009). SHOP: receptor-based scaffold HOPping by GRID-based similarity searches. *Journal of chemical information and modeling*, 49(3), 658-669.
- Bertacine Dias, M. V., Santos, J. C., Libreros-Zúñiga, G. A., Ribeiro, J. A., & Chavez-Pacheco, S. M. (2018). Folate biosynthesis pathway: mechanisms and insights into drug design for infectious diseases. *Future medicinal chemistry*, 10(8), 935-959.
- Bhabha, G., Lee, J., Ekiert, D. C., Gam, J., Wilson, I. A., Dyson, H. J., ... & Wright, P. E. (2011). A dynamic knockout reveals that conformational fluctuations influence the chemical step of enzyme catalysis. *Science*, 332(6026), 234-238.
- Biasini, M., Bienert, S., Waterhouse, A., Arnold, K., Studer, G., Schmidt, T., ... & Schwede, T. (2014). SWISS-MODEL: modelling protein tertiary and quaternary structure using evolutionary information. *Nucleic acids research*, 42(W1), W252-W258.
- Bickerton, G. R., Paolini, G. V., Besnard, J., Muresan, S., & Hopkins, A. L. Quantifying the chemical beauty of drugs. *Nat. Chem.* 4 (2), 90–98 (2012). *Crossref, Medline*.
- BIOVIA, D. S. (2021). BIOVIA Discovery Studio Academic Research Suite. *San Diego: Dassault Systèmes*.
- Blaser, H. U. (2013). Chirality and its implications for the pharmaceutical industry. *Rendiconti Lincei*, 24(3), 213-216.
- Boehm, H.J. et al. (2004) Scaffold hopping. *Drug Discov. Today: Technol.* 1, 217–224
- Böhm, H. J., Flohr, A., & Stahl, M. (2004). Scaffold hopping. *Drug discovery today: Technologies*, 1(3), 217-224.
- Brown, N. (2014). Bioisosteres and scaffold hopping in medicinal chemistry. *Molecular informatics*, 33(6-7), 458-462.
- Caldwell, J. (1992). The importance of stereochemistry in drug action and disposition. *Journal of clinical pharmacology*, 32(10), 925-929.

- Cardoso, N. C., Chibale, K., & Singh, V. (2022). Implications of *Mycobacterium tuberculosis* Metabolic Adaptability on Drug Discovery and Development. *ACS Infectious Diseases*, 8(3), 414-421.
- Cascioferro, S., Parrino, B., Spanò, V., Carbone, A., Montalbano, A., Barraja, P., ... & Cirrincione, G. (2017). 1, 3, 5-Triazines: A promising scaffold for anticancer drugs development. *European journal of medicinal chemistry*, 142, 523-549.
- Cava, F., & de Pedro, M. A. (2014). Peptidoglycan plasticity in bacteria: emerging variability of the murein sacculus and their associated biological functions. *Current opinion in microbiology*, 18, 46-53.
- Chakaya, J., Khan, M., Ntoumi, F., Aklillu, E., Fatima, R., Mwaba, P., ... & Zumla, A. (2021). Global Tuberculosis Report 2020—Reflections on the Global TB burden, treatment, and prevention efforts. *International Journal of Infectious Diseases*, 113, S7-S12.
- Cheeseright, T., Mackey, M., Rose, S., & Vinter, A. (2006). Molecular field extrema as descriptors of biological activity: definition and validation. *Journal of chemical information and modeling*, 46(2), 665-676. Spark, version, Cresset®, Litlington, Cambridgeshire, UK; <http://www.cresset-group.com/spark/>;
- Congreve, M., Carr, R., Murray, C., & Jhoti, H. (2003). A rule of three for fragment-based lead discovery?. *Drug discovery today*, 8(19), 876-877.
- Coronel Teixeira, R., Aguirre, S., & Pérez Bejarano, D. (2021). Thinking about tuberculosis in times of COVID-19. *Journal of Internal Medicine*, 289(4), 589-590.
- Daina, A., & Zoete, V. (2016). A boiled-egg to predict gastrointestinal absorption and brain penetration of small molecules. *ChemMedChem*, 11(11), 1117-1121.
- Daina, A., Blatter, M. C., Baillie Gerritsen, V., Palagi, P. M., Marek, D., Xenarios, I., ... & Zoete, V. (2017). Drug design workshop: A web-based educational tool to introduce computer-aided drug design to the general public. *Journal of Chemical Education*, 94(3), 335-344.
- Dallakyan, S., & Olson, A. J. (2015). Small-molecule library screening by docking with PyRx. In *Chemical biology* (pp. 243-250). Humana Press, New York, NY.



D'Amaral, M. C., Jamkhov, N., & Adler, M. J. (2021). Efficient and accessible silane-mediated direct amide coupling of carboxylic acids and amines. *Green Chemistry*, 23(1), 288-295.

Dunetz, J. R., Magano, J., & Weisenburger, G. A. (2016). Large-scale applications of amide coupling reagents for the synthesis of pharmaceuticals. *Organic Process Research & Development*, 20(2), 140-177.

Echeverria-Valencia, G., Flores-Villalva, S., & Espitia, C. I. (2018). Virulence factors and pathogenicity of Mycobacterium. *IntechOpen Mycobacterium Reserach and Development*, 231-55.

Eichelbaum, M., & Gross, A. S. (1996). Stereochemical aspects of drug action and disposition. In *Advances in drug research* (Vol. 28, pp. 1-64). Academic Press.

Elfiky, A. A. (2020). Ribavirin, Remdesivir, Sofosbuvir, Galidesivir, and Tenofovir against SARS-CoV-2 RNA dependent RNA polymerase (RdRp): A molecular docking study. *Life sciences*, 253, 117592.

El-Hamamsy, M. H., Smith, A. W., Thompson, A. S., & Threadgill, M. D. (2007). Structure-based design, synthesis, and preliminary evaluation of selective inhibitors of dihydrofolate reductase from *Mycobacterium tuberculosis*. *Bioorganic & medicinal chemistry*, 15(13), 4552-4576.

Evelyn, C. R., Bell, J. L., Ryu, J. G., Wade, S. M., Kocab, A., Harzdorf, N. L., ... & Larsen, S. D. (2010). Design, synthesis, and prostate cancer cell-based studies of analogs of the Rho/MKL1 transcriptional pathway inhibitor, CCG-1423. *Bioorganic & medicinal chemistry letters*, 20(2), 665-672.

Gajula, S. N. R., Nadimpalli, N., & Sonti, R. (2021). Drug metabolic stability in early drug discovery to develop potential lead compounds. *Drug Metabolism Reviews*, 53(3), 459-477.

Galagan, J. E., Sisk, P., Stolte, C., Weiner, B., Koehrsen, M., Wymore, F., ... & Schoolnik, G. K. (2010). TB database 2010: overview and update. *Tuberculosis*, 90(4), 225-235.

Gelbert, L. M., Cai, S., Lin, X., Sanchez-Martinez, C., Del Prado, M., Lallena, M. J., ... & de Dios, A. (2014). Preclinical characterization of the CDK4/6 inhibitor LY2835219: in-vivo cell cycle-dependent/independent anti-tumor activities alone/in combination with gemcitabine. *Investigational new drugs*, 32(5), 825-837.

Ghose, A. K., Viswanadhan, V. N., & Wendoloski, J. J. (1999). A knowledge-based approach in designing combinatorial or medicinal chemistry libraries for drug discovery. 1. A qualitative and quantitative characterization of known drug databases. *Journal of combinatorial chemistry*, 1(1), 55-68.

Gohlke, B. O., Overkamp, T., Richter, A., Richter, A., Daniel, P. T., Gillissen, B., & Preissner, R. (2015). 2D and 3D similarity landscape analysis identifies PARP as a novel off-target for the drug Vatalanib. *BMC bioinformatics*, 16(1), 1-9.

H Brooks, W., C Guida, W., & G Daniel, K. (2011). The significance of chirality in drug design and development. *Current topics in medicinal chemistry*, 11(7), 760-770.

Hall, A., Billinton, A., Brown, S. H., Chowdhury, A., Giblin, G. M., Goldsmith, P., ... & Theobald, P. J. (2008). Discovery of a novel indole series of EP1 receptor antagonists by scaffold hopping. *Bioorganic & medicinal chemistry letters*, 18(8), 2684-2690.

Hodge, C.N. and Pierce, J. (1993) A diazine heterocyclic replaces a six-membered hydrogen-bonded array in the active site of scytalone dehydratase. *Bioorg. Med. Chem. Lett.* 3, 1605–1608

Hong, W., Wang, Y., Chang, Z., Yang, Y., Pu, J., Sun, T., ... & Wang, H. (2015). The identification of novel Mycobacterium tuberculosis DHFR inhibitors and the investigation of their binding preferences by using molecular modelling. *Scientific reports*, 5(1), 1-14.

Huang, Q., He, R., & P Kozikowski, A. (2011). Stereochemistry at the forefront in the design and discovery of novel anti-tuberculosis agents. *Current topics in medicinal chemistry*, 11(7), 810-818.

Hussain, A., Singh, S., Das, S. S., Anjireddy, K., Karpagam, S., & Shakeel, F. (2019). Nanomedicines as drug delivery carriers of anti-tubercular drugs: from pathogenesis to infection control. *Current drug delivery*, 16(5), 400-429.

Hutchison, G. R., Morley, C., James, C., Swain, C., De Winter, H., Vandermeersch, T., & O'Boyle, N. M. (2011). Open Babel Documentation.

Hutt, A. G., & O'Grady, J. (1996). Drug chirality: a consideration of the significance of the stereochemistry of antimicrobial agents. *Journal of Antimicrobial Chemotherapy*, 37(1), 7-32.

- Ibrahim, I. M., Abdelmalek, D. H., Elshahat, M. E., & Elfiky, A. A. (2020). COVID-19 spike-host cell receptor GRP78 binding site prediction. *Journal of Infection*, *80*(5), 554-562.
- Jankute, M., Cox, J. A., Harrison, J., & Besra, G. S. (2015). Assembly of the mycobacterial cell wall. *Annual review of microbiology*, *69*, 405-423.
- Jia, H., Dai, G., Su, W., Xiao, K., Weng, J., Zhang, Z., ... & Bembenek, S. D. (2019). Discovery, optimization, and evaluation of potent and highly selective PI3K $\gamma$ -PI3K $\delta$  dual inhibitors. *Journal of medicinal chemistry*, *62*(10), 4936-4948.
- Jiang, T., Wang, G., Liu, Y., Feng, L., Wang, M., Liu, J., ... & Ouyang, L. (2021). Development of small-molecule tropomyosin receptor kinase (TRK) inhibitors for NTRK fusion cancers. *Acta Pharmaceutica Sinica B*, *11*(2), 355-372.
- Johnson, M. (2018). *Thalidomide Catastrophe*. Onwards and Upwards.
- Johnson, T. W., Richardson, P. F., Bailey, S., Brooun, A., Burke, B. J., Collins, M. R., ... & Edwards, M. P. (2014). Discovery of (10 R)-7-Amino-12-fluoro-2, 10, 16-trimethyl-15-oxo-10, 15, 16, 17-tetrahydro-2H-8, 4-(metheno) pyrazolo [4, 3-h][2, 5, 11]-benzoxadiazacyclotetradecine-3-carbonitrile (PF-06463922), a macrocyclic inhibitor of anaplastic lymphoma kinase (ALK) and c-ros oncogene 1 (ROS1) with preclinical brain exposure and broad-spectrum potency against ALK-resistant mutations. *Journal of medicinal chemistry*, *57*(11), 4720-4744.
- Kapopoulou, A.; Lew, J.M.; Cole, S.T. The MycoBrowser portal: A comprehensive and manually annotated resource for mycobacterial genomes. *Tuberculosis* 2011, *91*, 8–13.
- Kawasaki, Y., & Freire, E. (2011). Finding a better path to drug selectivity. *Drug discovery today*, *16*(21-22), 985-990.
- Keretsu, S., Bhujbal, S. P., & Cho, S. J. (2021). Molecular modeling studies of pyrrolo [2, 3-d] pyrimidin-4-amine derivatives as JAK1 inhibitors based on 3D-QSAR, molecular docking, molecular dynamics (MD) and MM-PBSA calculations. *Journal of Biomolecular Structure and Dynamics*, *39*(3), 753-765.
- Kobayashi, M., Kinjo, T., Koseki, Y., Bourne, C. R., Barrow, W. W., & Aoki, S. (2014). Identification of novel potential antibiotics against *Staphylococcus* using structure-based drug

screening targeting dihydrofolate reductase. *Journal of chemical information and modeling*, 54(4), 1242-1253.

Kosugi, T., & Ohue, M. (2021). Quantitative Estimate Index for Early-Stage Screening of Compounds Targeting Protein-Protein Interactions. *International journal of molecular sciences*, 22(20), 10925.

Kumar, R., Kumar, N., Roy, R. K., & Singh, A. (2018). 1, 3, 5-TRIAZINE: A VERSATILE SCAFFOLD. *Indian Journal of Drugs*, 6(1), 9-48.

Kushwaha, N., & Sharma, C. S. (2020). The Chemistry of Triazine Isomers: Structures, Reactions, Synthesis and Applications. *Mini Reviews in Medicinal Chemistry*, 20(20), 2104-2122.

Lagunin, A. A., Goel, R. K., Gawande, D. Y., Pahwa, P., Glorizova, T. A., Dmitriev, A. V., ... & Poroikov, V. V. (2014). Chemo- and bioinformatics resources for *in-silico* drug discovery from medicinal plants beyond their traditional use: a critical review. *Natural product reports*, 31(11), 1585-1611.

LaPlante, S. R., Fader, L. D., Fandrick, K. R., Fandrick, D. R., Hucke, O., Kemper, R., ... & Edwards, P. J. (2011). Assessing atropisomer axial chirality in drug discovery and development. *Journal of medicinal chemistry*, 54(20), 7005-7022.

Lauri, G., & Bartlett, P. A. (1994). CAVEAT: a program to facilitate the design of organic molecules. *Journal of computer-aided molecular design*, 8(1), 51-66.

Leelananda, S. P., & Lindert, S. (2016). Computational methods in drug discovery. *Beilstein journal of organic chemistry*, 12(1), 2694-2718.

Li, R., Sirawaraporn, R., Chitnumsub, P., Sirawaraporn, W., Wooden, J., Athappilly, F., ... & Hol, W. G. (2000). Three-dimensional structure of *M. tuberculosis* dihydrofolate reductase reveals opportunities for the design of novel tuberculosis drugs. *Journal of molecular biology*, 295(2), 307-323.

Li, X., Hilgers, M., Cunningham, M., Chen, Z., Trzoss, M., Zhang, J., ... & Finn, J. (2011). Structure-based design of new DHFR-based antibacterial agents: 7-aryl-2, 4-diaminoquinazolines. *Bioorganic & medicinal chemistry letters*, 21(18), 5171-5176.

- Lin, Y., & Gerson, S. L. (2014). Clinical Trials Using LV-P140K-MGMT for Gliomas. In *Gene Therapy of Cancer* (pp. 379-391). Academic Press.
- Lipinski, C. A. (2004). Lead-and drug-like compounds: the rule-of-five revolution. *Drug discovery today: Technologies*, 1(4), 337-341.
- Liu, S., Alnammi, M., Ericksen, S. S., Voter, A. F., Keck, J. L., Hoffmann, F. M., ... & Gitter, A. (2018). Practical model selection for prospective virtual screening. bioRxiv.
- Lundberg, H., Tinnis, F., Selander, N., & Adolfsson, H. (2014). Catalytic amide formation from non-activated carboxylic acids and amines. *Chemical Society Reviews*, 43(8), 2714-2742.
- Maass, P., Schulz-Gasch, T., Stahl, M., & Rarey, M. (2007). Recore: a fast and versatile method for scaffold hopping based on small molecule crystal structure conformations. *Journal of chemical information and modeling*, 47(2), 390-399.
- Macalino, S. J. Y., Basith, S., Clavio, N. A. B., Chang, H., Kang, S., & Choi, S. (2018). Evolution of *in-silico* strategies for protein-protein interaction drug discovery. *Molecules*, 23(8), 1963.
- Macalino, S. J. Y., Billones, J. B., Organo, V. G., & Carrillo, M. C. O. (2020). *In-silico* strategies in tuberculosis drug discovery. *Molecules*, 25(3), 665.
- Magazanik, M. (2015). *Silent Shock: The Men Behind the Thalidomide Scandal and an Australian Family's Long Road to Justice*. Text Publishing.
- Mak, K. K., & Pichika, M. R. (2019). Artificial intelligence in drug development: present status and future prospects. *Drug discovery today*, 24(3), 773-780.
- Mauldin, R. V., Sapienza, P. J., Petit, C. M., & Lee, A. L. (2012). Structure and dynamics of the G121V dihydrofolate reductase mutant: lessons from a transition-state inhibitor complex. *PLoS One*, 7(3), e33252.
- Mauri, A. (2020). alvaDesc: A tool to calculate and analyze molecular descriptors and fingerprints. In *Ecotoxicological QSARs* (pp. 801-820). Humana, New York, NY.
- McGrath, N. A., Brichacek, M., & Njardarson, J. T. (2010). A graphical journey of innovative organic architectures that have improved our lives. *Journal of chemical education*, 87(12), 1348-1349.

Mencher, S. K., & Wang, L. G. (2005). Promiscuous drugs are compared to selective drugs (promiscuity can be a virtue). *BMC clinical pharmacology*, 5(1), 1-7.

Menéndez, C. A., Accordino, S. R., Gerbino, D. C., & Appignanesi, G. A. (2016). Hydrogen bond dynamic propensity studies for protein binding and drug design. *PLoS One*, 11(10), e0165767.

Menichincheri, M., Ardini, E., Magnaghi, P., Avanzi, N., Banfi, P., Bossi, R., ... & Orsini, P. (2016). Discovery of entrectinib: a new 3-aminoindazole as a potent anaplastic lymphoma kinase (ALK), c-ros oncogene 1 kinase (ROS1), and pan-tropomyosin receptor kinases (Pan-TRKs) inhibitor. *Journal of medicinal chemistry*, 59(7), 3392-3408.

Montanha, M. C., Fabrega, F., Howarth, A., Cottura, N., Kinvig, H., Bunglawala, F., ... & Siccardi, M. (2022). Predicting Drug–Drug Interactions between Rifampicin and Ritonavir-Boosted Atazanavir Using PBPK Modelling. *Clinical Pharmacokinetics*, 61(3), 375-386.

Morris, G. M., D. S. Goodsell, M. E. Pique, W. Lindstrom, R. Huey, S. Forli, W. E. Hart, S. Halliday, R. Belew, and A. J. Olson. "User Guide Autodock 4.2." *The Scripps Research Institute* (2009).

Morris, G. M., Huey, R., Lindstrom, W., Sanner, M. F., Belew, R. K., Goodsell, D. S., & Olson, A. J. (2009). AutoDock4 and AutoDockTools4: Automated docking with selective receptor flexibility. *Journal of computational chemistry*, 30(16), 2785-2791.

Mugumbate, G., Abrahams, K. A., Cox, J. A., Papadatos, G., Van Westen, G., Lelièvre, J., ... & Besra, G. S. (2015). Mycobacterial dihydrofolate reductase inhibitors identified using chemogenomic methods and in vitro validation. *PloS one*, 10(3), e0121492.

Munchhof, M. J., Li, Q., Shavnya, A., Borzillo, G. V., Boyden, T. L., Jones, C. S., ... & Tkalcevic, G. T. (2012). Discovery of PF-04449913, a potent and orally bioavailable inhibitor of smoothened. *ACS medicinal chemistry letters*, 3(2), 106-111

Murray, C. W., Newell, D. R., & Angibaud, P. (2019). A successful collaboration between academia, biotech and pharma led to discovery of erdafitinib, a selective FGFR inhibitor recently approved by the FDA. *MedChemComm*, 10(9), 1509-1511.

Nagasaka, M., Ge, Y., Sukari, A., Kukreja, G., & Ou, S. H. I. (2020). A user's guide to lorlatinib. *Critical reviews in oncology/hematology*, 151, 102969.

- Nayariseri, A., Khandelwal, R., Tanwar, P., Madhavi, M., Sharma, D., Thakur, G., & Singh, S. K. (2021). Artificial Intelligence, Big Data, and Machine Learning Approaches in Precision Medicine & Drug Discovery. *Current Drug Targets*, 22(6), 631-655.
- Newman, D. J., Cragg, G. M., & Snader, K. M. (2000). The influence of natural products upon drug discovery. *Natural product reports*, 17(3), 215-234.
- Niederweis, M., Danilchanka, O., Huff, J., Hoffmann, C., & Engelhardt, H. (2010). Mycobacterial outer membranes: in search of proteins. *Trends in microbiology*, 18(3), 109-116.
- Oktavia, L., Krishna, V. S., Rekha, E. M., Fathoni, A., Sriram, D., & Agusta, A. (2020, November). Anti-mycobacterial activity of two natural Bisanthraquinones:(+)-1, 1'-Bislunatin and (+)-2, 2'-Epicytoskyrin A. In *IOP Conference Series: Earth and Environmental Science* (Vol. 591, No. 1, p. 012025). IOP Publishing.
- Othman, I. M., Mahross, M. H., Gad-Elkareem, M. A., Rudrapal, M., Gogoi, N., Chetia, D., ... & Kadri, A. (2021). Toward a treatment of antibacterial and antifungal infections: Design, synthesis and in vitro activity of novel arylhydrazothiazolylsulfonamides analogues and their insight of DFT, docking and molecular dynamic simulations. *Journal of Molecular Structure*, 1243, 130862.
- Pelay-Gimeno, M., Glas, A., Koch, O., & Grossmann, T. N. (2015). Structure-based design of inhibitors of protein–protein interactions: mimicking peptide binding epitopes. *Angewandte Chemie International Edition*, 54(31), 8896-8927.
- Peloquin, C. A., & Davies, G. R. (2021). The Treatment of Tuberculosis. *Clinical Pharmacology & Therapeutics*.
- Petkova, Z., Valcheva, V., Momekov, G., Petrov, P., Dimitrov, V., Doytchinova, I., ... & Stoyanova, M. (2014). Antimycobacterial activity of chiral aminoalcohols with camphane scaffold. *European Journal of Medicinal Chemistry*, 81, 150-157.
- Popovici-Muller, J., Lemieux, R. M., Artin, E., Saunders, J. O., Salituro, F. G., Travins, J., ... & Yen, K. (2018). Discovery of AG-120 (Ivosidenib): a first-in-class mutant IDH1 inhibitor for the treatment of IDH1 mutant cancers. *ACS medicinal chemistry letters*, 9(4), 300-305.

- Prasasty, V. D., Cindana, S., Ivan, F. X., Zahroh, H., & Sinaga, E. (2020). Structure-based discovery of novel inhibitors of Mycobacterium tuberculosis CYP121 from Indonesian natural products. *Computational Biology and Chemistry*, 85, 107205.
- Raja, A., Gajalakshmi, P., Raja, M., & Mahroop, M. (2010). Drugs from the natural bio sources for human disease. *International Journal of Pharmacology*, 6(4), 360-363.
- Ramachandran, P. V., & Hamann, H. J. (2021). Ammonia-borane as a Catalyst for the Direct Amidation of Carboxylic Acids. *Organic Letters*, 23(8), 2938-2942.
- Reddy, A. S., & Zhang, S. (2013). Polypharmacology: drug discovery for the future. *Expert review of clinical pharmacology*, 6(1), 41-47.
- Reddy, T. B. K., Riley, R., Wymore, F., Montgomery, P., DeCaprio, D., Engels, R.,... & Schoolnik, G. K. (2009). TB database: an integrated platform for tuberculosis research. *Nucleic acids research*, 37(suppl\_1), D499-D508.
- Remm, S., Earp, J. C., Dick, T., Dartois, V., & Seeger, M. A. (2022). Critical discussion on drug efflux in *Mycobacterium tuberculosis*. *FEMS microbiology reviews*, 46(1), fuab050.
- Rod, T. H., Radkiewicz, J. L., & Brooks III, C. L. (2003). Correlated motion and the effect of distal mutations in dihydrofolate reductase. *Proceedings of the National Academy of Sciences*, 100(12), 6980-6985.
- Roughley, S. D., & Jordan, A. M. (2011). The medicinal chemist's toolbox: an analysis of reactions used in the pursuit of drug candidates. *Journal of medicinal chemistry*, 54(10), 3451-3479.
- Rush, T. S., Grant, J. A., Mosyak, L., & Nicholls, A. (2005). A shape-based 3-D scaffold hopping method and its application to a bacterial protein– protein interaction. *Journal of medicinal chemistry*, 48(5), 1489-1495.
- Ryu, J. Y., Lee, J. H., Lee, B. H., Song, J. S., Ahn, S., & Oh, K. S. (2022). PredMS: A random Forest model for predicting metabolic stability of drug candidates in human liver microsomes. *Bioinformatics*, 38(2), 364-368



Salomon-Ferrer, R., Case, D. A., & Walker, R. C. (2013). An overview of the Amber biomolecular simulation package. *Wiley Interdisciplinary Reviews: Computational Molecular Science*, 3(2), 198-210.

Sander, T., & Freyss, J. (2015). Mütevazı von Korff, Christian Rufener. DataWarrior: Kimya İçin Veri Görselleştirme ve Analizini Destekleyen Açık Kaynaklı Bir Program. *J Chem Inf Model*, 55, 460-473.

Sarathy, J. P., Dartois, V., & Lee, E. J. D. (2012). The role of transport mechanisms in *Mycobacterium tuberculosis* drug resistance and tolerance. *Pharmaceuticals*, 5(11), 1210-1235.

Schneider, G., Neidhart, W., Giller, T., & Schmid, G. (1999). “Scaffold-hopping” by topological pharmacophore search: a contribution to virtual screening. *Angewandte Chemie International Edition*, 38(19), 2894-2896.

Schreiber, S. L. (2011). Organic synthesis toward small-molecule probes and drugs. *Proceedings of the National Academy of Sciences*, 108(17), 6699-6702.

Scott, W. J., Hentemann, M. F., Rowley, R. B., Bull, C. O., Jenkins, S., Bullion, A. M., ... & Lefranc, J. (2016). Discovery and SAR of novel 2, 3-dihydroimidazo [1, 2-c] quinazoline PI3K inhibitors: identification of copanlisib (BAY 80-6946). *ChemMedChem*, 11(14), 1517.

Sharma, K., Neshat, N., Sharma, S., Giri, N., Srivastava, A., Almalki, F., ... & Akhter, M. (2020). Identification of novel selective Mtb-DHFR inhibitors as antitubercular agents through structure-based computational techniques. *Archiv der Pharmazie*, 353(2), 1900287.

SIB Swiss Institute of Bioinformatics Members. (2016). The SIB Swiss Institute of Bioinformatics’ resources: focus on curated databases. *Nucleic acids research*, 44(D1), D27-D37.

Silakari, O., & Singh, P. K. (2021). Chapter 11 - Scaffold hopping: An approach to improve the existing pharmacological profile of NCEs. *Concepts and Experimental Protocols of Modelling and Informatics in Drug Design*, 255-265.

Silakari, O., & Singh, P. K. (2021). Chapter 6—Molecular docking analysis: Basic technique to predict drug-receptor interactions. *Concepts and Experimental Protocols of Modelling and Informatics in Drug Design*, 131-155.

Smeyne, D. (2020). Structure-activity relationship (SAR) studies of neurotoxin quinoline-derivatives.

Smithells, R. W., & Newman, C. G. (1992). Recognition of thalidomide defects. *Journal of medical genetics*, 29(10), 716.

Sousa da Silva, A. W., & Vranken, W. F. (2012). ACPYPE-Antechamber python parser interface. *BMC research notes*, 5(1), 1-8.

Spark, version, Cresset®, Litlington, Cambridgeshire, UK; <http://www.cresset-group.com/spark/>;  
Cheeseright, T., Mackey, M., Rose, S., & Vinter, A. (2006). Molecular field extrema as descriptors of biological activity: definition and validation. *Journal of chemical information and modeling*, 46(2), 665-676.

Stelitano, G., Sammartino, J. C., & Chiarelli, L. R. (2020). Multitargeting compounds: a promising strategy to overcome multi-drug resistant tuberculosis. *Molecules*, 25(5), 1239.

Stop TB Partnership. UNHLM on TB: key targets and commitments. Geneva, Switzerland: STOP TB Partnership; 2020.

Storace, L., Anzalone, L., Confalone, P. N., Davis, W. P., Fortunak, J. M., Giangiordano, M., ... & Wood, C. C. (2002). An efficient large-scale process for the human leukocyte elastase inhibitor, DMP 7771. *Organic process research & development*, 6(1), 54-63.

Sui, J., Zhang, J., Ching, C. B., & Chen, W. N. (2009). Expanding proteomics into the analysis of chiral drugs. *Molecular BioSystems*, 5(6), 603-608.

Sun, H., Tawa, G., & Wallqvist, A. (2012). Classification of scaffold-hopping approaches. *Drug discovery today*, 17(7-8), 310-324.

Sunduru, N., Gupta, L., Chaturvedi, V., Dwivedi, R., Sinha, S., & Chauhan, P. M. (2010). Discovery of new 1, 3, 5-triazine scaffolds with potent activity against *Mycobacterium tuberculosis* H37Rv. *European Journal of Medicinal Chemistry*, 45(8), 3335-3345.

Taha, M. O., Habash, M., Al-Hadidi, Z., Al-Bakri, A., Younis, K., & Sisan, S. (2011). Docking-based comparative intermolecular contacts analysis as new 3-D QSAR concept for validating

docking studies and *in-silico* screening: NMT and GP inhibitors as case studies. *Journal of chemical information and modeling*, 51(3), 647-669.

Tatum, N. J., Liebeschuetz, J. W., Cole, J. C., Frita, R., Herledan, A., Baulard, A. R., ... & Pohl, E. (2017). New active leads for tuberculosis booster drugs by structure-based drug discovery. *Organic & Biomolecular Chemistry*, 15(48), 10245-10255.

TBFACTS.ORG (2022). <https://tbfacts.org/tb-statistics/>.

Tiberi, S., du Plessis, N., Walzl, G., Vjecha, M. J., Rao, M., Ntoumi, F., ... & Zumla, A. (2018). Tuberculosis: progress and advances in the development of new drugs, treatment regimens, and host-directed therapies. *The Lancet Infectious Diseases*, 18(7), e183-e198.

Tuberculosis, Self-study Modules On. n.d. "Epidemiology of Tuberculosis."

Uehara, S., Higuchi, Y., Yoneda, N., Kawai, K., Yamamoto, M., Kamimura, H., ... & Suemizu, H. (2022). An improved TK-NOG mouse as a novel platform for humanized liver that overcomes limitations in both male and female animals. *Drug Metabolism and Pharmacokinetics*, 42, 100410.

Upadhyay, S. S., Gadhari, N. S., & Srivastava, A. K. (2020). Biomimetic sensor for ethambutol employing  $\beta$ -cyclodextrin mediated chiral copper metal organic framework and carbon nanofibers modified glassy carbon electrode. *Biosensors and Bioelectronics*, 165, 112397.

Valeur, E., & Bradley, M. (2009). Amide bond formation: beyond the myth of coupling reagents. *Chemical Society Reviews*, 38(2), 606-631.

Vargesson, N. (2019). The teratogenic effects of thalidomide on limbs. *Journal of Hand Surgery (European Volume)*, 44(1), 88-95.

Vieth, M., Siegel, M. G., Higgs, R. E., Watson, I. A., Robertson, D. H., Savin, K. A., ... & Hipskind, P. A. (2004). Characteristic physical properties and structural fragments of marketed oral drugs. *Journal of medicinal chemistry*, 47(1), 224-232.

Vilchèze, C., & Kremer, L. (2017). Acid-fast positive and acid-fast negative *Mycobacterium tuberculosis*: the Koch paradox. *Microbiology spectrum*, 5(2), 5-2.

Wajja, A. (2004). Prevalence and Risk Factors for Drug Resistant Tuberculosis at an Urban Hospital in Uganda. *University of Toronto: Graduate Department of Public Health*.

- Wang, J., Wolf, R. M., Caldwell, J. W., Kollman, P. A., & Case, D. A. (2004). Development and testing of a general amber force field. *Journal of computational chemistry*, 25(9), 1157-1174.
- Watney, J. B., Agarwal, P. K., & Hammes-Schiffer, S. (2003). Effect of mutation on enzyme motion in dihydrofolate reductase. *Journal of the American Chemical Society*, 125(13), 3745-3750.
- World Health Organization. (2021). WHO consolidated guidelines on tuberculosis: module 2: screening: systematic screening for tuberculosis disease. World Health Organization.
- Wu, Y., Islam, A., Yang, X., Qin, C., Liu, J., Zhang, K., ... & Han, L. (2014). Retarding the crystallization of PbI<sub>2</sub> for highly reproducible planar-structured perovskite solar cells via sequential deposition. *Energy & Environmental Science*, 7(9), 2934-2938.
- Xiong, Y., Ba, X., Hou, A., Zhang, K., Chen, L., & Li, T. (2018). Automatic detection of *Mycobacterium tuberculosis* using artificial intelligence. *Journal of thoracic disease*, 10(3), 1936.
- Yadav, G., & Ganguly, S. (2015). Structure activity relationship (SAR) study of benzimidazole scaffold for different biological activities: A mini-review. *European Journal of Medicinal Chemistry*, 97, 419-443.
- Yang, H., Sun, L., Wang, Z., Li, W., Liu, G., & Tang, Y. (2018). ADMETopt: a web server for ADMET optimization in drug design via scaffold hopping. *Journal of chemical information and modeling*, 58(10), 2051-2056.
- Yuan, H., Ma, Q., Ye, L., & Piao, G. (2016). The Traditional Medicine and Modern Medicine from Natural Products, *Molecules* 21.
- Zhang, Y., Zhang, H., Chen, Y., Qiao, L., Han, Y., Lin, Y., ... & Jiang, J. D. (2021). Screening and identification of a novel anti-tuberculosis compound that targets dUTPase. *Frontiers in microbiology*, 2934.
- Zhou, C., Min, J., Liu, Z., Young, A., Deshazer, H., Gao, T., ... & Kallenbach, N. R. (2008). Synthesis and biological evaluation of novel 1, 3, 5-triazine derivatives as antimicrobial agents. *Bioorganic & medicinal chemistry letters*, 18(4), 1308-1311.